ANALYSIS OF THE EFFECT OF THE MACROSCALE OF TURBULENCE ON THE TOTAL DRAG OF A SPHERE

TEDDY SHANSONGA

A thesis presented for the degree
of Doctor of Philosophy of
The City University

Department of Mechanical Engineering
The City University
London.

April 1988

To my Mother, Father and wife Elizabeth.

ABSTRACT

The dependence of the drag coefficient of a sphere on the free-stream turbulence characteristics and Reynolds number has been acknowledged by researchers for many years now. Over the same period, a correlation between the drag coefficient and a combination of the various characteristics has also been sought. This project analyses the effects of the characteristics of importance in this respect and provides a correlation between the drag coefficient and a variation of characteristics.

The effects on the drag coefficient of varying the macroscale of turbulence keeping all other characteristics constant have been presented. These show that the magnitude of variation of the drag coefficient caused by this characteristic is such that it should be included in any correlation between the drag coefficients and characteristics that may be sought.

The effect on the pressure distribution of the various characteristics has also been presented, from which it has been shown that the macroscale of turbulence introduces a dynamic boundary layer which conforms with the physical model built in the earlier chapters. The mechanisms by which the dynamic boundary layer is formed and is affected by the various characteristics have been analysed together with the resulting variations of the drag coefficient. It has also been shown that because of the dynamic boundary layers introduced, the skin friction drag increases and raises its percentage contribution to the total drag to values much greater than those quoted by previous researchers who investigated flows of low macroscale of turbulence. Additionally, a resonance position of the drag coefficient values has been shown to exist at a fixed frequency ratio with an amplitude dependent on the Reynolds number.

A series of correlations have been shown to exist between the drag coefficient and the characteristics, with the scale ratio being identified as the characteristic upon which the correlations are made unique. Because of the nature of the correlation, a vibrations equation for a similar phenomenon has been used to define the curves. Within the determined limits this equation has been found to be an accurate method of predicting the drag coefficient from the characteristics.

In determining the macroscale of turbulence from the experiments conducted, a method of predicting the position of the peak of a Gaussian curve when this has been cut-off has been developed. This has been derived from the von Karman equation which defines the spectral density of turbulence.

CONTENTS

List of figures

ACKNOWLEDGEMENTS

I wish to express my sincere gratitude to Dr. R. S. Neve for his assistance and encouragement during the course of my research: to J. Spencer and J. Lee for their unrelenting assistance with my experimental equipment: and last but not least, to the other research students with whom I shared an office, for their constructive critisim from which I have learnt a lot.

I wish also to thank the trustees of the Robert Kitchen Award for their assistance.

DECLARATION

I grant powers of discretion to the University Librarian to allow this thesis to be copied in whole or in part without further reference to me. This permission covers only single copies made for study purposes, subject to normal conditions of acknowledgement.

NOMENCLATURE

A,B,C	Constants
b	Grid slat width
Cd	Total drag coefficient
C_f	Skin-friction coefficient
Cp	Pressure coefficient
Cp_b	Base pressure coefficient
d	Sphere diameter
E(n)	One-dimensional energy spectrum
f(r)	Longitudinal correlation coefficient
g(r)	Lateral correlation coefficient
h	Heat transfer coefficient
I	Relative turbulence intensity
k	Thermal conductivity / Empirical constant / roughness height
l	Characteristic linear dimension
L	Macro(integral)scale of turbulence
Lx	Longitudinal macroscale of turbulence
Ly	Lateral macroscale of turbulence
Lx/d	Scale ratio
m,n	Empirical constant
M	Grid mesh size
∂n	Vertical component to surface
n	Frequency / Shedding frequency
N	Nusselt number
q_s	Heat transfer
$Q_{ij}(x,x+r)$	Double velocity correlation tensor

r	Distance between points
$R(t)$	Eulerian correlation coefficient
$R_{ij}(x,x+r)$	Correlation coefficient
Re	Reynolds number based on sphere diameter
Re_{crit}	Critical Reynolds number
Re_x	Reynolds number based on circumferential distance x from the front stagnation point
S	Strouhal number
T	Time / Temperature
u,v,w	Fluctuating components of velocities
u',v',w'	Root-mean-square velocities
$\bar{u}\ \bar{U}$	Mean time-averaged velocity
U	Turbulent velocity
v	Fluctuating output voltage
$\bar{V}$	Mean output voltage
V_{CTA}	Anemometer output voltage
V_{LIN}	Linearizer output voltage
x,y,z	Cartesian directions
θ	Angle from front stagnation point
λ	Microscale of turbulence
μ	Dynamic viscosity
ν	Kinematic viscosity of air
ρ	Density of air
τ_s	Wall shear stress

CHAPTER 1. INTRODUCTION.

Turbulence is the most common form of fluid state found in engineering and industrial use. This therefore necessitates the ability to determine the ultimate effects that characteristics of such turbulent fields will have on various fluid applications. It follows from this that for a particular category, e.g. pneumatic and hydraulic transportation applications, there must be a precise determination during design of what the effect of the turbulent flow field will be on the drag of the bluff objects being transported. Another example of a category of fluid application would be the determination of the heat transfer to turbulent flow fields. Here again, the effect that the turbulent flow fields will have on the rate and degree of heat transfer must be determined in the early stages of design. It is of course recognized, that numerous other categories of applications exist for which the importance of the turbulence effects need special consideration at an early stage during design. However, concentration in this project will be on the first category of which an example is the design of a pipeline for the transportation of spherical objects. In this case, the effect of the turbulence flow field on the drag needs to be determined so that the pressure drop in the pipeline can be calculated. This will affect amongst others, the pump size (flow rate and head developed), pipe diameter, and pipe thickness used. Unfortunately, because of the

current limited understanding of the ultimate effects of the turbulence characteristics, there is insufficient information available to designers, providing only a limited basis for them to strive towards greater accuracy of design or analyses of various safety factors employed.

The determination of the effect that a turbulent flow field has on the total drag of a sphere is very useful, both in increasing the understanding of turbulence itself and in increasing the ability to predict the effects that such a field would have on similar objects in industrial applications. To achieve this, the effects of individual characteristics of a turbulent field have to be identified and isolated. Only by identification and isolation is it possible to spot an effect that is not due to any of the expected characteristics of a field, and also to build up the expected individual effects to enable prediction of the total effect.

There are many characteristics of a turbulent flow field, the importance of which are dependent on the effect that is being observed at the time. For instance, the turbulence characteristics of importance in determining total drag may differ from those in determining heat transfer, mass transfer, cavitation, or even noise production. Therefore, only by being able to identify and isolate the effects of the individual turbulence characteristics is it possible to predict the total effect

that a turbulent flow field may have on each of the factors being considered.

Turbulence as defined by Hinze [1959] "is an irregular condition of flow in which the various quantities show a random variation with time and space co-ordinates, so that statistically distinct average values can be discerned". Because of this irregularity and randomness, mathematical approaches to the solution of determining the effects due to turbulence can be very involved and are limited to statistical averages only. Cooper and Tuplin [1955] summed up the problem by saying "the fluctuation which is superimposed on the principal motion is so hopelessly complex in its details that it seems to be inaccessible to mathematical treatment". A total determination of the effects is therefore possible only by considering experimental results, until the advancement of mathematics becomes such that these complex motions may be analysed.

Identification of the effects due to individual turbulence characteristics initially involves isolating the characteristics that are considered to be of importance. In the determination of the effect on the total drag coefficient of a sphere, the important turbulence characteristics are considered to be: the Reynolds number; the turbulence intensity; and the macroscale of turbulence. Additional factors such as the method of support, blockage and end effects are also of importance and therefore need special attention during the conducting

of experiments. Investigations into the effects of most of the turbulence characteristics on the total drag of a sphere have been conducted by many researchers, with the exception of the effect due to the macroscale of turbulence. This, until recently (Neve [1986]) was not considered to be of any importance in the determination of the total drag. Because of this total lack of co-ordinated information on the effects of macroscale, many researchers have treated the importance of this turbulence characteristic with scepticism. This scepticism has probably arisen because insufficient research has been carried out on the effects of macroscale. The isolation and identification of macroscale effects on total drag was therefore the prime concern of this research project.

1.1. Review of previous work.

The drag of a sphere and the static pressure at the back of it were initially used as criteria for determining the degree of turbulence in an airstream. A critical Reynolds number defined by Dryden and Kuethe [1930], was the value of the Reynolds number for which the drag coefficient of a sphere was 0.3. At this critical value, the pressure coefficient was determined as -0.22 for a pressure tapping hole at 157.5^{o} from the front stagnation point. Though not considered a direct measure of the turbulence, the critical Reynolds number was considered a measure of the aerodynamic effect of turbulence on a particular body.

Interest in the sphere as an object of aerodynamic study, rather than a means of calibrating wind tunnels (Prandtl [1914]), was the beginning of a study into the resistance of spheres in wind tunnels, jets, air, water, and many other media, thus enabling a better understanding of the effects of the turbulence characteristics. Because of the mathematical limitations in handling problems associated with turbulence, most of the work conducted on the effects of some of the turbulence characteristics has been experimental. This experimental work has been dependent on, and simplified by the theoretical work carried out by a few researchers, the most prominent of whom were G. I. Taylor, and T. von Karman.

Bacon and Reid [1924] working on spheres in wind tunnels observed that factors such as the method of support, intensity, and scale of turbulence, were contributing factors in the difference, beyond experimental error, of the data that were obtained from different wind tunnels. One of the conclusions they drew was that:

> "The one determined effect of scale of turbulence is to control the degree with which true dynamic similarity may be maintained throughout a series of tests with spheres of different sizes. If the scale is fine, as compared with the diameter of the smallest sphere, a good approximation may be had throughout; if it is coarse, Reynolds law no longer serves even as an indicator."

Though this was apparently not considered seriously by researchers until many years after, it is a very relevant contribution to the present research because of its identification of the importance of the macroscale in

experiments with aerodynamic objects immersed in turbulent flow fields. There is no apparent indication as to which length scale (longitudinal or lateral) Bacon and Reid referred, but a generalization of both seems probable.

To generate turbulent flow fields, grids of various shapes and sizes were used. This meant that a careful study of the characteristics of the turbulent flow fields generated by the grids had to be initiated. Dryden et.al. [1937] determined the scale and intensity of turbulence downstream of square grids of different size and construction. They recommended that measurements closer than a few mesh lengths from the grids should be avoided, as the "shadows" of the grids were still prevalent in that region of the field. Ower and Warden [1934] had also previously noticed the "shadows" due to wire and cord networks a few mesh lengths downstream of the networks in their experiments. Baines and Peterson [1951] conducted a more detailed investigation using grids of different shapes, size, and construction, and recommended a distance of 5 to 10 mesh lengths downstream from grids as the minimum required "to ensure reasonable flow establishment". Measurements by Bearman [1971] showed that the intensity and scale of turbulence were both independent of the free-stream velocity. Laurence [1956] working on jets, carried out a thorough investigation into the variations of the intensity, scales (lateral and longitudinal), and spectra of turbulence downstream of a

nozzle. His results show the variation of these turbulence characteristics in the vertical plane of a jet.

Experiments investigating the effect of turbulence intensity on the critical Reynolds number were carried out by many researchers including Millikan and Klein [1933], Hoerner [1935a], Serby and Morgan [1936], Platt [1936] and Dryden et.al. [1937]. Observed by all was the variation that the increase or decrease of the turbulence intensity had on the critical Reynolds number. Hoerner additionally observed that the effect of the turbulence intensity on the sphere drag was similar to that of surface roughness. Dryden et.al. noted further that the sphere drag can vary "by a factor of 4 in airstreams of different turbulence".

In experiments by Torobin and Gauvin [1961], they tested moving spheres in fluid flows with turbulence intensities of up to 45%, and found results similar to those of Hoerner [1935b] who used fixed spheres. The significant difference was that the critical Reynolds numbers they found were much lower than those found by Hoerner, the difference being a factor of 100. This, Torobin and Gauvin concluded to be due to the difference of effects between fixed and moving spheres. Clamen and Gauvin [1969] continued the work by Torobin and Gauvin and extended the range of the Reynolds numbers to higher values. They found that in the low Reynolds number region, the curves formed a series of minimum drag coefficients whose position was

dependent on the intensity. The higher the turbulence intensity, the lower the Reynolds number value at which the minimum drag coefficient occurred. Beyond these minimum positions, increase in Reynolds number produced corresponding increases in the drag coefficient until maximum peak values were attained, beyond which increase in Reynolds number caused corresponding decrease in drag coefficient. The positions of the peaks of the drag coefficients were again dependent on the turbulence intensity, so the peaks of curves with a higher intensity occurred at lower Reynolds numbers than those of lower intensities. Neve and Jaafar [1982] extended these results to an even higher Reynolds number range, and obtained results that formed the decreasing drag coefficient portions of the curves. The combination of all the results gave, superposed onto the standard drag coefficient against Reynolds number curve (Achenbach [1972]), a series of 'S' curves (figure 1.1) dependent on the turbulence intensity. These 'S' curves showed the possible existence of two critical Reynolds numbers for a fixed intensity curve, at Reynolds number differing by a factor of 100.

Although the effect of the scale of turbulence as first mentioned by Bacon and Reid [1924] was considered in relation to other aerodynamic objects (van der Hegge Zijnen [1958] on circular cylinders; Bearman [1971] on flat plates; and Lee [1975/6] on square prisms), the effect on spheres was not readily investigated. It is this

use of complicated aerodynamic shapes which introduce further unnecessary complications that has delayed the isolation of the distinct effects due to the scale of turbulence. Torobin and Gauvin [1961], who quoted scale ratio values (Lx/d) of between 0.16 and 0.5, observed no effect due to the scale of turbulence. The reason for this is that for such small scale ratio values, the effect of the scale compared to that of the turbulence intensity is expected to be negligible.

Neve [1986] considered the importance of the scale in determining the drag coefficient of spheres. He observed that the variations of the drag coefficients with Reynolds numbers were dependent on both the scale and intensity of turbulence and that the magnitude of their variations deserved them special consideration. It is thus against this background that the current research was conducted.

1.2. Aim of the project.

As an extension to the work by Neve [1986], the aims of this project were to achieve the following:

1). To establish the relationship between the macroscale of turbulence and the total drag of a sphere.

2). To establish whether the variations in the drag coefficients have corresponding base pressure coefficient variations.

3). To establish the dynamic relationship between the drag and pressure coefficients, and also to ascertain the existence of "resonance" at given vortex shedding

frequencies.

4). To establish whether the effects of individual vortices passing the sphere can be detected.

2.1. Turbulence generation.

Generation of turbulent flow fields in laboratories is usually achieved by the use of grids although other methods such as frictional force generation of turbulence can also be used. Grids are also used as reducers of large scale turbulence, the distinction between grids used as generators and those used as reducers generally depending on their size and positioning. Goldstein [1938] made the distinction based on the position relative to a contraction nozzle leading to the working section. He observed that grids placed at the entrance to the contraction were reducers and those placed at the exit of the contraction were generators. Baines and Peterson [1951] made a rigorous investigation of the flow fields downstream of different grids and concluded that particular combinations of grid characteristic were most efficient for particular types of grid application. Tan-Atichat et.al. [1982] on the other hand summed up the distinction between generators and reducers as being dependent on: the Reynolds number of operation; the turbulence properties in the absence of the grids; the turbulence properties created by the grids; and the downstream decay time provided.

Von Karman [1937a] stated that turbulent flow fields were normally generated in one of two ways:

1). Boundary layer or wall turbulence; generated by friction forces at the wall, and is continuously affected by fixed walls.

2). Free-stream turbulence; turbulence in the absence of walls, generated by the flow of layers of fluids of different velocities past or over one another.

The second of these two ways is the general method by which grids generate turbulence.

2.1.1. Mechanics of turbulence generation.

The mechanics by which turbulent flow fields are generated by grids was studied amongst others by Owen and Zienkiewicz [1957], Ho and Nosseir [1981], and Laufer [1981]. Owen and Zienkiewicz provided the basic explanation by showing that the static pressure differences between the downstream and upstream faces of the grid cause the downstream ~~moving~~ pressure field to interact with the initial vortices of the shear layer. Such an interaction produces a contracting-expanding motion which results in an acceleration and deceleration of the flow, and this in turn changes the stability characteristics of the layer. During the unstable deceleration phase, initial vortices coalesce and roll up into a large vortical structure, whereas in the stable acceleration phase the vortices do not coalesce. By this process a turbulent flow field comprising of large and small vortical structures propagating downstream from the grid is generated. Figure 2.1 shows this early development

of the vortical structures.

Each individual slat of the grid forms its own wake which, with increasing distance away from the grid, begins to interact with the wakes of other slats. It is this early region of the interactions that Ower and Warden [1934] and Dryden et.al [1937] described as having the "shadow" of the grid prevalent. Beyond this region, when the interaction between the wakes of individual slats is complete, a uniform flow field is formed which can be considered to be self-preserving. Self-preserving as defined by Stewart and Townsend [1951] is a term used to define a flow for which the structure of turbulence can be assumed to maintain its similarity during decay. The notion of self-preservation during decay is one that had been introduced in theoretical literature by many researchers, in particular von Karman [1937b], von Karman and Howarth [1938], von Karman and Lin [1951] and Dryden [1941,1943], where its value in relatively simplifying equations is incalculable.

For turbulent flow fields generated in open section wind tunnels, this initial region forms a "potential core", which is of almost uniform cross-sectional velocity and therefore of very low shear stress. Surrounding this core will be the mixing region, a region of high shear stress caused by the velocity gradient between the fast flowing potential core and the stationary surrounding fluid. These shear layers formed increase both the level of intensity

and the size of the vortices in the turbulent flow field. The interaction which increases the vorticity spreads, reducing the core region until it disappears. Beyond this region the shear stresses decrease until a fully developed self-preserving region is attained.

The significant distances away from the grids in the turbulent flow field are those at which:-

- the grid shadow disappears,
- the potential core disappears,

and - the flow becomes fully developed.

Various researchers have found different distances for these occurrences, a summary of which would be:

1). Grid shadow disappears.

Dryden et.al. [1937]	15 mesh lengths.
Baines and Peterson [1951]	5 - 10 mesh lengths.

2). Potential core disappears.

Davies et.al. [1963]	4 - 5 times wind tunnel width.

3). Start of fully developed region.

Goldstein [1938]	5 - 7 times wind tunnel width.
Wygnanski and Fiedler [1969]	5 times wind tunnel width.
Comte-Bellot and Corrsin [1966]	20 - 30 mesh lengths.

Variations of these distances are only to be expected because the characteristics of the turbulent flow fields

generated will depend on the level of turbulence in the flow approaching the grids, the wind tunnel size, and the grid size, mesh, and construction. Therefore identical grids placed in two similar sized wind tunnels will not necessarily produce identical turbulent flow fields, unless the characteristics of the flow approaching the grid position are also identical.

The dependence of the characteristics of the turbulent flow field on the grids has been investigated by many researchers. Dryden et.al. [1937] stated that although the scale of the turbulence near the grids corresponds more nearly to the wire size than the mesh size, this did not imply that the wire size necessarily determined the initial scale. Rose [1970] demonstrated that the turbulent scale imposed initially by the grid fixed the level of turbulence intensity, and that below some minimum initial scale the turbulence was always found to decay. Baines and Peterson [1951] showed from their results the dependence of the initial characteristics on the grid dimensions.

Although the decay of turbulence and the increase of scale in the potential core is independent of the grid dimensions, as indicated by the results of Dryden et.al. [1937], Baines and Peterson [1951], Bearman [1971], Lee [1975/6] and Neve [1986], the start of the mixing region appears from the results of Neve [1986] to be dependent on the grid dimensions. This is only to be expected because

the mixing region, for open section wind tunnels, also starts to develop just downstream of the grids where the grid dimensions are of great importance. The spreading vorticity of the mixing region is therefore directly dependent on the grid dimensions which will cause the position at which the potential core disappears also to be dependent on the grid dimensions. The results of Neve [1986] also show that as the flow becomes fully developed, self-similar and self-preserving the dependence of the characteristics of turbulence on the grid dimensions disappears, and the development of the turbulence characteristics is proportional to the distance from the grid position as observed by many researchers including Townsend [1956], Davies et.al. [1963], and Wygnanski and Fiedler [1970].

2.2. Turbulent flow fields.

Turbulence, was defined by Hinze [1959], as an irregular condition of flow in which the various quantities show a random variation with time and space co-ordinates. The other essential features of this turbulence are the vorticity and mixing. Vorticity is a vector quantity, which gives a measure of the rotation of a particle of fluid, and mixing plays a major and important role in the energy interchange within the turbulent flow field.

The turbulent velocity consists of two components; a mean flow that is steady in time, and a fluctuating flow whose time-averaged velocity is zero ($U = \overline{u} + u$). Three spatial

components of the fluctuating velocity components are denoted as u, v, and w and the corresponding root-mean-square values as u', v', and w', with the u component in the direction of mean flow.

The first person to show any understanding of the phenomenon of turbulence was Reynolds in 1883. His investigations of pipe flow clearly established two fundamental modes of flow, laminar and turbulent, the latter of which he called "sinuous" flow. In 1895 Reynolds introduced the ideas which have led to what are now known as Reynolds number and Reynolds stresses. He showed that as a result of turbulence, additional stresses were introduced and superimposed on the mean motion. These Reynolds stresses are proportional to the product of any two components of fluctuating velocity averaged over a long period of time. There are nine of these stresses, three normal compressive components and six shear components and they are essential in determining the behaviour of the mean flow.

A number of theories have been suggested regarding the interrelationship between the Reynolds stresses and the mean flow, to determine how the turbulent viscosity varies with distance from a wall. These include the similarity theory of von Karman [1930] and the mixing theories of Prandtl [1926] (the momentum-transfer theory) and Taylor [1932] (the vorticity-transfer theory). Although these

theories permitted the prediction of certain gross characteristics of some boundary layer type turbulent flows, they offered limited understanding of the mechanism of turbulence itself. Goldstein [1938a] gives a detailed description of these theories. The books of Townsend [1956], Hinze [1959], and Batchelor [1971] also give a detailed analysis of the state of the knowledge on turbulence at the respective times of publications.

2.2.1. The statistical theory.

Taylor [1935,1938] introduced the application of statistical terms and concepts, to turbulence problems. (Hinze [1959] gives the mathematical approach to the statistical theory of turbulence). Some of these important concepts which led to the definition of certain quantities important in the characterization of turbulent flow fields are:-

1). The spectrum of turbulence (a function of time) at any point in the flow field may be considered as an infinite sum of harmonic components each of which has a different and characteristic scale (eddy size) associated with it. Batchelor [1971] considered a turbulent flow field at any instant in time as being defined in space by a three-dimensional Fourier integral.

2). The correlation coefficients in a turbulent flow field describes the structure of the field to the degree with which the velocity components at

neighbouring points are correlated. This correlation between velocities at two points increases with decrease in the distance between the points.

3). The degree of isotropy of a turbulent flow field is the degree to which the quantitative description of the field at a certain point depends upon the orientation of the physical co-ordinate system. An isotropic flow field has all spatial components of the fluctuating flow equal.

2.2.2. The characteristics of turbulence.

A turbulent flow field is usually described quantitatively only in terms of its statistical properties and in general the lowest frequencies of importance in the turbulence signal are sufficiently large to permit a determination of statistical quantities from a time sampling no longer than a few seconds. These statistical properties include:

1) The turbulence intensities. (u', v', w')

These are the most commonly measured quantities, because of the ease with which this can be done. The turbulence intensities are defined as the root-mean-square values of the fluctuating velocity components.

$$u' = \left[\lim_{T \to \infty} \frac{1}{T} \int_0^T u^2 \, dt \right]^{1/2}$$

The averaging time T cannot be taken as infinitely long, so is taken as a finite time interval sufficiently large compared with the time scale of turbulence. The magnitude

of the time scale as stated by Hinze [1959], "is determined by the dimensions of and the velocities within the apparatus in which the turbulent flow occurs". The free-stream turbulence intensity is of practical importance because of its effect on the boundary layer transition point. This effect on the transition point has important effects on drag, maximum lift and heat transfer.

The energy density of a turbulent field is derived from the turbulence intensities as:

$$(u'^2 + v'^2 + w'^2) / 2.$$

2). The one-dimensional energy spectrum. (E(n)).

If the turbulent velocity u(t) is resolved into harmonic components, the component of turbulent energy u'^2 may be regarded as consisting of the sum of contributions from all frequencies. Therefore the quantity E(n)dn is the energy contribution from frequencies between n and n + dn.

Or $$u'^2 = \int_0^\infty E(n)\, dn.$$

The shape of the energy spectrum against frequency curve, provides useful information about the structure of the turbulent field enabling concepts of the mechanism of turbulence to be phrased in terms of energy transfer through the energy spectrum. The low frequency components (large eddy sizes) contain most of the turbulent energy and are known as energy-containing eddies. These interact

with the mean flow through the action of the shear stresses and receive mean flow energy. This energy, converted to turbulence, is transferred through the spectrum to the high frequency end (large eddies are broken down into smaller ones) and there dissipated into heat through the rapid viscous decay of the smaller eddies.

3). The double velocity correlation tensor. ($Q_{ij}(x,x+r)$)
The elements of this symmetrical tensor are the mean (time averaged) products of various velocity components measured at the same or neighbouring points.

$$Q_{ij}(x,x+r) = \lim_{T \to \infty} \frac{1}{T} \int_0^T u_i(x)u_j(x+r)\, dt$$

$$\text{or} \quad Q_{ij}(x,x+r) = \overline{u_i(x)u_j(x+r)}$$

where r is the distance between the two points with respective velocities u_i and u_j. When the points are coincident, i.e. r = 0, the diagonal elements are the turbulent energy components u'^2, v'^2, and w'^2, while the remaining elements are the Reynolds shear stresses.

A correlation coefficient defined by

$$R_{ij}(x,x+r) = \frac{\overline{u_i(x)u_j(x+r)}}{u'_i(x)u'_j(x)}$$

is most commonly used.

For isotropic homogeneous turbulence;

a longitudinal correlation coefficient

$$f(r) = \frac{\overline{u_i(x)u_i(x+r)}}{u'^2}$$

and a lateral correlation coefficient

$$g(r) = \frac{\overline{u_j(x)u_j(x+r)}}{u'^2}$$

are defined. It can be shown from the Schwarzian inequality (Batchelor [1971]) that both f(r) and g(r) are always less than or equal to unity. Because of the homogeniety of the flow field, the correlation must be a symmetrical function of r. The maximum value (unity) occurs at r=0, and decreases with increasing r. Only in the neighbourhood of r=0 is it possible to say anything about the shape of the correlation function because the shape will depend on the character of the turbulence.

The measure of the curvature at the origin of the correlation curve was defined by Taylor [1935] with a length λ defined by

$$f(r) = 1 - \frac{r^2}{\lambda^2}$$

$$\text{or} \quad \frac{1}{\lambda^2} = -\frac{1}{2}\left[\frac{\partial^2 f}{\partial r^2}\right]_{r=0}$$

$$\text{or} \quad \frac{1}{\lambda^2} = \frac{1}{2u'^2_i}\overline{\left[\frac{\partial u_i}{\partial r}\right]^2_{r=0.}}$$

Since the local change in u_i is caused by the smallest eddies present in the turbulent flow field, then λ may also be considered a measure of the average dimension of the smallest eddies.

λ is the microscale of turbulence or the dissipation scale. It is a measure of the dimension of eddies which are responsible for the dissipation of kinetic energy of the flow field into heat by the effect of molecular viscosity determined by the value of

$$\overline{\left[\frac{\partial u_i}{\partial r}\right]^2_{r=0.}}$$

A length "L" which is a measure of the longest correlation distance between velocities at two points of the flow field, or velocities at the same point separated by a time interval, is called the macro or integral scale of turbulence. This is defined by

$$L = \int_0^{\infty} f(r)\, dr$$

$$\text{or} \quad L = \int_0^{\infty} R(t)\, dt$$

where R(t) is the Eulerian correlation coefficient defined by

$$R(t) = \frac{\overline{u_1(t')u_1(t'-t)}}{u'^2_1}$$

where the average is taken with respect to time t'. The relationship justifying the determination of spatial integrals from time integrals is from Taylor's hypothesis (Taylor's "frozen flow field hypothesis"), which assumes that the turbulent eddies are advected (mean energy transportation) past the point of observation by a mean flow so fast that they do not have time to change substantially during their time of passage and so can be represented by the equation

$$\frac{\partial}{\partial t} = -\bar{U}\frac{\partial}{\partial r} .$$

Hinze [1959], showed also that $f(r) = R(t)$.

Longitudinal and lateral macroscales of turbulence Lx and Ly are defined from the longitudinal and lateral correlation coefficients respectively. The longitudinal macroscale of turbulence is in the direction of the general fluid flow and as determined by Baines and Peterson [1951], is twice the magnitude of the lateral macroscale of turbulence. These macroscales are also a measure of the average size of the energy containing eddies.

The correlation tensors that have been considered in the preceeding sections are of the second order type. A first order correlation tensor correlates a scalar (such as

pressure) at a point A to the fluctuating velocity component at a point B. A second order correlation tensor, as in this case, correlates fluctuating velocities at points A and B. A third order tensor would therefore correlate fluctuating velocities at points A, B, and C.

CHAPTER 3. FLOW AROUND A SPHERE.

The flow around a sphere has been analysed and observed by many researchers since the time of Prandtl [1904], when he introduced his theory of boundary layers. This theory bridged the gap between the theoretical science of classical hydrodynamics of an inviscid fluid and the empirical practical subject of hydraulics. Boundary layers are the region close to a body between the moving fluid and the stationary body. The flow in this region is retarded by the friction at the surface, to which it gives up some of its momentum to balance the frictional drag of the body. It is only in this region therefore (restricted to the viscous sub-layer for a turbulent boundary layer) that the viscosity effects of the fluid are considered. These result in viscous stresses which are proportional to the velocity gradient, with the constant of proportionality being the coefficient of viscosity of the fluid.

3.1. Steady incompressible flow.

Two types of boundary layers are found to exist around a sphere: namely, laminar and turbulent boundary layers. For a sphere immersed in a sufficiently fast steady incompressible flow, the flow around a sphere may be divided into the following regions:-

1). Front stagnation point.

2). Laminar boundary layer.

3). Transition region.

4). Turbulent boundary layer.

5). Separated region (wake).

1). Stagnation point.

At the front of the sphere i.e. $\theta = 0^{o}$, the fluid is brought to rest. This position of zero velocity is known as the forward stagnation point. Here all the kinetic energy of the fluid is converted into pressure, and the sphere experiences its greatest pressure.

2). Laminar boundary layer.

Downstream of the stagnation point, a favourable (negative) pressure gradient results in an increase in the velocity of the fluid nearest to the sphere. The thickness of the laminar boundary layer increases from this point with increase in the distance x. The growth of the laminar boundary layer is proportional to $Re_x^{-1/2}$, where Re_x is the Reynolds number based on the circumferential distance x from the forward stagnation point.

In the laminar boundary layer, the flow is smooth and proceeds in streamlines roughly parallel to the surface. The equations of continuity and motion, for the steady flow of an incompressible fluid are valid here. These form a series of equations, generally termed "boundary layer equations". Because of the numerical difficulties involved in obtaining exact solutions of these equations for the general case, approximate methods have been developed for

predicting the overall characteristics of the boundary layer, rather than specific details of the boundary layer flow. These overall characteristics predicted include: the momentum thickness, the displacement thickness, and the skin friction. The earliest developed approximate methods include the Pohlhausen's method [1921], Young's method [1940], Holstein and Bohlen's method [1940], and Thwaites' method [1949]. These methods are all based on the momentum integral equation, from which the approximations are made in the assumptions adopted to solve them. The momentum integral equation was originally derived by von Karman [1912] by balancing the momentum transport to an element and the wall shear force acting on the element. The limitations of these approximate methods is generally that the pressure gradient should be less than or equal to zero, after which modifications to the methods are necessary.

An adverse (positive) pressure gradient has the effect on a laminar boundary layer of causing either separation of the boundary layer or transition to a turbulent boundary layer to occur.

a). Separation.

This is when the laminar boundary layer leaves the surface of the body, and reverse flow occurs beyond this point on the body. The zero velocity line is then detached from the body allowing circulation of flow to occur in the region beyond the point of separation. This region is known as

the wake.

For the flow around a sphere this separation occurs at an angle of around 80^{o} from the front stagnation point. Separation of this type occurs at low Reynolds numbers of typical value less than 2.3×10^{5} (Schlichting [1968]) for zero turbulence of the free-stream fluid flow. This Reynolds number is based on the sphere diameter.

Calculations by Boltze [1908] showed that separation actually begins at the rear stagnation point after the equivalent of a sphere starting impulsively from rest has moved through a distance equal to about two-fifths of its radius. This line of separation then moves towards the front of the sphere. The line of separation forms a circle at a fixed angle from the forward stagnation point. The idea by Boltze that separation begins at a point can be developed to encompass the results of Achenbach [1974] who observed that vortex shedding from a sphere occurred at a point which rotated around the sphere. The idea therefore that the point of separation originates at the rear stagnation point and travels along the line of separation shedding vortices as it progresses seems feasible. The angle from the front stagnation point at which the line of separation finally settles is dependent on the prevailing flow conditions around the sphere.

Associated with boundary layer separation is the aforementioned phenomenon of vortex (eddy) formation. These vortices are generally unstable, so they detach and move downstream from the body, while new ones are formed in their place. The wake that is formed downstream of the body therefore includes large scale vortices, the size of which is dependent on the position of the boundary-layer separation, and corresponds to the width of the wake. The energy that is carried downstream and ultimately dissipated in such vortices is large and proportional to their size. This wastage of energy in the cast-off (shed) vortices, results in a large drag of the sphere which is manifest in the pressure distribution on the sphere and is termed the pressure drag.

The cast-off vortices move alternately clockwise and anti-clockwise in a regular pattern. This is known as the Karman vortex street (von Karman [1911]) and moves with a velocity smaller than the fluid in which the sphere is immersed. Different values for the ratio of these velocities have been found including: 0.88 to 0.89 by Bearman [1967] and 0.77 by Fage and Johansen [1927]. The dimensionless frequency for the measure of the rate at which vortices are shed from the sphere is the Strouhal number (Strouhal [1878]) given by:

$$\frac{nd}{U} = S$$

where S = Strouhal number

n = shedding frequency

d = sphere diameter

and U = free-stream velocity.

Roshko [1954] working on circular cylinders showed that there existed a unique relationship between the Strouhal number and the Reynolds number. Other researchers also determined this unique relationship for spheres and found a Strouhal number of around 0.2. These include: Mujumdar and Douglas [1970], 0.2; Achenbach [1974], 0.19; and Pao et.al. [1977], 0.14 to 0.22. Bearman [1967] put forward a relationship between the product of the Strouhal number and the total drag coefficient (S x Cd), and a function of the base pressure coefficient $(1 - Cp_b)^{0.5}$ (this relationship was used by Pao et.al. in their determination of the Strouhal number for a sphere). From this relationship, the Strouhal number for an object can be verified with the knowledge of Cd and Cp_b.

A non-dimensional constant called the frequency ratio can be defined here. This is the ratio of the frequency of the approaching free-stream vortices to the frequency of the shed vortices. Van der Hegge Zijnen [1958] who was working on circular cylinders observed that for particular frequency ratios Nusselt number values that deviated significantly from the standard values were obtained. This deviation he referred to as a "resonance effect" of the frequency ratio. Hinze [1959] suggested that this effect for circular cylinders occurred at a frequency ratio value of 2.

Two types of drag components contribute to the total drag of the sphere; the pressure drag, and the skin-friction drag. The pressure drag, as previously discussed, has been determined by Achenbach [1972] as contributing not less than 87.5% of the total drag, the rest being due to the skin-friction drag. The skin-friction drag is the resultant of frictional stresses in the boundary layer and is related to the defect of momentum of the fluid in the wake relative to the fluid outside it.

b). Transition.

An adverse pressure gradient and free-stream turbulence may also cause transition from a laminar to a turbulent boundary layer to occur. The occurrence of this transition, as will be seen in the following section, enables separation to be delayed.

3). Transition.

Transition is the process by which a laminar boundary layer transforms into a turbulent boundary layer. With the occurrence of this transition is an accompanying noticeable change in the law of resistance. Because of the turbulent mixing motion introduced, there is now a greater resistance to an adverse pressure gradient, and separation occurs at a much later stage. Associated with transition is also the element of stability of the boundary layer. The laminar boundary layer at low Reynolds numbers is very stable. Increase of the Reynolds number reduces the

stability of the boundary layer until transition occurs when the flow becomes unstable. A comprehensive account of the theory of boundary layer stability is given by Lin [1955].

Initially the process of transition occurs over a region referred to as the "transition region" where the characteristics change from those of laminar to those of turbulent flow. With increase in the Reynolds number, the transition region becomes smaller until the region is sufficiently small relative to the size of the body to be called a point, - the "transition point".

The precise physical nature of the process of transition and its causes are not at present fully understood, although the spot theory of Emmons [1951] is the generally accepted process. This suggests that in naturally developing transition, random spots of turbulence arise while the flow outside the spots is still laminar. As new spots are formed in the transition region, the existing spots grow by contaminating the fluid around them until there are no more laminar gaps left and the flow is turbulent.

The factors that cause transition to occur, on the other hand, are known and generally accepted as:

1). An adverse (positive) pressure gradient

2). Roughness or imperfections of the surface

3). High degree of turbulence in the free-stream

4). A sufficiently high Reynolds number ($Re_x > 2 \times 10^6$).

The study of transition has become of great importance because of problems associated with boundary-layer control and stability.

4). Turbulent boundary layer.

The turbulent boundary layer has all the characteristics (including equations) of a turbulent flow field as discussed in chapter 2. Because of the mixing, which is responsible for the increased resistance to the adverse pressure gradient, the turbulent boundary layer is much thicker than the laminar one. The growth of this boundary layer is proportional to $Re_x^{-1/5}$, which gives a higher velocity to the fluid nearest the sphere and thus increased resistance.

Because of this increased resistance, separation of a turbulent boundary layer takes place at a much later stage than with a laminar boundary layer. A typical separation angle for this boundary layer would be 120^o, this being dependent on the Reynolds number and the degree of disturbance in the free-stream. As a result of this delay in the position of separation, a narrower wake is formed behind the sphere and smaller vortices are shed from it. These smaller vortices dissipate less energy and a significant drop in the drag of the sphere is therefore observed. This phenomenon was first demonstrated by Eiffel [1912] who experimented with spheres of three different

diameters for the same velocity and obtained three corresponding drag values. Prandtl [1914] gave an explanation for this phenomenon by inducing artificial turbulence in the boundary layer using a trip wire and obtained varying drag values depending on the degree of disturbance introduced by the trip wires of varying sizes.

This ability of turbulent boundary layers to give a lower drag on bluff objects, or a fuller energy recovery, is what makes them very attractive to the engineer who is very much concerned with reducing the drag on objects and obtaining the fullest energy recovery possible.

3.2. Unsteady incompressible flow.

An unsteady free-stream (turbulent) flow has the effect of introducing fluctuating components which affect the stability of the boundary layer. Experimental work by Schubauer and Skramstad [1947] showed that the theory of stability of the boundary layer for small disturbances provided a useful guide as to the importance of external disturbances on the transition to turbulent flow. Lin [1957], put forward a theory which shows the effect of the fluctuating components, by considering a free-stream flow with a periodic oscillation superimposed. He obtained a relationship between the free-stream oscillations and the oscillation of the point of laminar separation. From this, it can therefore be implied that a turbulent flow field imposes instabilities in the boundary layers which affect

the transition point, the degree by which it is affected being proportional to the degree of disturbance in the flow field.

The resulting effect of disturbances in the free-stream affecting the transition point, is its variation of the drag and of the heat transfer from a body. It is for these principal reasons that a lot of work has gone into determining the importance of free-stream turbulence on the transition point of the boundary layer (boundary layer control). In chapter 4, the effects of the characteristics of a turbulent field on the transition point (known and expected) are fully discussed.

3.3. Effect of support on boundary layers.

In conducting experiments to observe various effects of objects, the support of these objects in test sections is very important. In the case of spheres, experiments are conducted using either free or fixed spheres. Although free spheres have the advantage of not having complications with supports, unknown factors on the effects being observed in the form of extra degrees of freedom and limitations on readings that can be observed are introduced. Readings such as pressure distributions are impossible on free spheres because, amongst other reasons, the freedom to rotate will constantly alter the angles at which pressure tapping values are being taken. Generally, free spheres (Torobin and Gauvin [1961]) are only used to determine drag effects.

Fixed spheres have been used in a number of wind tunnel experiments by a number of researchers because of the ease with which various instruments can be attached and readings taken. The problem had initially been the method by which the spheres were held, but during the years it has evolved from the experiments of various researchers that the most effective means of holding the sphere without interference with the flow is by the use of a sting. Sting-held spheres were the most effective because they did not interfere with the boundary layers, although a proviso for the size of the sting was necessary. The sting to sphere diameter ratio is of great importance during experiments, because if this is high, the effect of the sting will be to streamline the sphere thus altering the pressure at the rear of the sphere and ultimately the drag on it. Experiments by Owen [1945] showed that for Mach numbers between 1.2 and 4.4, the sting had no effect on drag if its frontal area was less than one-tenth of that of the sphere. Pope and Harper [1966] recommended a sting to sphere diameter ratio of no more than 1/4 for sting/wake interactions not to occur.

CHAPTER 4. PHYSICAL MODEL.

In this chapter, a physical model of flow approaching the sphere, and the effect of this flow on the boundary layer of the sphere will be discussed. Only the major factors that are deemed important to the problem will be modelled; and from these factors, explanations for the expected changes in the total drag will be suggested in justification of the model.

Characteristics of the turbulent flow field (chapter 2) that are considered important and are represented in the model are; the time averaged velocity (and hence Reynolds number), the macroscale of turbulence, and the turbulence intensity of the flow field. The reason for isolating these characteristics is because of the negligible comparative effects of the other turbulence characteristics.

For the purposes of modelling, the turbulent flow field approaching the sphere, as shown in figure 4.1, is modelled as a series of fixed size vortices propagating with alternate clockwise and anticlockwise direction. Although the simplification of this model may appear extreme, the important details of the flow field whose effects are of consequence are contained. A summary of these would be as follows:-

1). Although the actual flow is three dimensional, the model is considered in two dimensions. This is

because all experimental positions are taken along the centreline of the wind tunnel exit plane, for which the existence of planes of symmetry due to the square and circular shapes of the turbulence generators serve as a means of simplification. For a sphere, therefore, an analysis of the effects due to vortices in a fixed plane can be considered because of the minimal interplanary effect of the flow around it.

2). Vortices are modelled as having a fixed size whereas in practice each vortex bundle consists of numerous different sized vortices. These modelled vortices are such that they represent the macroscales of turbulence which by definition are the size of the energy containing eddies. This definition, implicitly determines that these macroscales will be responsible for any effect due to the scale of turbulence.

3). Vortex shedding is generally considered as occurring on alternating sides of objects. Therefore, for a given plane, the successive vortices at the centreline after the "potential core" of a turbulent flow field, are from alternate sides and have varying clockwise and anticlockwise directions.

4). The vortices represent the longitudinal macroscale of turbulence, because the comparative effects due to the lateral macroscales of turbulence are negligible. (Batchelor [1971]).

Other equally important characteristics of turbulence, such as the Reynolds shear stress, the spectra and macroscale of turbulence, have not been considered in the model because, as previously stated, their effects on the total drag of a sphere are small compared to those of the characteristics modelled.

Results by Achenbach [1972] (chapter 3) show that the maximum contribution of the skin-friction drag to the total drag is only 12.5% with the major contributor being the pressure drag (maximum 87.5%). It is therefore necessary in building up this physical model to ensure that the characteristics modelled are those that make significant contributions to the pressure drag variations. These are therefore the aforementioned Reynolds number, turbulence intensity and macroscale of turbulence.

1). The Reynolds number.

Increase in the Reynolds number increases the total energy available in the free-stream. This increase in energy results in a delay in separation occurring which alters the wake size and thereby the pressure drag.

2). The turbulence intensity.

Increase in turbulence intensity introduces additional mixing between the free-stream and the boundary layers. This induces transition to turbulent boundary layers to occur which further increases the energy transfer from the high energy, free-stream layers to

the low energy regions close to the surface. The increased energy in the layers closest to the surface increases the resistance to the adverse pressure gradient, thus delaying the occurrence of separation and consequently varying the pressure drag.

3). The macroscale of turbulence.

The macroscale of turbulence is expected to affect the pressure drag in two distinct ways:-

a). When the macroscale of turbulence is comparable to the sphere diameter (i.e. macroscale is equal, just less than, or just greater than the sphere diameter ($1.5 > L_x/d > 0.7$), the vortices will interact with the wake altering the pressure at the rear of the sphere and thus the pressure drag.

b). When the macroscale of turbulence is much larger than the sphere diameter, the flow around the sphere begins to resemble that of normal laminar (or turbulent) flow with a cyclically altering angle of incidence. This introduces a dynamic pressure distribution and a corresponding pressure drag.

The other turbulence characteristics tend to contribute mainly to the variations in the skin-friction drag and can therefore, for the purposes of this model, be neglected.

From the physical model shown in figure 4.1, the resultant effect on the total drag of the approaching vortices can be categorized according to the following flow

characteristics:-

a). Low turbulence intensity and small macroscale of turbulence.

b). Low turbulence intensity and large macroscale of turbulence.

c). High turbulence intensity and small macroscale of turbulence.

d). High turbulence intensity and large macroscale of turbulence.

All these flow characteristics can be further sub-divided to include their differing effects for low and high Reynolds numbers.

The following discussions on the effects of each category of flow characteristics on the total drag of the sphere, will cover the most likely effects and provide an explanation for the reasoning behind such drag variation expectancies.

a). Low turbulence intensity and small macroscale of turbulence.

This type of flow/~~is~~ (a) and (b) are the closest examples to a laminar free-stream flow. It is therefore expected that at the extreme, when the macroscale of turbulence is of the same order of magnitude as the boundary-layer thickness, and the turbulence intensity is below about two percent, then the drag will be dependent only on the Reynolds number. Hancock [1980] who conducted experiments with turbulence

characteristics of this magnitude found that the effects of free-stream turbulence decrease with increasing length scale. Although working on heat transfer from a flat plate, his observations can be applied here to imply that an increase in the scale at this magnitude will result in the effect due to scale being greater than that due to turbulence intensity. His results can be considered qualitatively because of the existence of an analogy between heat transfer and drag. This analogue is discussed in greater detail later in this section.

Technically length scales that are of the same order of magnitude as the boundary-layer thickness are usually regarded as the microscale of turbulence. (Typical size of microscales of turbulence is 1 mm (Cebeci and Smith [1974])). But because, by definition, microscales of turbulence dissipate the turbulence energy that is produced by macroscales of turbulence, the largest length scales in a turbulent field are always the macroscales of turbulence even when this is of the same order of magnitude as the thickness of the boundary layers. The length scales therefore referred to by Hancock [1980] are in effect the macroscales of turbulence.

The drag coefficient values for this category are generally expected to be almost the same as those for a sphere immersed in a laminar fluid flow.

b). Low turbulence intensity and large macroscale of turbulence.

When the scale of turbulence is comparable to the diameter of the sphere, the expected effect on the drag is two-fold. Firstly, for lower scale values, the large vortices interact with the wake modifying the base pressure and thereby the separation point and consequently the drag. Secondly, at larger scale values, the vortices of the turbulent flow field are "seen" by the sphere as an approaching laminar flow with an oscillating angle of incidence.

The effect of the low turbulence intensity on the drag by altering the transition point will, compared to the scale effects, be comparatively small and may thus be assumed negligible. The resulting effects on the drag coefficient by this category are therefore expected to be an initial increase from the standard drag curve at low scale values, and then a return to approximately standard drag curve values at larger scale values.

c). High turbulence intensity and small macroscale of turbulence.

The effects of the turbulence intensity in this category are expected to heavily outweigh those due to the scale of turbulence. At high values of turbulence intensity, the disturbance introduced to the boundary layer causes very early transition to occur. This early occurrence of transition results in a delay of separation, and thereby a

reduction of the drag values obtained.

The effects of this category are expected to be a reduction of the drag coefficient values to below the standard drag curve.

d). High turbulence intensity and large macroscale of turbulence.

Unlike the previous categories where the effect of one turbulence characteristic always outweighed the effect of the other and thereby allowing the effects of one to be ignored, in this category the resultant effects from both characteristics are expected. The general tendency of intensity to reduce drag and that of scale to increase it, gives rise to situations where very slight modifications in the value of one of the characteristics can cause considerable change in the drag values being obtained. Situations can therefore be envisaged here whereby certain combinations of the turbulence characteristic values give unstable drag values which cover a distinct range, for all other values unchanged. This phenomenon has been observed by both Neve [1986] and van der Hegge Zijnen [1958]. Although van der Hegge Zijnen, who was working on the heat transfer from a cylinder, also noticed this phenomenon, an analogy between the heat transfer and drag coefficient indicates the similarities between the two phenomena and therefore the reason why heat transfer observations should also show this similar feature of instability.

The effects of this category are expected to be very marked deviations of drag coefficient values from the standard drag curve, with various combinations of turbulence characteristics giving apparently uncorrelated values.

Superimposed on the effects of the characteristics discussed above is the effect due to the variation in the Reynolds number. The underlying effect of the Reynolds number is generally the same; that is, an increase in Reynolds number raises the energy of the free-stream and therefore causing smaller interactions between layers to transmit an equal amount of energy. The resulting effect of this is that either: when the effect of one of the turbulence characteristics is negligible, increase in Reynolds number may cause its effect to increase to a level where it has to be taken into consideration, although the magnitudes of the characteristics themselves remain unchanged; or an increase in Reynolds number may cause a variation in the effect of the turbulence characteristics giving different drag values for the same combination of characteristics.

From the preceeding discussion, the problem of predicting the drag for a given set of turbulence characteristics is evident. A number of possible methods of solution to this problem exist, some of which are less probable than others. The most promising are the numerical and physical

modelling methods.

1). Numerical modelling.

A numerical model representing the turbulent fluid flow in which the sphere is immersed can show in detail the variation of the drag coefficient of the sphere for varying combinations of turbulence characteristics. Unfortunately, numerical models, such as may be required here, using various computer codes are as yet not possible both because of the limitations in our knowledge of the total effects of turbulence and also because of the inabilities of modern day computers to handle the size of data necessary for such a feat.

To date, computer codes that can predict laminar fluid flow and its effects with great accuracy exist, as do computer codes that can predict laminar and turbulent boundary-layers, although great accuracy is obtained only for the former case. Computer codes representing fully turbulent fluid flows are generally only in their trial periods, this despite the fact that turbulent flows are the most common types of flows in general industrial applications. "Large eddy simulation" computer codes are the closest of the available progressions to a break-through because of their ability to model the production, transmission, and dissipation of energy by the various sized eddies.

Development of computer codes that will reflect the effects of large eddies on boundary layers are (to the author's knowledge) still in the "pre-conception" stages. This is not surprising because the effects of these large eddies on flow around objects are still being ascertained and isolated. With the increase in the knowledge of these effects (to which this project makes a major contribution) the possibility of developing these computer codes will become feasible.

2). Physical modelling.

Since the early days of trying to understand turbulence and its effects, this approach has always led the way with mathematicians and numerical modellers following behind with more detailed and compounding explanations for the observations and analyses made by "physical modellers". By this same token, the physical modelling method merits its attraction in the accumulation of reliable data on the effects that various combinations of turbulence characteristics have on the drag coefficients. Unfortunately, the quantity of data necessary to achieve absolute correlations between various combinations of turbulence characteristics and drag is incalculable. To this end, collective data from different experimenters working with different wind tunnels and turbulence generators is necessary to

enable the full ranges of the various characteristic combinations to be covered, and thus enabling the absolute correlations to be obtained.

Experimenters who have to date attempted similar work as the present project have either worked on objects that have complicated aerodynamic shapes which introduce unnecessary complications to the problem of the effects being analysed, or have concentrated on other effects of which only analogies with the drag coefficient may be drawn and thus making the quantitative value of their results minimal. An example of an experimenter in the first category is Lee [1975/6], who worked on square based prisms, and an example of an experimenter of the second category is van der Hegge Zijnen [1958] who worked on the heat transfer effect from horizontal cylinders. Although the analogy between heat transfer and drag can be evaluated, the difference in aerodynamic shape of the objects being considered does not assist in actually providing data for correlations. These results may therefore only be used as a guide for the correlations being formulated.

To analyse in detail the effects that the macroscale of turbulence has on the total drag of a sphere, it is imperative that the effects of the other turbulence characteristics that have the same magnitude of variation of the total drag as the macroscale are considered. These,

as previously discussed, are the turbulence intensity and the Reynolds number. Because the major contributor to the variation of the total drag is the pressure drag, a means of measuring the variations in the pressure distribution is necessary. For varying combinations of turbulence characteristics, the knowledge of both the total drag and the pressure distribution is therefore necessary. From this information effects of the various characteristics can be identified and isolated, and also a correlation developed of the combined characteristics and the drag variation. A similar analysis of the dynamic variation of the data can also be made.

The aims of this research project, as stated in chapter 1, are:

1). To establish the relationship between the macroscale of turbulence and the total drag of a sphere. Dryden et.al. [1937] used the theoretical relationship suggested by Taylor [1936]

$$Re_{crit} \propto \frac{u'}{\bar{U}} \left[\frac{d}{L}\right]^{1/5}$$

relating the critical Reynolds number to a function of intensity and scale. The results obtained by Dryden et.al., were determined to be in close proximity with this theory suggesting the existence of some complex relationship between the drag and the Reynolds number, intensity, macroscale, and maybe spectra of turbulence. This assumption, made from

this theory, is based on the definition of the critical Reynolds number which is directly linked to the drag of a sphere.

2). To establish whether variations in the drag coefficients have corresponding base pressure coefficient variations. Achenbach [1972] observed that the maximum contribution of skin-friction drag to the total drag was 12.5%. Therefore, as discussed earlier in the chapter, variations in the total drag of the magnitude associated with the turbulence characteristics are expected to have a corresponding variation of the pressure drag, since these characteristics are known to mainly affect the pressure distribution.

3). To establish the dynamic relationship between the drag and base pressure coefficients, and also to ascertain the existence of resonance at given vortex shedding frequencies. Van der Hegge Zijnen [1958] working on the heat transfer from circular cylinders observed resonance effects when a particular frequency ratio existed between the free-stream vortices and the shed vortices. Hinze [1959] suggested that this resonance occurred at a frequency ratio of 2:1.

4). To establish whether the effects of individual vortices passing the sphere can be detected. As suggested by the physical model, the distinct effect

of individual vortices passing the sphere should be detectable. The establishment of this particular aim, would further enhance the use of the model in further mathematical considerations of this general problem.

4.1. Analogy between Nusselt number and drag coefficient.

The need to use the results of experimenters who have worked on similar turbulence characteristic problems but have observed effects other than those of drag coefficient has been discussed earlier. Due to the scarcity of similar results, it is necessary to establish the analogy that exists between the heat transfer and the drag coefficient of an object so as to enable the qualitative use of the available heat transfer results to be made. The main indicator of heat transfer is the Nusselt number, defined by

$$N = \frac{hl}{k}$$

where N is the Nusselt number

h is the heat transfer coefficient

k is the thermal conductivity

and l is a characteristic linear dimension.

This non-dimensional term is a measure of the overall heat transfer from the body. The component of the total drag coefficient for which an analogy with the Nusselt number is usually drawn (Reynolds analogy) is the skin-friction drag coefficient defined by

$$C_f = \frac{\tau_s}{(1/2)\rho V^2}$$

where C_f is the skin-friction coefficient

and τ_s is the wall shear stress.

This skin-friction drag coefficient is a measure of the drag force exerted on the body by the friction.

The heat transfer coefficient and the wall shear stress can be expanded to show more clearly the analogy which exists between the thermal and the velocity boundary layers.

1). The wall shear stress by definition is proportional to the velocity gradient, the coefficient of proportionality being the viscosity μ.

$$\tau_s = \mu \left(\partial u / \partial y\right)_s$$

This equation determines the velocity gradient in the velocity boundary layer.

2). The heat transfer coefficient which is proportional to the actual heat transfer between the wall and the free-stream is implicitly included in the equation

$$q_s = -k \left(\partial T / \partial n\right)_s .$$

This equation determines the temperature gradient in the thermal boundary layer.

From the above, the analogy between heat transfer and drag can therefore be reduced to an analogy between the velocity gradient in the velocity boundary layer, and the

temperature gradient in the thermal boundary layer.

The skin-friction drag has earlier been discussed as contributing only a maximum of 12.5% to the total drag, and that the turbulence characteristics included in the model affect mainly the pressure drag component of the total drag. Therefore a more meaningful analogy would, in this particular case, be one between the Nusselt number and the pressure drag coefficient, which unfortunately, does not give a mathematically meaningful analogy. Confirmation of the need to take an analogy between the Nusselt number and the pressure drag is from experiments by Schmidt and Wenner [1941] who showed that the heat transfer from an object is greater in the wake region where there is greater mixing compared to the regions with velocity boundary layers. These results also indicate that an increase in the Reynolds number causes separation to be delayed thus resulting in a smaller wake and therefore a net reduction in the amount of heat transfer. This is analogous to the pressure drag, in that the narrower the wake the lower is the pressure drag. From this a direct relationship between the pressure drag and the Nusselt number can be assumed because of their direct dependence on the conditions of the wake.

Because of the significant difference in magnitude of the Nusselt number in areas outside the wake as compared to that in it, as observed by Schmidt and Wenner, the contribution to the total heat transferred in the thermal

boundary layers and in the wake can be assumed to be in the same ratio as that of the contributions of the drag components to the total.

Results taken of the Nusselt numbers for aerodynamic objects placed in turbulent flow fields may therefore be related analogously to the total drag coefficient variation on the same object. The major contributors to both the Nusselt number and the drag coefficient therefore are those respective components which are dependent on the wake conditions.

CHAPTER 5. EXPERIMENTAL ARRANGEMENT.

5.1. Introduction.

The design of the experimental rig was one which enabled the desired effects of the characteristics of the turbulent flow field to be observed with a minimal introduction of undesired effects from external complicating factors. These factors include blockage effects, effects of reflected vortices (end effects), limitations on the maximum wavelengths attainable by the vortices, nonlinear trajectory of the sphere, translational oscillations of the sphere, acceleration effects, and model mounting effects. To alleviate these effects, an open section wind tunnel with a "rigidly" sting-held sphere was used.

To determine the effects that the characteristics of the turbulent flow field were having on the drag of the sphere, two main approaches were used: namely, a strain-gauged cantilever to measure the force exerted on the sphere which was attached to the sting; and pressure tapping holes on the sphere to determine the pressure distribution for which purpose both the sphere and the sting were hollow. Plate 1 shows the experimental arrangement including the instrumentation used.

5.2. Wind tunnel.

The open section wind tunnel used, as shown in plate 2, consisted of a variable speed 10 bhp motor attached to a

centrifugal impeller which drew air in from the atmosphere to the settling chamber. Eight sets of honeycombs were placed in the chamber to help improve the mean flow uniformity and to reduce the large vortices and instabilities induced by the impeller. Beyond the settling chamber, the shape of the wind tunnel was made into a nozzle so as to increase the velocity of the air in the jet produced while reducing the pressure to atmospheric at the exit. This nozzle had a contraction ratio of 8:1, with dimensions in the exit plane of the nozzle of 240 x 405 mm. Air speeds of up to 47 m/s and turbulence intensities no greater than 0.7 % were experienced in this exit plane.

5.3. Turbulence generation grids.

To generate turbulent flow fields, three grids shown in plate 3 were used. Labelled grids A, B and C, these three placed individually at the exit of the wind tunnel generated turbulent flow fields of varying turbulence characteristics, thus increasing the range of the turbulence characteristics whose effects were to be observed.

The holes in the grids were square, circular and square respectively. The turbulent flow fields generated by grid B, with the circular holes, were approximated to an equivalent grid of square holes using the method devised by Baines and Peterson [1951]. Therefore for the purpose of dimensioning, the dimensions of the square holed

equivalent to grid B were used.

The horizontal and vertical solid pieces of the grids of width b are the slats, while the mesh of the grid, M, is the distance between centrelines of two parallel slats. These dimensions for the respective grids were:- grid A, b = 25 mm, and M = 90 mm; grid B, 6 and 20 mm; and grid C, 2 and 14 mm respectively.

5.4. Spheres.

High quality table tennis balls of diameter 37.68 mm were used as the spherical objects. Their surfaces were tested for smoothness with a Talysurf and found to have an equivalent sand roughness k/d of less than 11×10^{-5}, thus qualifying as hydraulically smooth.

The spheres were hollow with pressure tapping holes of 0.5 mm diameter drilled in them enabling the pressure at the tapping point to be transmitted via the hollow sting to the micromanometer. A number of identical spheres were used each with the pressure tapping hole(s) at varying angles from the front stagnation point of 0^{o}, 30^{o}, 45^{o}, 60^{o}, 90^{o}, 100^{o}, 110^{o}, 125^{o}, 140^{o}, and 155^{o} respectively.

Spheres used for the static testing each had four holes drilled at 90^{o} to each other but at the same angle from the front stagnation point. This enabled the average pressure at any particular angle from the front stagnation point to be observed. Spheres used for the dynamic testing, on the other hand, had only a single hole each

thus enabling the dynamic pressure variation at a particular point of known angle and orientation to be determined.

Each sphere as shown in plate 4 could be screwed onto a hollow sting of outside diameter 6 mm. This dimension, giving a sting to sphere diameter ratio of less than 1/6, was considered slender enough for the sting not to cause any problems with sting/wake interactions, and was within the sting size limitations of Owen [1945] and of Pope and Harper [1966] discussed in section 3.3.

5.5. Traversing mechanism.

The traversing mechanism was the basic means by which the spheres were held, traversed, and the drag on the sphere measured. Appendix A gives a detailed analysis of the method by which the drag was measured using a basic force balance method and strain-gauges on a cantilever arm.

The test section extended to over 2000 mm from the exit plane of the wind tunnel and had, perpendicular to the exit plane, two tracks on which the traversing mechanism could be moved. This mechanism, shown in plate 5, was very stable and massive so as to avoid the introduction of any undesired vibrations during testing. Movement of the sting-held sphere was possible in the x direction (see figure 5.1 for cartesian directions), by movement of the mechanism along the tracks, and in the y and z directions, by movement of the attachment to which the sting was

connected. Movement in the x direction was necessary so as to expose the sphere to varying parts of the field which had increasing macroscales of turbulence the further away from the exit plane they were, whilst the y and z adjustments were principally used to position the sphere along the centreline of the jet.

Shown in figure 5.1 is also the detailed attachment of the sting to the traversing mechanism. Two aspects of this attachment are of importance:

1). The threaded portion labelled could be loosened, enabling the sting to be rotated to all four 90^{o} cardinal positions in the y-z plane. This feature was of particular importance in the dynamic testing where the spheres had only one hole each and varying orientations were necessary.

2). The vertical part of the attachment which formed a cantilever had a reduced size portion which was strain-gauged. This could measure, by further calibration, the force exerted onto the attached sting.

To prevent the strain-gauges from being strained by other forces apart from those transmitted by the sting, a vertical wedge-shaped guard was attached upstream of these strain-gauges. On this guard was attached at respective distances of 3 and 4 sphere radii above the centreline, a pitot-static tube and a hot-wire probe. These distances

and positions were judged to be a fair compromise between the probes not interfering with the fluid flow around the sphere, and the probes not being influenced by the sphere's localised effects.

5.6. Probes.

5.6.1. Pitot-static tube.

For measuring the velocity of the air in which the sphere was immersed, the standard pitot-static tube connected to a micromanometer was used. The pitot-static tube was positioned three sphere radii above the centreline so as to ensure that it was measuring as closely as possible, and without causing interference to the flow around the sphere, the time average velocity of the fluid. The micromanometer to which the pitot-static tube was connected had a maximum capability of only 19.99 mmH_2O, so beyond this head value readings for the calculation of the average velocity were taken from the CTA anemometer which was connected to the hot-wire probe.

5.6.2. Hot-wire probe.

In figure 5.2 a schematic view of the essential parts of the probe are shown. The important component is the platinum-plated tungsten wire of diameter 5 microns and length 1 mm. It is this wire whose resistance is measured to determine the fluctuating conditions of the flow field. The small diameter and material used are to enable the rapid fluctuations of the flow field to be matched as

closely as possible by the rapid change in the resistance of the wire.

This probe was used to determine the turbulence intensity and the average velocity of the flow field around the sphere, and also to determine the macroscales of turbulence at various positions away from the grid. Its position of four sphere radii above the centreline was considered satisfactory to ensure that the turbulence characteristics it was measuring, were not being influenced by the localised effects of the fluid flow around the sphere.

A wire type probe was chosen instead of a film type probe because of its greater accuracy in monitoring rapid fluctuations of the air around it. The film type probe, because of its relatively robust make and slow response time, is more generally used in mediums that would break the very thin and delicate wire probe and with slow fluctuations of the turbulence characteristics being measured.

This probe was connected to a CTA anemometer from which the turbulence intensities and the average velocities were calculated from the readings.

5.7. Instrumentation.

5.7.1. Micromanometers.

Standard digital micromanometers were used. These had a measuring range of 0.000 to 1.999 mmH_2O on the first range setting and 0.00 to 19.99 mmH_2O on the second.

5.7.2. Anemometry.

In the measurement of the turbulence intensity and the average velocity, the standard DISA anemometer used was connected to the hot-wire probe. The circuitry used was of the constant-temperature anemometer (CTA) type. This was chosen in preference to the constant-current anemometer (CCA) circuitry because of its suitability for measuring high frequency velocity fluctuations as opposed to the CCA circuit suitable for measuring low frequency temperature fluctuations.

In the CTA circuit, the hot-wire probe is maintained at a constant resistance, and thus a constant temperature. A change in the flow acting on the probe affects its temperature by causing it to get cooler or hotter resulting in a change of its resistance. This resistance change causes a variation in the current required to maintain the temperature, giving an error voltage across the bridge. Because the error voltage is dependent upon the instantaneous velocity of the air around the probe, a calibration would determine the actual value of the instantaneous velocity. In the CCA circuit, on the other

hand, the probe is maintained at a constant current and it is the resistance imbalance in the bridge that causes the error voltage.

Plate 6 shows the components of the CTA circuitry used. These were the 55M10 standard bridge, 55D10 linearizer, 55D31 digital voltmeter and the 55D35 r.m.s. unit. Because of the tendency for the linearizer to be most effective for only a small voltage range per setting, this range was set in this particular case to occur from the position where the micromanometer connected to the pitot-static tube exceeded 19.99 mmH_2O. In this way, when the pitot-static tube could no longer be used to measure the velocity, because of the range limitations of the micromanometer, the hot-wire probe and CTA circuitry could be used instead with the same accuracy.

5.7.3. Band pass filter.

To determine the macroscales of turbulence for the generated turbulent fields, a Brüel and Kjaer tunable band pass filter (type 1621) was inserted into the CTA circuit. Positioned between the linearizer and the r.m.s. unit, the frequency variations on the filter enabled the energy distribution of the vortices per frequency band width to be determined from the r.m.s. unit readings. From these readings the macroscales of turbulence were determined.

5.7.4. Wheatstone bridge.

For the determination of the drag on the sphere, a strain-gauged cantilever arm as discussed earlier was used. These strain-gauges formed one arm of a Wheatstone bridge network from which the out-of-balance (error) voltage was time-averaged to give a value which when calibrated gave the drag on the sphere. A Solartron true time averager was connected to the bridge to give a digital display of these readings, thus avoiding any reading errors and increasing the speed at which the readings could be taken.

5.7.5. Data logger.

For the dynamic testing, readings of all the instruments needed to be taken simultaneously, to which end the data logger was used. Capable of scanning at up to 500 channels/second, and with a memory of up to 1000 digits, the readings from the 5 channels scanned were digitized for analysis using various computer based methods.

The data logger was programmed to compute the readings taken to give four sets of data: namely drag coefficient, pressure coefficient, turbulence intensity, and the Reynolds number, in which form the digitizing took place. Twenty such scans of the channels performed continuously constituted an individual run of the test rig.

5.7.6. Computer terminal.

This terminal was connected to the Gould super-mini computer system and was capable of reading data from an

RS232 port at a rate of 1.2 kilobauds. It is via this terminal located at the experimental site that the digitized data was input into the computer.

CHAPTER 6. EXPERIMENTAL PROCEDURE.

6.1. Calibration of instruments.

The calibration of the instrumentation used was carried out very rigorously so as to avoid an introduction of unidentified errors into the results. Three of the instruments used required calibration: namely the linearizer, the Wheatstone bridge, and the digital voltmeter.

6.1.1. Linearizer.

The linearizer was introduced into the CTA circuit to compensate for the distortion produced by the non-linearity of the hot-wire probe calibration. This distortion was given by the DISA instruction manual as:

a). Non-linearized anemometer.

$$\frac{\sqrt{\overline{u^2}}}{\overline{U}} = \frac{2}{n(1 - (V_o/V)^2)} \times \frac{\sqrt{\overline{v^2}}}{\overline{V}}$$

b). Linearized anemometer.

$$\frac{\sqrt{\overline{u^2}}}{\overline{U}} = C \frac{\sqrt{\overline{v^2}}}{\overline{V}}$$

where $\overline{U}$ = mean flow velocity.

u = flow velocity fluctuation.

$\overline{V}$ = mean value of anemometer output voltage.

v = fluctuation of anemometer output voltage.

V_o = anemometer output voltage at zero velocity.

n = constant found empirically.

C = constant.

The calibration of the linearizer was based on the relation between the flow velocity U and the anemometer output voltage V_{CTA} expressed by the equation

$$V_{CTA}^2 = A + BU^n = A + BU^{1/m}$$

where A and B are constants whose values depended on the probe. This equation is referred to as King's law, from which the transfer function of the linearizer is obtained.

$$V_{LIN} = K(V_{CTA}^2 - A)^m$$

where K is a constant dependent on the conditions of measurement.

This function is such that a substitution between the two previous equations gives a resultant equation of $V_{LIN} = kU$. This shows that the linearizer output voltage V_{LIN} is proportional to the mean flow velocity U.

Obtaining the exponent m, which was a required setting of the linearizer, was done by plotting the logarithmic curve of $(V_{CTA}/V)^2 - 1$ vs U, the slope being the inverse of m. An alternative method of plotting V^2 against $\sqrt{U}$ can also be used. From the graph the value of m was found to be 2.05. A trial and error method was used as a check from which a similar value was also obtained. With the other settings of the linearizer set accordingly, the linearizer was duly

calibrated.

6.1.2. Wheatstone bridge.

Calibration of the Wheatstone bridge was conducted by hanging known masses at the position where the sphere was attached to the sting. For various known masses, the strains on the strain-gauges as indicated by the Wheatstone bridge meter readings were noted and the forces causing the strains on the strain-gauges could be determined by taking moments. Appendix C gives the method and calculations by which these forces were determined.

The slope from a graph of the determined forces against the Wheatstone bridge meter readings, gave the calibration factor of the strain-gauged cantilever as 2.206 N/volt. By the use of this calibration factor the forces exerted on the sphere could be directly calculated. It was therefore for this reason that the wedge-shaped metal guard was placed upstream of the strain-gauges, to ensure that only forces exerted on the sphere produced strains in the strain-gauges as was the case during calibration.

6.2. Determination of the turbulent flow field characteristics.

The effects due to the u components of the fluctuating velocites were considered to be of a greater magnitude than those of the v and w components (chapter 2), so only a single hot-wire probe was used connected to the CTA circuit to measure the u components. Before experimental

testing was started, it was required that the turbulence characteristics in the testing region be determined both in the presence and in the absence of the grids. In the absence of the grids relative turbulence intensities in the exit plane of the wind tunnel were determined to be no greater than 0.7%.

For simplicity, the term turbulence intensity will be used from here and onwards to refer to the relative turbulence intensity ((u'/U) x 100) expressed as a percentage.

Along the test section, the variation of the characteristics of the turbulent flow fields generated by each of the three grids also needed to be determined. These characteristics were the longitudinal macroscale of turbulence and the turbulence intensity.

6.2.1. Turbulence intensity.

To obtain the turbulence intensity at a particular position a known distance x from the grids, the ratio of the r.m.s. voltmeter and the voltmeter readings expressed as a percentage were taken. At increasing distances x, the turbulence intensities for each grid were determined. These were plotted against the non-dimensional ratio x/b, where b is the grid slat width, and curves as shown in figure 6.1 were obtained.

The individual curves show distinctly the transitions of the flow into the different regions of the flow field:

a). The "potential core".

The turbulence intensities in this region are independent of the grid dimensions. This is indicated by the curves of all three grids falling onto the same curve. The turbulence intensities decrease at the same rate for all grids as the distance from the grids is increased, because the flow is almost self-preserving during its decay.

b). The mixing region.

Measurements which are taken along the centreline of the exit plane of the wind tunnel suddenly begin to increase. This increase occurs in a manner which distinctly indicates dependence on the grid dimensions. The curve for grid A, which has the largest slat widths, deviates first from the decreasing potential core curve. The curve for grid B, which has the second largest slat widths, deviates next with that for grid C deviating last. The minimum turbulence intensities attained with grid B before commencement of the mixing region are lower than those for grid A, but larger than those for grid C which has the lowest turbulence intensities.

This mixing region introduces high shear stresses and high mixing, which cause the turbulence intensities to increase sharply, as soon as the effect of these shear stress and mixing reaches the centreline.

c). The developing region.

In this region of reducing shear stresses, the development of the flow into a developed, self-preserving, and self-similarity region progressively occurs. The prevailing turbulence intensities then seem to approach a steady constant turbulent intensity value with increasing distance from the exit plane.

6.2.2. Longitudinal macroscale of turbulence.

Determining the longitudinal macroscale of turbulence was done using a power spectral density (PSD) technique. Two versions of this technique were available:

1). Plotting the spectral density against the frequency, (the spectral density being the energy in a waveband divided by the bandwidth), the curve obtained extrapolated to zero frequency would give a parameter proportional to the longitudinal macroscale of turbulence.

2). Plotting the product of the spectral density and the frequency against the frequency. The curve obtained would be a quasi-Gaussian curve, and the frequency at which the peak occurred would be inversly proportional to the longitudinal macroscale of turbulence.

E.S.D.U. Data Sheet 74031 (superseded by Data Sheet 85020) gives a detailed analysis of the equations governing these curves and the parameters of proportionality for each method. The second of the two

techniques was used here, for which the relationship between the frequency and the macroscale at the position where the peak occurred was:

$$Lx = 0.146\bar{U}/\hat{n}$$

where Lx is the macroscale of turbulence

$\bar{U}$ is the average velocity

and $\hat{n}$ is the frequency at which the peak occurs.

An alternative method for determining the macroscale using the knowledge of energy at high and low frequencies has been developed during this project to assist in determing the position of the peak when distinct peaks on the Gaussian curves are not available. Detailed in appendix B, this method can give the frequency of the peak at which the peak should occur with an accuracy of $\pm$ 40%.

The spectral density was determined by the voltage r.m.s. value for a specific setting of frequency on the band pass filter. The filter was inserted into the circuit between the CTA Wheatstone bridge and the linearizer. With this, the effects due to the fluctuating velocity components could be filtered so as to allow only fluctuations of a preset frequency band.

For the three grids, the macroscales were obtained for the various distances x away from the grids. The curves obtained for the non-dimensional ratios Lx/b vs. x/b are shown in figure 6.2. Here again the characteristics of the three regions previously discussed in section 6.2.1

are evident.

a). The potential core.

An increase in scale independent of the grid dimensions is observed, because the flow is almost self-preserving in its decay.

b). The mixing region.

Rapid increases in the scale occur, as the curves deviate from the "potential core" curve at positions dependent on grid dimensions.

c). The developing region.

An increase of scale independent of grid dimensions is approached, as the flow develops into a self-preserving, self-similar region.

6.3. Static testing.

For the static testing, the spheres with four pressure tapping holes each were used. For each of the predetermined distances x, the following sequence was followed:-

The speed setting knob, which was attached to a rheostat in the variable speed motor circuitry and had marked divisions on it of 0 to 10 in steps of 0.1 was progressively increased. With successive speed settings in steps of 0.5 of the rheostat, the velocity of the fluid flow was increased. For each setting the following readings were taken; the two micromanometer readings, the voltmeter and the r.m.s.

voltmeter readings, and the Solartron true time averager reading. The integrating settings on these instruments were; slow for the micromanometers, and 3 seconds for the voltmeter and the Solartron true time averager.

This sequence was repeated for all speed settings, at each position x from the grid and for all three grids. These were then repeated for all the spheres which had varying angles from the front stagnation point of the setting of the pressure tapping holes.

6.4. Dynamic testing.

For the dynamic testing, the spheres with single pressure tapping holes were used. In these experiments the data logger was used to take readings from the five instruments as discussed previously. The connections of the data logger to these instruments was via the output ports of each of the instruments. The readings which were digitized were then transmitted via RS232 ports to the Gould super-mini computer terminal. This enabled readings to be taken from all five instruments simultaneously.

For the same sequence as discussed in section 6.3, for each speed setting, the data logger was programmed to take 20 consecutive sets of simultaneous readings of the instruments, at time spans of 10 ms between sets of readings. This was repeated at each speed setting and position for all four orientations of the pressure tapping

hole.

The sequence was repeated for all speed settings, with all four orientations at each position x from the grid and for all three grids. These were again repeated for all the spheres.

The data logger was programmed to compute the data read so as to obtain the following; Reynolds number, turbulence intensity, total drag coefficient, and pressure coefficient. These were the quantities that were transmitted to the computer for further analysis.

To ensure that these dynamic results taken were of the actual variations of the effects on the sphere, a few preliminary calculations were done. These can be classified as follows:-

a). Determining the natural frequency of the traversing mechanism, so that the possibility of resonance occuring between the mechanism and sphere can be eliminated from any unexpected peaking results.

b). Determining the response time of the air in the hollow sphere to pressure changes at the pressure tapping holes to ensure that the response time of the air to pressure changes is less than the sampling time of the data logger.

The first was carried out by recording the signal taken from the vibrations of the mechanism after the sphere

attached to it had been released from an initial displacement. The natural frequency of the mechanism was determined from this as 35HZ (period 28.36 ms). The second was calculated from the Helmholtz resonator which is detailed by Kinsley and Frey [1962]. From this the response time was calculated to be 4.5ms, which is much less than the 10ms sampling time of the data logger. The requirement that the transverse time of the vortex should be between 10ms and 28.36ms for the drag variation effects to be uniquely attributed to an individual vortex passing the sphere can be observed from the following table of traversing times of different sized vortices at varying Reynolds numbers.

Taking the vortex velocity as 0.8 times the free-stream velocity, the traversing times in milliseconds are:

Re	1.5×10^4	2.5×10^4	3.5×10^4	4.2×10^4
Lx (mm)				
167.41	22.4	13.9	9.6	8.0
148.31	19.9	11.9	8.5	-
119.94	16.1	9.6	-	-

6.5. Accuracy.

The accuracy of each of the parameters was dependent on the instruments and method by which they were measured. The total contributions of the errors in the end results are therefore due mainly to the following:-

a). The errors due to measurements using the hot-wire probe are summed up by Cooper and Tuplin [1955], as being between 3% and 15% depending on the free-stream velocity. The graphs of figures 6.1 and 6.2 show the scatter of data that is obtained due to these errors. A maximum error of 15% is evident from the graphs.

The method by which the macroscale of turbulence was determined was found not to give, on occasions, a precise peak in the Gaussian curve. A truncated curve was then obtained from which the peak position had to be estimated. Despite this, the maximum error of the readings taken was still less than 15%.

Cooper and Tuplin [1955] and Bradshaw [1971] give detailed analyses of the factors that contribute to the errors in readings found using hot-wire probes. These include the zero drift, a factor found with the zero temperature adjustment on the linearizer, for which regular adjustment before commencing a series of experiments was found to be necessary.

b). By positioning the two probes (pitot-static tube and hot-wire) at the compromised positions of three and four sphere radii above the centreline (section 5.6) the characteristics of the flow being measured were not actually those in which the sphere was immersed. The errors caused by the probe positionings is very small, as was observed when the vertical variations of the turbulent flow field characteristics were

observed. Laurence [1956], Davies et.al. [1963] and Grant [1958] all conducted similar experiments to observe the characteristics of turbulence in jets. They also found that for small vertical distances (in this case 75.36 mm) above the centreline, the change in characteristics was very small.

The regions in which the potential core disappeared were avoided because it was possible in these regions for the sphere to be in the potential core and the probes to be in the mixing region, thus getting uncorrelated readings between the regions in which the readings are supposed to be taking place.

The major contributing factor to the errors in the readings are therefore those of turbulence intensity from the CTA circuit. As these readings were used only to determine the velocity at high velocity ranges where the errors decrease, then the errors in the results of total drag and pressure coefficients are expected to be small and much less than the quoted 15%.

CHAPTER 7. RESULTS.

7.1. Sample of results.

Listed below is a sample of the static and dynamic results as derived from the instruments indicated in chapters 5 and 6. Because of the large quantity of data accumulated, analysis was only made possible with the use of a computer. A microcomputer package was found to be much faster for analysis and to this end a Lotus 1-2-3 spreadsheet on an IBM/compatible computer was used. Data for the spreadsheet was put on floppy disks and from these graphic analyses performed. Appendix C contains the description of the means by which the full results may be accessed from the floppy disks enclosed, and the means of manipulating these results to enable the curves presented in chapter 8 to be obtained is also discussed.

7.1.1. Static results.

Angle (deg.)	Slat width (mm)	Mesh (mm)	Scale ratio	Intensity (%)	Reynolds number	Drag Coefficient	Pressure coefficient
155.0	25.0	90.0	0.663	25.0	6.16E+03	0.618	-0.297
155.0	25.0	90.0	0.663	23.4	1.19E+04	0.789	-0.237
155.0	25.0	90.0	0.663	21.6	1.69E+04	0.835	-0.179
155.0	25.0	90.0	0.663	20.0	2.20E+04	0.755	-0.131
155.0	25.0	90.0	0.663	19.7	2.77E+04	0.805	-0.092
155.0	25.0	90.0	0.663	19.7	3.37E+04	0.823	-0.056
155.0	25.0	90.0	0.663	18.1	3.93E+04	0.789	-0.029
155.0	25.0	90.0	0.663	18.0	4.49E+04	0.696	-0.008
155.0	25.0	90.0	0.663	17.6	5.12E+04	0.677	0.007
155.0	25.0	90.0	0.663	17.0	5.70E+04	0.634	0.017
155.0	25.0	90.0	0.663	16.4	6.13E+04	0.648	0.022
155.0	25.0	90.0	0.663	16.2	6.66E+04	0.596	0.030
155.0	25.0	90.0	0.663	16.1	7.18E+04	0.576	0.034
140.0	6.0	20.0	1.593	20.8	5.36E+03	0.163	-0.250
140.0	6.0	20.0	1.593	20.3	9.92E+03	0.095	-0.385

140.0	6.0	20.0	1.593	20.0	1.40E+04	0.289	-0.405
140.0	6.0	20.0	1.593	19.8	1.79E+04	0.422	-0.427
140.0	6.0	20.0	1.593	20.3	2.19E+04	0.547	-0.442
140.0	6.0	20.0	1.593	21.8	2.55E+04	0.628	-0.450
140.0	6.0	20.0	1.593	21.7	2.96E+04	0.647	-0.448
140.0	6.0	20.0	1.593	19.4	3.44E+04	0.632	-0.429
140.0	6.0	20.0	1.593	17.0	3.86E+04	0.617	-0.418
140.0	6.0	20.0	1.593	15.7	4.35E+04	0.573	-0.406
140.0	6.0	20.0	1.593	15.8	4.60E+04	0.658	-0.428
140.0	6.0	20.0	1.593	15.2	4.95E+04	0.650	-0.435
140.0	6.0	20.0	1.593	14.1	5.35E+04	0.649	-0.428
140.0	6.0	20.0	1.593	14.3	5.63E+04	0.639	-0.423
140.0	6.0	20.0	1.593	14.4	5.93E+04	0.627	-0.416
125.0	25.0	90.0	2.003	12.5	6.94E+03	0.194	-0.319
125.0	25.0	90.0	2.003	16.1	1.28E+04	0.457	-0.381
125.0	25.0	90.0	2.003	16.6	1.90E+04	0.534	-0.410
125.0	25.0	90.0	2.003	15.9	2.45E+04	0.552	-0.410
125.0	25.0	90.0	2.003	16.4	3.00E+04	0.582	-0.411
125.0	25.0	90.0	2.003	17.0	3.60E+04	0.577	-0.391
125.0	25.0	90.0	2.003	15.3	4.28E+04	0.576	-0.352
125.0	25.0	90.0	2.003	15.9	4.52E+04	0.586	-0.338
125.0	25.0	90.0	2.003	15.6	5.03E+04	0.563	-0.293
125.0	25.0	90.0	2.003	14.3	5.73E+04	0.563	-0.249
125.0	25.0	90.0	2.003	14.2	6.38E+04	0.524	-0.221
125.0	25.0	90.0	2.003	14.3	7.06E+04	0.514	-0.202
110.0	2.0	14.0	3.183	11.7	9.44E+03	0.105	-0.322
110.0	2.0	14.0	3.183	12.5	1.54E+04	0.353	-0.348
110.0	2.0	14.0	3.183	11.2	2.23E+04	0.567	-0.368
110.0	2.0	14.0	3.183	11.2	2.96E+04	0.696	-0.390
110.0	2.0	14.0	3.183	10.7	3.54E+04	0.788	-0.400
110.0	2.0	14.0	3.183	11.3	4.10E+04	0.837	-0.423
110.0	2.0	14.0	3.183	11.2	4.47E+04	0.830	-0.423
110.0	2.0	14.0	3.183	9.0	4.97E+04	0.859	-0.443
110.0	2.0	14.0	3.183	9.4	5.31E+04	0.910	-0.462
110.0	2.0	14.0	3.183	9.2	5.58E+04	0.978	-0.481
110.0	2.0	14.0	3.183	9.3	5.94E+04	0.927	-0.495
110.0	2.0	14.0	3.183	9.2	6.28E+04	0.896	-0.519
100.0	25.0	90.0	4.145	19.4	6.32E+03	0.352	-0.333
100.0	25.0	90.0	4.145	22.2	1.14E+04	0.540	-0.433
100.0	25.0	90.0	4.145	21.7	1.61E+04	0.864	-0.500
100.0	25.0	90.0	4.145	20.2	2.11E+04	0.939	-0.543
100.0	25.0	90.0	4.145	21.0	2.59E+04	1.057	-0.584
100.0	25.0	90.0	4.145	20.8	3.10E+04	1.240	-0.634
100.0	25.0	90.0	4.145	20.3	3.65E+04	1.270	-0.671
100.0	25.0	90.0	4.145	19.5	4.31E+04	1.184	-0.700
100.0	25.0	90.0	4.145	19.8	4.53E+04	1.229	-0.717
100.0	25.0	90.0	4.145	18.8	4.75E+04	1.246	-0.727
100.0	25.0	90.0	4.145	19.3	4.90E+04	1.212	-0.786
100.0	25.0	90.0	4.145	19.4	5.12E+04	1.175	-0.780
90.0	2.0	14.0	0.095	6.5	9.33E+03	0.215	-0.294
90.0	2.0	14.0	0.095	5.7	1.45E+04	0.357	-0.312
90.0	2.0	14.0	0.095	5.2	1.94E+04	0.433	-0.339
90.0	2.0	14.0	0.095	5.1	2.57E+04	0.476	-0.373
90.0	2.0	14.0	0.095	5.0	2.94E+04	0.476	-0.396
90.0	2.0	14.0	0.095	5.0	3.39E+04	0.468	-0.439

90.0	2.0	14.0	0.095	5.0	3.79E+04	0.481	-0.510
90.0	2.0	14.0	0.095	5.0	4.33E+04	0.469	-0.547
90.0	2.0	14.0	0.095	5.1	4.53E+04	0.468	-0.566
90.0	2.0	14.0	0.095	4.9	5.18E+04	0.449	-0.585
90.0	2.0	14.0	0.095	5.1	5.47E+04	0.444	-0.600
90.0	2.0	14.0	0.095	5.0	5.84E+04	0.433	-0.601
60.0	2.0	14.0	2.653	10.0	9.33E+03	0.108	-0.365
60.0	2.0	14.0	2.653	9.6	1.55E+04	0.449	-0.380
60.0	2.0	14.0	2.653	10.6	2.24E+04	0.712	-0.383
60.0	2.0	14.0	2.653	9.6	2.78E+04	0.879	-0.398
60.0	2.0	14.0	2.653	10.4	3.37E+04	0.925	-0.409
60.0	2.0	14.0	2.653	10.9	3.82E+04	0.883	-0.411
60.0	2.0	14.0	2.653	10.2	4.12E+04	0.950	-0.417
60.0	2.0	14.0	2.653	9.8	4.53E+04	1.017	-0.417
60.0	2.0	14.0	2.653	9.0	5.06E+04	0.920	-0.419
60.0	2.0	14.0	2.653	8.8	5.59E+04	0.951	-0.407
60.0	2.0	14.0	2.653	8.7	6.10E+04	0.849	-0.423
60.0	2.0	14.0	2.653	8.6	6.97E+04	0.783	-0.419
45.0	2.0	14.0	3.183	13.0	1.03E+04	0.264	0.029
45.0	2.0	14.0	3.183	11.8	1.85E+04	0.618	0.015
45.0	2.0	14.0	3.183	12.4	2.44E+04	0.787	0.010
45.0	2.0	14.0	3.183	11.6	3.07E+04	0.843	0.003
45.0	2.0	14.0	3.183	11.7	3.71E+04	0.971	-0.004
45.0	2.0	14.0	3.183	10.9	4.53E+04	1.015	-0.005
45.0	2.0	14.0	3.183	10.3	5.09E+04	0.971	-0.021
45.0	2.0	14.0	3.183	10.6	5.91E+04	0.936	-0.027
45.0	2.0	14.0	3.183	10.2	6.75E+04	0.871	-0.030
45.0	2.0	14.0	3.183	9.2	7.60E+04	0.762	-0.037
45.0	2.0	14.0	3.183	9.4	8.33E+04	0.673	-0.041
45.0	2.0	14.0	3.183	10.0	9.13E+04	0.600	-0.048

7.1.2. Dynamic results.

Orientation	Angle (deg)	Slat width	Mesh	Macro-scale (mm)	Time (ms)	Intensity (%)	Reynolds number	Drag Coefficient	Pressure Coefficient
4	100	2	14	119.9	1	19.7	3.34E+04	0.469	-0.577
4	100	2	14	119.9	2	17.9	3.49E+04	0.658	-0.517
4	100	2	14	119.9	3	17.0	3.51E+04	0.310	-0.501
4	100	2	14	119.9	4	16.6	3.47E+04	1.452	-0.522
4	100	2	14	119.9	5	15.0	3.66E+04	0.085	-0.504
4	100	2	14	119.9	6	16.5	3.63E+04	0.393	-0.469
4	100	2	14	119.9	7	18.6	3.44E+04	2.125	-0.599
4	100	2	14	119.9	8	18.6	3.40E+04	2.112	-0.579
4	100	2	14	119.9	9	16.3	3.50E+04	0.382	-0.479
4	100	2	14	119.9	10	16.2	3.65E+04	0.745	-0.461
4	100	2	14	119.9	11	20.8	3.15E+04	2.785	-0.660
4	100	2	14	119.9	12	18.8	3.47E+04	0.690	-0.567
4	100	2	14	119.9	13	17.4	3.36E+04	1.127	-0.551
4	100	2	14	119.9	14	19.3	3.47E+04	0.235	-0.540
4	100	2	14	119.9	15	19.7	3.42E+04	0.378	-0.556
4	100	2	14	119.9	16	18.5	3.52E+04	1.485	-0.504

4	100	2	14	119.9	17	18.0	3.41E+04	1.687	-0.614
4	100	2	14	119.9	18	20.4	3.24E+04	1.647	-0.621
4	100	2	14	119.9	19	20.9	3.30E+04	0.025	-0.611
4	100	2	14	119.9	20	17.0	3.54E+04	0.717	-0.555
1	110	2	14	119.9	1	13.0	2.12E+04	0.271	-0.342
1	110	2	14	119.9	2	13.6	2.15E+04	0.208	-0.316
1	110	2	14	119.9	3	14.2	2.14E+04	0.142	-0.336
1	110	2	14	119.9	4	10.5	2.22E+04	0.082	-0.284
1	110	2	14	119.9	5	9.7	2.21E+04	0.605	-0.295
1	110	2	14	119.9	6	15.7	2.20E+04	0.942	-0.317
1	110	2	14	119.9	7	20.2	2.15E+04	0.486	-0.336
1	110	2	14	119.9	8	18.3	2.21E+04	1.322	-0.331
1	110	2	14	119.9	9	15.0	2.15E+04	0.379	-0.318
1	110	2	14	119.9	10	16.8	2.21E+04	1.204	-0.303
1	110	2	14	119.9	11	17.1	2.21E+04	0.646	-0.342
1	110	2	14	119.9	12	15.2	2.22E+04	0.572	-0.282
1	110	2	14	119.9	13	15.0	2.12E+04	0.498	-0.362
1	110	2	14	119.9	14	13.3	2.18E+04	0.125	-0.340
1	110	2	14	119.9	15	12.4	2.16E+04	0.453	-0.336
1	110	2	14	119.9	16	23.5	2.15E+04	0.415	-0.364
1	110	2	14	119.9	17	15.1	2.18E+04	0.637	-0.299
1	110	2	14	119.9	18	13.4	2.15E+04	0.180	-0.367
1	110	2	14	119.9	19	21.9	2.13E+04	0.699	-0.396
1	110	2	14	119.9	20	19.6	2.19E+04	0.947	-0.353
1	125	2	14	119.9	1	17.3	3.39E+04	0.440	-0.567
1	125	2	14	119.9	2	17.5	3.45E+04	0.971	-0.568
1	125	2	14	119.9	3	16.4	3.63E+04	0.980	-0.508
1	125	2	14	119.9	4	17.0	3.55E+04	0.040	-0.495
1	125	2	14	119.9	5	18.8	3.35E+04	0.017	-0.592
1	125	2	14	119.9	6	18.0	3.38E+04	1.705	-0.585
1	125	2	14	119.9	7	17.5	3.33E+04	0.568	-0.615
1	125	2	14	119.9	8	18.4	3.42E+04	0.287	-0.575
1	125	2	14	119.9	9	15.5	3.66E+04	0.541	-0.451
1	125	2	14	119.9	10	18.2	3.30E+04	0.508	-0.578
1	125	2	14	119.9	11	15.9	3.58E+04	0.793	-0.485
1	125	2	14	119.9	12	17.5	3.43E+04	1.291	-0.525
1	125	2	14	119.9	13	17.8	3.51E+04	0.320	-0.531
1	125	2	14	119.9	14	17.4	3.41E+04	1.394	-0.544
1	125	2	14	119.9	15	16.7	3.50E+04	0.317	-0.553
1	125	2	14	119.9	16	19.6	3.31E+04	0.982	-0.601
1	125	2	14	119.9	17	18.8	3.52E+04	0.541	-0.536
1	125	2	14	119.9	18	17.4	3.55E+04	0.179	-0.519
1	125	2	14	119.9	19	17.7	3.53E+04	0.665	-0.544
1	125	2	14	119.9	20	17.5	3.56E+04	0.428	-0.526
1	125	2	14	119.9	1	17.1	3.61E+04	0.384	-0.616
1	125	2	14	119.9	2	16.7	3.74E+04	1.111	-0.533
1	125	2	14	119.9	3	14.4	3.93E+04	0.919	-0.540
1	125	2	14	119.9	4	15.9	3.81E+04	0.330	-0.489
1	125	2	14	119.9	5	18.5	3.77E+04	2.179	-0.548
1	125	2	14	119.9	6	18.1	3.74E+04	0.342	-0.553
1	125	2	14	119.9	7	16.2	3.91E+04	1.144	-0.498
1	125	2	14	119.9	8	14.1	3.78E+04	0.421	-0.521
1	125	2	14	119.9	9	15.1	4.01E+04	1.513	-0.424
1	125	2	14	119.9	10	17.2	3.82E+04	0.311	-0.526
1	125	2	14	119.9	11	16.5	3.79E+04	0.972	-0.570

1	125	2	14	119.9	12	18.0	3.82E+04	0.064	-0.502
1	125	2	14	119.9	13	20.8	3.51E+04	0.949	-0.631
1	125	2	14	119.9	14	15.3	3.85E+04	0.262	-0.518
1	125	2	14	119.9	15	15.4	3.80E+04	0.354	-0.529
1	125	2	14	119.9	16	14.7	3.93E+04	1.330	-0.516
1	125	2	14	119.9	17	17.0	3.87E+04	1.532	-0.508
1	125	2	14	119.9	18	17.6	3.75E+04	1.019	-0.582
1	125	2	14	119.9	19	15.9	3.85E+04	0.398	-0.491
1	125	2	14	119.9	20	17.2	3.77E+04	0.930	-0.553
1	125	2	14	119.9	1	17.4	4.51E+04	2.158	-0.531
1	125	2	14	119.9	2	15.3	4.74E+04	1.283	-0.476
1	125	2	14	119.9	3	13.5	4.63E+04	0.492	-0.496
1	125	2	14	119.9	4	16.3	4.59E+04	0.842	-0.509
1	125	2	14	119.9	5	15.2	4.52E+04	0.828	-0.559
1	125	2	14	119.9	6	16.3	4.37E+04	0.379	-0.571
1	125	2	14	119.9	7	18.6	4.39E+04	1.883	-0.605
1	125	2	14	119.9	8	16.6	4.45E+04	0.599	-0.548
1	125	2	14	119.9	9	15.7	4.57E+04	1.327	-0.566
1	125	2	14	119.9	10	15.5	4.53E+04	1.106	-0.529
1	125	2	14	119.9	11	14.7	4.61E+04	0.233	-0.500
1	125	2	14	119.9	12	16.6	4.55E+04	0.634	-0.534
1	125	2	14	119.9	13	17.6	4.44E+04	0.321	-0.596
1	125	2	14	119.9	14	17.5	4.34E+04	0.201	-0.645
1	125	2	14	119.9	15	16.0	4.60E+04	1.320	-0.536
1	125	2	14	119.9	16	14.7	4.59E+04	0.772	-0.505
1	125	2	14	119.9	17	13.4	4.74E+04	0.510	-0.523
1	125	2	14	119.9	18	15.1	4.61E+04	1.698	-0.532
1	125	2	14	119.9	19	18.2	4.36E+04	1.209	-0.615
1	125	2	14	119.9	20	16.4	4.43E+04	0.002	-0.559

CHAPTER 8. DISCUSSION OF RESULTS.

A preliminary analysis of the results obtained can be made by presenting the results in some of the recognizable standard forms from which the effects, if any, of the turbulence characteristics can be observed. A few non-standard forms which effectively portray the relevant information in a clearer manner will also be presented. In this particular case, the recognizable standard curves are the pressure distribution, and the drag coefficient variation with Reynolds number. Non-standard forms include curves of drag coefficient variation with both the scale ratio and the frequency ratio. The scale ratio has been defined as the ratio of the longitudinal macroscale of turbulence to the sphere diameter, and the frequency ratio as the ratio of the frequencies of the free-stream vortices to that of the vortices shed from the sphere.

8.1. Pressure distribution.

A number of results have been published which show the pressure distribution of a sphere immersed in turbulence free flows of varying free-stream Reynolds numbers. Amongst these results are those by Fage [1937], who gave comprehensive details of all the free-stream velocities, Reynolds numbers, and total drag coefficients relating to the pressure distributions that he presented. His results have since been, and continue to be, used as standard references for comparisons with all similar results by

many researchers. Use of these results has been made for comparison with the present results.

The pressure distributions obtained from the present results form a number of different shaped curves for which an attempt to present all of them would be cumbersome and would cover hundreds of pages. A summary of the important pressure distributions resulting from variations in the free-stream turbulence characteristics are therefore presented in figures 8.1 to 8.5. These figures also show for comparison, two curves taken from the previously mentioned results by Fage for respective Reynolds number and drag coefficients of 1.57×10^5; 0.471 and 4.24×10^5; 0.143 (laminar and turbulent boundary layer flows). Because the Reynolds number range investigated by Fage encompasses the position of the standard transitional region, it is expected that results such as the present ones which are in a lower Reynolds number range, should give laminar drag values and pressure distributions similar to the laminar pressure distribution curve of Fage. Figures 8.1 to 8.5 show that the variation in the turbulence characteristics prevents the above explanation from being universally true.

1). Effect of increasing Reynolds number at low scale ratio and intensity values.

Figure 8.1 shows the effect on the pressure distribution of increasing the free-stream Reynolds number. At low values of scale ratio and turbulence intensity, of ranges

between 0.1 to 0.3 and 2% to 5% respectively, the effect of these characteristics on the drag and pressure distribution is expected to be minimal. The effect of these characteristics is considered to be minimal rather than negligible because if it were negligible then the first data set would completely overlap the laminar pressure distribution curve of Fage. At the low Reynolds number range of between 1.5×10^4 and 2×10^4, the curve obtained is very close to the laminar pressure drag curve. Its position of slightly above this curve is reflected by its drag coefficient value of 0.329 compared to that of 0.471 by Fage. The delayed separation point, from 87^o to 97^o, which gives a narrower wake, and the slightly increased pressures at the rear of the sphere account for this reduction in the drag coefficient. The presence of small disturbances in the free-stream therefore alters slightly the pressure distribution and also gives a corresponding drag coefficient alteration. Further increase of the Reynolds number to between 9.5×10^4 and 1.2×10^5, as given by the second data set, results in a further increase in the rear pressures while the rest of the pressure distribution apparently remains quasi-laminar. This can be taken as implying that the increased Reynolds number enhances the interaction between the wake and the free-stream caused by the prevailing small disturbances which results in the increased rear pressures. Because the pressure increase due to the

wake/free-stream interactions begins at the 180^{o} position (implied from Boltze [1908]) and "spreads" towards the front of the sphere, only the rear pressures have at this stage been affected whilst those points towards the front of the sphere remain unaffected by this increased interaction. The obtained drag coefficient value of 0.345 does not seem to correspond to the pressure distribution obtained for this data set. A pressure drag calculation of this data set as shown in figure 8.1a shows that the pressure drag coefficient contribution is only approximately 0.2. This implies that the contribution of the frictional drag is about 42% of the total drag coefficient distinct from a maximum of 12.5% quoted by Achenbach for turbulent-free flows. The increase in Reynolds number appears therefore to enhance the effects of the turbulence characteristics which introduces a dynamic boundary layer causing an increase in the frictional area thereby reducing the effective wake and increasing the frictional drag.

2). Effect of increasing turbulence intensity at low scale ratio and Reynolds numbers.

From the first set of results (scale ratio range; 0.1 to 0.3: intensity range; 2% to 5%: and Reynolds number range; 1.5 x 10^{4} to 2 x 10^{4}) discussed in figure 8.1, the effect of increasing turbulence intensity to a higher range of 12% to 14% is shown in figure 8.2. The previously observed phenomenon of an increase in the rear pressures is again

observed even at these low Reynolds numbers. The previously discussed "spread" of the rear high pressures is again observed, with the magnitude of increase resulting from the rear high pressures reducing as the front of the sphere is approached. Up to an angle of about 97^{o} from the front stagnation point, it is observed from the figure that there is still no apparent effect due to the increase in the free-stream turbulence intensity. As the flow at this position has already separated, (identified by a constant pressure coefficient in the first set of results), this increase of rear pressure can be considered not to have spread far enough as yet, for it to begin to affect the position of the separation point and thus on the shed vortices and drag.

The effect on the drag coefficient of increasing the free-stream turbulence intensity at such low Reynolds numbers is therefore equivalent to the previously observed increase in the Reynolds number for the same characteristics combination. The increased contribution of the frictional drag is another similar feature to be observed. An important point indicated here is that if from the characteristics combination of the second set of results, either the Reynolds number or the free-stream turbulence intensity were increased, the effect of the spreading rear high pressures will reach the separation point and begin to affect both it, the shed vortices, and consequently the drag values.

3). Effect of progressively increasing scale ratios for low Reynolds numbers and medium turbulence intensities.

From the second set of results (scale ratio range; 0.1 to 0.3: intensity range; 12% to 14%: and Reynolds number range; 1.5×10^4 to 2×10^4) discussed in figure 8.2, the effect on the pressure distribution of progressively increasing the scale ratio on this set of results is shown in figure 8.3.

Increasing the scale ratio increases the disturbance in the free-stream which affects the effective separation point, shed vortices, and the rear pressure levels. For a scale ratio range of between 0.5 and 0.6, figure 8.3 shows a distinct reduction in the rear pressures to near laminar values. This effect as discussed previously also begins at the rear of the sphere and spreads towards the front of it. Previous discussion of the first set of results in this figure have shown that at turbulence intensity levels of between 12% and 14%, the effect of increased pressures due to the prevailing turbulence characteristics would have spread and affected positions up to angles of around 97°. The scale ratio which has the apparent effect of reducing the rear pressures, nullifies the effect caused by the intensity as its effect spreads to smaller angles. This gives rise to the situation indicated in the figure of having regions around the sphere where, for a given point, a partial contribution of effects from both

characteristics is evident with the proportion of contribution varying. Further increase in the scale ratio increases the dominance of this characteristic over the intensity causing the pressure distribution to become quasi-laminar.

Observation of figure 8.3 indicate that an increase of the scale ratio appears to "push" the region and to reduce the level of turbulence intensity influence towards the front of the sphere thereby causing the separation point to become affected by the turbulence intensity. The effect of this is to cause separation to occur earlier as indicated by the other two sets of results. As the scale ratio is further increased, its dominance over the turbulence intensity increases reducing further the level of intensity acting over the transition region. This affects further the separation point position causing the distribution to become even more quasi-laminar. The movement of the separation point is reflected in the corresponding drag coefficient values obtained for the three sets of results. An initial assertion may thus be made here, that for fixed Reynolds number and turbulence intensity values, an increase in the scale ratio results in an increase of the drag values as the dominance of the scale ratio over the intensity increases. The increased scale ratio causes wider effective wakes to be achieved with corresponding drag coefficient values. The pressure drag coefficient calculation shown in figure 8.3a for the

third data set shows that the contribution of the skin frictional drag to the total, progressively reduces with increasing scale ratio.

The physical model developed in chapter 4 gives an indication of the means by which the scale ratio introduces lower pressures to the rear of the sphere. As the vortices approach the sphere, a cyclically oscillating angle of approach of the free-stream flow is "observed" by the sphere, thereby giving a dynamic front stagnation point position. Taking a time-frozen frame, as shown in figure 8.3b, it will be noticed that because of the wake variation due to this dynamic stagnation point, the effective rear pressures of the sphere, will be an average of the pressures near the 90^{o} position and those near the 180^{o} position. Because pressures near the 90^{o} position are lower than those in the separated region, the general tendency of averaging the pressures will be to lower the effective pressure recorded by pressure tapping holes located in the separated region. The amount by which the pressures are reduced is dependent on the scale ratio which directly relates to the amplitude of the wake oscillations. By this mechanism an increase in scale ratio will produce low effective rear pressures. The spread of the scale characteristic effect as the scale ratio increases can therefore be considered as being caused by the increased amplitudes of oscillation resulting in a net reduction of the effective pressure at angles

progressively approaching the stagnation point. Dynamic testing results shown in figures 8.3c and 8.3d for pressure tapping angles of 0^{o} and 155^{o} respectively show the dynamic effect of both the stagnation point and the wake as previously discussed. Amplitudes of these oscillations can be expected to increase with the scale ratio depending on the instanteneous boundary layer flow. At these low Reynolds numbers, the instanteneous prevailing boundary layer flow during oscillations is always laminar. The difference in effects between this and an oscillating turbulent boundary layer will be discussed later.

4). Effect of increasing Reynolds numbers for high scale ratio and medium turbulence intensity values.

The effect of increasing the Reynolds number from the case of the third set of results considered in figure 8.3 is shown in figure 8.4.

An increase in the Reynolds number gives pressure distribution values that match very closely the laminar curve values of Fage, although a much higher drag coefficient value is obtained. From the earlier discussion on the effect of the combination of Reynolds number and intensity on the dominance between scale and intensity characteristics, it can be deduced from the second set of results that an increase in Reynolds number enhances the dominance of the scale characteristic.

An increased drag coefficient value of 0.782 is obtained for this second data set which can be explained as being due to either or both of the following factors: The prevailing large scale characteristics modifies the effective pressure distribution thereby producing much higher drag values as the dominance of this characteristic over the intensity characteristic becomes complete; or the increase of the free-stream Reynolds number increases the velocity of the free-stream vortices which in turn increases the frequency of oscillation of the dynamic boundary layer and wake. This increased frequency of oscillation increases the skin frictional drag component to contribute around 44% of the total drag coefficient. Figure 8.4a shows a pressure drag calculation curve from which the preceeding has been deduced.

5). Effect of progressively increasing scale ratios at high intensity and Reynolds number.

For certain combinations of high intensity and Reynolds numbers, the previously discussed effect of the spread of the high pressures due to the intensity can reach the angles towards the front of the sphere thereby giving turbulent boundary layer pressure distributions with corresponding drag values. This is shown in the first set of results in figure 8.5. If on this set of results is superposed the effect of an increased scale characteristic, then the oscillating flow pressure distribution (which when time-frozen gives a turbulent

boundary layer flow) will vary the distribution to effectively form a quasi-laminar pressure distribution. The increased amplitude of oscillation gives an increased frictional drag coefficient contribution giving the high drag coefficient values of 0.636 as indicated by the second set of results. Further increase of the scale ratio to values above 2.0 gives a pressure distribution which is again quasi-turbulent. This is because by increasing the scale ratio, the amplitude of the wake oscillation increases and the frequency of the wake oscillation reduces. The combination of these two factors in addition to reducing the vorticity of the shed vortices and thereby the drag also cause a narrower effective wake to be formed which reintroduces the quasi-turbulent pressure distribution. The reduction of the drag coefficient value to 0.606 is therefore attributed directly to the pressure distribution variation. This new characteristic combination effectively reduces the scale characteristic dominance over the intensity characteristic. Previously, it has been shown that the dominance of the scale characteristic over the intensity characteristic is enhanced by the Reynolds number for a fixed combination of scale and intensity characteristics, an increase of the scale ratio for fixed Reynolds number and intensity characteristic will therefore have the opposite effect as has been shown here.

The results of figure 8.5 show that for a fixed high Reynolds number and turbulence intensity characteristic, an increase of the scale ratio will result in a turning point in the drag coefficient values caused by the interchange of dominance between the scale and intensity characteristics.

6). Summary of effects due to turbulence characteristic combinations.

From the results obtained, pressure distributions of spheres immersed in turbulent flows have been shown to vary depending on the prevailing combinations of turbulence characteristics. Various distributions are formed ranging from quasi-laminar to quasi-turbulent distributions including combinations of both, depending on the dominance between the scale and intensity characteristics. A careful study of these distributions, coupled with the knowledge of the prevailing characteristics combination can give a general indication of the resulting total drag value.

The results obtained have indicated the existence of turning points in the attainable drag values for specific characteristic combinations. The type of turning point obtained (maximum and minimum) is dependent on the characteristics. The effect of the Reynolds number which generally increases the frequency of the free-stream vortices and thereby the oscillating wake, would generally account for the presence of a turning point but not for

the specific type of turning point present. The scale ratio on the other hand is a means by which the specific type of turning point present can be identified. The type of turning point can be identified as: Minimum for low Reynolds numbers, when the increasing dominance of the scale characteristic "pushes" the region of turbulence intensity influence to the transition position thus affecting the separation point before totally removing the effect of the intensity characteristic; and maximum for high Reynolds numbers when the increasing scale ratio causes the turbulent boundary layer flow to form wide and narrow effective wakes for varying characteristics combinations and depending on the degree of the scale characteristic dominance over the intensity characteristic. Although the turning points discussed so far have resulted from an increase in scale ratio, it is not inconceivable that an increase in one of the other characteristics can also form turning points.

The general effect of the turbulence intensity, as observed so far, is to cause an increase in the rear pressures. The region in which this effect is prevalent spreads towards the front of the sphere as the free-stream turbulent intensity increases. The effect of the scale ratio on the other hand, is to cause a reduction in the rear pressures achieved by the dynamic wake effect. The region in which this effect is prevalent also spreads towards the front of the sphere "pushing" forwards the

region of intensity characteristic influence as the free-stream scale ratio increases. This also increases the amplitude of wake oscillations which affects the vorticity of the shed vortices and the dissipated energy. The effect of increasing the Reynolds number is to modify these effects; either by amplifying the effect of the scale ratio thus causing the spread of the reduced pressures to increase, or by increasing the frequency of the wake oscillations and thus affecting the effective wake size formed. The Reynolds number can be generalised as having the effect of increasing the dominance of the scale characteristic over the intensity characteristic.

8.2. Drag variation with Reynolds number.

Neve [1986] has given very detailed results and analyses showing the drag coefficient variation with Reynolds number for varying free-stream combinations of scale and intensity characteristics. Reproductions of his results are presented here as figures 8.6, 8.7 and 8.8. Because the present project was an extension of the work conducted by Neve, the reproduced graphs are similar to those determined from the present results. As confirmation of this, a sample of the present results have been added onto these figures from which the similarity is obvious.

These results confirm the previously made assertion that an increase in Reynolds number also forms maxima and minima of the drag coefficient values, and also that the

amplitudes and Reynolds number positions of these turning points depend on the prevailing combinations of the scale and intensity characteristics. Another feature shown is that a curve with a fixed combination of scale and intensity characteristics can produce upon increasing the Reynolds number both a minimum and a maximum of the drag coefficient. The 'S' curve effect discussed in chapter 1 can be observed in these figures indicating a sequence of minima and maxima for each curve of constant characteristic combination. For a fixed Reynolds number the validity of the previously made assertion that maxima and minima can occur with increase in the scale ratios (keeping all other characteristics constant) can be observed here again together with its dependence on the Reynolds number. Although turning points due to an increase in the scale ratio can still be discerned at all Reynolds numbers, maxima and minima due to an increase in the Reynolds numbers occur only in particular Reynolds number regions.

From the preceeding discussion it can be stated that there exist particular regions in the Reynolds number range in which turning points are most likely to occur. Because the Reynolds number increases the frequency of the free-stream vortices and also the dominance of the scale characteristic over the intensity characteristic, in the Reynolds number ranges where turning points occur, the prevailing frequency ratios are expected to be such that they induce "resonance". This feature would therefore explain the heat

transfer resonance effect observed by van der Hegge Zijnen [1958] for circular cylinders, for which a frequency ratio of 2.0 was suggested by Hinze [1959]. Further analysis of the variation of the drag with frequency ratio will be discussed later in the chapter.

8.3. Drag variation with scale ratio.

The effect of an increase in the scale ratio on the drag, is expected to be dependent on the Reynolds number range of the free-stream flow. This, as has been previously discussed, is because of the dependence that the scale ratio has on the Reynolds number. Figures 8.9 to 8.14 show the effect of the scale ratio on the drag coefficient for varying Reynolds number and intensity characteristic combinations.

a). Graphs.

Figure 8.9.

For a characteristic combination of: Reynolds number range, between 5×10^3 and 6.3×10^3; and turbulence intensity range, between 13% and 20%, the high intensity in the free-stream has a considerable effect on the boundary layer causing transition to occur and turbulent drag values to be obtained. The very low Reynolds numbers give a low frequency of wake oscillation and, as discussed previously, this reduces the effectiveness of the scale ratio. Because of the high turbulence intensity in the free-stream, it is observed from the figure that an

increase of the scale ratio has no significant effect on the total drag, although at the high scale ratio range, there is a slight tendency for the drag values to increase. The slight increase at the high scale ratio range is because the low Reynolds numbers begin to affect the dominance between the scale and intensity characteristics. Figure 8.9 verifies the previously made assertion that because the degree of dominance of the scale ratio characteristic over the intensity characteristic is enhanced by the high Reynolds numbers, at low Reynolds numbers the dominance of the intensity characteristic over the scale characteristic is more or less total.

Figure 8.10.

Increasing the Reynolds number to between 1×10^4 and 1.1×10^4 increases the dominance of the scale characteristic, which at this stage, has the tendency of increasing the obtained drag values at low and high scale ratios. The resulting effect observed is that a turning point in the form of a minimum at a scale ratio value of around 1.5 is formed. At scale ratio values greater than 4, drag values similar to the standard laminar values are obtained showing that the dominance of the scale characteristic has totally nullified that of the intensity characteristic. A pressure distribution similar to the second data set of figure 8.5 is obtained.

Figure 8.11.
At a Reynolds number range of between 2.1 x 10^4 and 3 x 10^4 the effect of the scale characteristic on the drag is evident even at very low scale ratio values. The curve obtained indicates that the tendency for the increase in scale ratio to yield laminar drag values results in the equivalent of a "low damping" effect of the curve. Because of this low damping effect, the drag values oscillate about the laminar drag values yielding turning points at scale ratio values of 0.7, 1.5 and 3.2.

An increase of the intensity range to between 18% and 20% (figure 8.12) produces a curve that now oscillates about a higher drag value. This curve also shows that the increase in the scale ratio causes the turning points of the curve to occur at closer intervals.

Figure 8.13.
For a higher Reynolds number range of between 8 x 10^4 and 8.5 x 10^4, figure 8.13 shows that a "near critical damping" effect on the curve is obtained with the curve "gently" oscillating about a laminar drag value. This near critical damping is indicated in the figure by the reduction in the amplitude of oscillation of the curve with increase of the scale ratio values. Because the increased scale ratio increases the amplitude of the wake oscillations, the effective wake size is also increased which results in a corresponding increase of the effective drag value obtained. The curve further indicates that a maximum

is likely to occur at a scale ratio value of around 4.0 thereby giving drag values that are approaching the the standard laminar drag coefficient value of 0.5.

Implicit in the figure, is the indication that with such high Reynolds numbers, the dominance of the scale characteristic over the intensity characteristic is such that an intensity range of between 3.5% and 15% as used in the figure produces no variation on the curve obtained. On the other hand, the sensitivity of the curve to variations of Reynolds numbers is shown in figure 8.14 where the Reynolds number range is increased to between 9×10^4 and 1×10^5. Here it is seen that the damping effect on the curve is increased and a maximum is now obtained at a scale ratio value of 3.0 for which a very low amplitude is achieved.

An analogy between the Nusselt number and the drag coefficient which has been discussed in chapter 4 can be used as a basis for comparing the Nusselt-number ratio variation with scale ratio. Results of van der Hegge Zijnen [1958] shown in figure 8.14a, show that turning points occur with increase in the scale ratio of the Nusselt-number ratio. Although these results are for heat transfer from a circular cylinder which makes them of little quantitative value, their qualitative value in showing the trend of the effect of the scale ratio is enormous. Hinze [1959] discussing the results of van der Hegge Zijnen, associated

the increased Nusselt-number ratio with resonance occurring between the free-stream vortex frequency and the frequency of the shed vortices. This is similar to the above obtained effects in a qualitative sense.

b). Summary of effects.

From the graphs shown in figures 8.9 to 8.14 the following deductions can be made:

1). In the absence of free-stream turbulence, standard drag coefficient values of around 0.5 are obtained. For the Reynolds number range considered, this value can be considered to be the "relaxed equilibrium position". The introduction of free-stream turbulence causes the drag values to deviate from this equilibrium position by an amount dependent on the prevailing characteristics combination. For a fixed Reynolds number and turbulence intensity combination, drag coefficient values will generally tend to increase to laminar drag values with increase of the scale ratio. This occurs because the scale ratio characteristic cause wider effective wakes and thereby higher drag values.

2). The levels of the prevailing Reynolds number and intensity characteristics determine the degree by which the drag values approach the aforementioned relaxed equilibrium position. The dominance of the high turbulence intensity characteristic over the scale characteristic is very evident at low Reynolds

numbers which gives low drag values. Increase of the Reynolds number enhances the dominance of the scale characteristic over the intensity characteristic giving increased drag coefficients. This enhanced dominance is observed in the rapid increase of the drag values for only slight increases of the scale ratio at low scale ratio values. Increase in the Reynolds numbers increases the rate of this drag increase and reduces the scale ratio at which this increase occurs.

3). At sufficiently high Reynolds numbers, the effects of the intensity characteristic become negligible. This is shown by the drag values approaching the relaxed equilibrium position with oscillations of variable damping. The amplitude of these oscillations reduce with increase in the Reynolds number introducing an effect similar to "critical damping" in vibrating systems.

8.4. Drag variation with frequency ratio.

A relationship has previously been suggested between the drag coefficient and the frequency ratio. This relationship has also been previously determined by researchers to cause resonance effects of the drag values. Curves of the drag coefficient variation with frequency ratio for the present results are given in figures 8.15 and 8.16. These figures, shown expanded in figures 8.15a and 8.16a respectively, show the presence of resonance at a frequency

ratio of 8.0 although the amplitude of this resonance reduces with increase in the Reynolds number to between 4.1×10^4 and 4.5×10^4 in figure 8.16. Both figures show that at very low frequency ratios there is a rapid drop in the drag coefficient values with very little corresponding change of the frequency ratios. This resonance position identified by van der Hegge Zijnen [1958], Hinze [1959] and Neve [1986] is indicated in figures 8.15a and 8.16a as positions such that when the particular frequency ratio is attained high drag coefficient values, out of character with those for the nearest frequency ratios, are attained. In the region where resonance occurs, the high scale ratio values give wakes of large amplitudes and low frequency of oscillation resulting in high drag values. Increase of the frequency ratio causes a rapid reduction in the drag values as its effect of reducing the effective wake becomes evident. An increase in the Reynolds number as shown in figure 8.16, shows that this reduces the amplitude and increases the wavelength of the oscillation covering the whole frequency ratio range.

8.5. Drag variation with both scale ratio and turbulence intensity.

Another method of analysing the effect of the turbulence characteristics on the drag coefficient is to observe the drag variation for particular combinations of scale ratio and turbulence intensity. This is achieved by plotting regions of various drag coefficient values for variations

of the scale ratio with turbulence intensity. Figures 8.17 to 8.24 show these variations for increasing Reynolds numbers. On the graphs are shown points and contour lines of constant drag coefficients and also shaded regions of low drag values. Drag coefficient values are shown by numbers which are 100 times the actual drag coefficients.

Figure 8.17 shows that at a low Reynolds number of 6×10^3 the low drag values fall on a line which shows a linear increase of scale ratio with turbulence intensity. Increased drag coefficient values occur at positions of increasing distances from this line. Increase in the Reynolds number to 1×10^4, as shown in figure 8.18, reduces along the linearity line the maximum intensity and scale ratio values to which the low drag value regions are attained. The region of the highest drag coefficients is observed to occur at increased turbulence characteristic values. Progressive increases in the Reynolds number [figures 8.19 to 8.24] show that the high drag coefficient region appears to rotate via the high scale ratios to lower intensity values. At a Reynolds number of 7×10^4 as in figure 8.24, the high drag coefficient value region forms a linearity relationship between the scale ratio and turbulence intensity. The low drag coefficient region also rotates via the low scale ratios to concentrate at high Reynolds numbers to only the low scale ratio values.

These figures show that for a given combination of turbulence characteristics, the varying corresponding drag coefficient values can be identified.

8.6. Prediction of drag coefficient.

The preceeding methods discussed isolate and ascertain the importance of the individual characteristics in determining the drag coefficient of the sphere. Although the variation of the drag coefficient with these characteristics has been isolated, a method by which the prediction of the drag coefficient from the knowledge of turbulence characteristics has as yet not been provided. A method which can be used to predict the drag coefficient has been derived and discussed in the following section.

From a combination of the frequency ratio, Reynolds number and turbulence intensity, a product function is obtained which is equal to the product F.R. x Re x I. The variation of the drag coefficient with this product function is given in figure 8.25. A total of over 2,000 data points are included in this figure resulting in what appears to be a distinct trend. Analysis of these trends shows that individual curves exist which are dependent on the scale ratio. Figure 8.25a shows the extracted curve for a scale ratio of 0.1. The curve for this low scale ratio is similar to a vibrations curve with a very high damping factor. The drag values increase very rapidly to a laminar drag coefficient value of 0.5, forming a peak at a very low function value, before gradually reducing at very high

product function values. Increasing the scale ratio to a value of 0.5 as shown if figure 8.25b gives a curve with a high amplitude peak which occurs at an even lower product function value and is much "sharper". Further increases in the scale ratio to 1.5, 3.2 and greater than 4.0, as shown in figures 8.25c, 8.25d and 8.25e respectively shows the trend of peaks becoming progressively sharper, occurring at higher drag coefficient values, and at lower product function values. The general trend of all these results can therefore be seen as being similar to a reduction in the damping factor of a vibrations curve.

The preceeding graphs therefore give a distinct method by which the drag coefficient of a sphere can be predicted from the knowledge of the free-stream turbulence characteristics with great accuracy. With the previously mentioned similarity to a vibrations curve, an analogy can be drawn between the series of graphs of figure 8.25 and the graph of a forced vibration with a rotating unbalanced mass as given by Thomson [1981]. The equation derived by Thomson for this forced vibration with an out-of-balance is as follows:-

$$\frac{MX}{me} = \frac{K^2}{((1 - k^2)^2 + (2ZK)^2)^{0.5}}$$

and $K = (w / w_n)$

where M is the mass of the system

X the amplitude of oscillation

m the mass out-of-balance

e the eccentricity of out-of-balance

w the frequency of oscillation

w_n the natural frequency

and Z the damping factor.

The analogy drawn between the two systems would therefore be:

$\frac{MX}{me}$ equivalent to Cd ratio

K equivalent to product function ratio

and Z equivalent to the inverse of the scale ratio

The two ratios introduced in the analogy are the drag coefficient ratio and the product function ratio. These terms are defined as follows:

a) Drag coefficient ratio: Ratio of the actual drag coefficient to the approximate drag coefficient value to which the drag coefficients tend at high product function values - 0.4.

b) Product function ratio: Ratio of the actual product function to the product function value at which most of the peaks occur at high scale ratio values - 100.

A reproduction of figure 8.25 is shown in figure 8.26 but with the aforementioned ratios used for the axes instead.

Using the available data, theoeretical drag coefficient ratios can be obtained using the equation derived by Thomson to give the series of curves shown in figure 8.26a. These curves are again dependent on the scale ratio in the same manner as has been previously discussed.

To compare the accuracy with which the equation can be used to predict the drag coefficient, a graph of the actual drag coefficient ratio over the theoretical drag coefficient ratio against the function ratio is given in figure 8.26b. This graph shows very good agreement for function ratios greater than 1.0 which corresponds to the peak positions in figure 8.25. For function ratio values less than 1.0 the agreement is not as good because of the difference in approach to the peak positions of the actual results compared to the theoretical results. A further restriction to the comparison is for scale ratio values less than 0.6 for which there is also poor agreement.

Within the limitations of a scale ratio greater than 0.6 and product functions greater than 100, this equation can be used to predict the obtained drag coefficient to an accuracy of $\pm$ 20%, which compared to the present accuracies in determining the drag coefficients is acceptable.

The implication of this analogy applied to the drag coefficient variation of a sphere can be taken to be as follows:

The turbulent flow field sets up an effective out-of-balance effect probably due to the oscillating wake which varies the magnitude of the drag component. This out-of-balance varies with the combination of the characteristics given by the frequency ratio, free-stream turbulence intensity and free-stream Reynolds number to give a series of curves dependent on the scale ratio. At a given product function, which is equivalent to the ratio of the frequency of the sphere oscillations caused by the wake to its natural frequency, resonance will occur with its position and amplitude determined by the macroscale size of the free-stream vortices. At low scale ratios, when the effect of the wake oscillations is negligible, there is no resonance effect at all, but with increase in the scale ratio and hence the amplitude of the wake oscillations, the drag at which the turning point (resonance) occurs increases and varies with the characteristic combination at which it occurs. Noted in the figure also is that although when the drag was varied with individual characteristics both maxima and minima were obtained, the drag variation with the product function for a fixed scale ratio forms only a single maximum.

To enable comparisons of figure 8.26b to be made with results of previous researchers, the turbulence intensity, Reynolds number and macroscale of turbulence characteristics together with the frequency ratio and the drag coefficient all need to be known. A literature survey

conducted failed to reveal publications containing all the information necessary to make this comparison possible. Comparisons of the individual characteristics which culminated in this figure have been made in the preceeding sections and have been found to agree either in values or in trends with the published results.

CHAPTER 9. CONCLUSIONS.

From the analysis of the results on the effects of the macroscale of turbulence on the total drag of a sphere, the following conclusions can be drawn:

1). The total drag coefficient of a sphere for any given flow condition is dependent on the prevailing turbulence characteristics combination. The characteristics whose combination is of importance in this respect are: the turbulence intensity; and the macroscale of turbulence. The free-stream Reynolds number is also important because of its influence on the characteristics dominance for a given characteristics combination.

The effects of the individual characteristics and the Reynolds number on the total drag coefficient can be summarized as follows:

a). Turbulence intensity: This causes mixing to occur between the fast flowing high energy free-stream and the slow flowing low energy boundary layer. By receiving energy from the free-stream flow, the boundary layer flow increases its energy and resists the adverse pressure gradient around the sphere. This causes transition from a laminar to a turbulent boundary layer to take place earlier than usual and for the separation point of the boundary layer from the sphere to be delayed. Resulting from this is a higher energy recovery and narrower wake giving a reduced drag coefficient.

b). Macroscale of turbulence: This characteristic, depending on its size compared to that of the sphere diameter, introduces a dynamic boundary layer with an oscillating wake. In its simplest form, this characteristic can be considered as two-dimensional and non-interactive. At low scale ratio values, (macroscale of turbulence to sphere diameter ratio) the effects of this characteristic are negligible, although an increase in the Reynolds numbers will enhance these effects. At high scale ratio values, this characteristic forms a dynamic pressure distribution and an oscillating wake which, depending on the frequency of oscillation, will vary the size of the effective wake and thereby vary the drag. The effect of this characteristic on a "free sphere" in a turbulent flow field would be to cause it to oscillate in the vertical (or horizontal) plane because of the presence of a varying lift component resulting from the resolution of the force component. Upon averaging, this lift component cancels out, or in the case of a free sphere, it would oscillate about a fixed line.

c). Reynolds number: The velocity of the free-stream vortices together with the frequency of oscillation of the wakes that they produce are affected by changes in this characteristic. This causes a dependence to develop between the effects of the scale characteristic and the prevailing Reynolds number. For a given combination of turbulence characteristics, the Reynolds number enhances the dominance of the effects of the scale characteristic

over those of the intensity characteristic.

A relationship has been found to exist between the drag coefficient and a product function comprising the frequency ratio, the Reynolds number and the turbulence intensity. This relationship forms a series of curves defined uniquely only by the scale ratio which has the effect of causing an increased damping with decrease in the scale ratio. The similarity of this relationship to that of a standard "out-of-balance rotating mass" vibrations curve, enabled the same equation to be used and was found to give a good agreement between the values calculated from the equation and the experimental values within limits. The limits within which this relationship may thus be used are: a scale ratio value greater than 0.6; and a function ratio greater than unity.

2). The dynamic pressure distributions caused by the scale characteristic have been shown from pressure drag calculations to increase the percentage contribution of the friction drag to the total drag. Achenbach [1972] working with turbulence-free flows determined maximum skin friction drag contributions of not more than 12.5%. Present results have shown that the effects of the scale characteristic can increase the skin friction drag contributions to over 40%. Generally, the initially made assertion that the variation in the pressure distributions should have a corresponding drag variation was shown to be correct.

3). Resonance, initially observed by van der Hegge Zijnen [1958] who was working on the heat transfer from cylinders, has been shown to occur in the drag coefficient values of the present results. In variations between the drag coefficient and the frequency ratio, resonance was found to occur repeatably at a frequency ratio of 8.0. The amplitude of this resonance was observed to be dependent on the prevailing Reynolds number. This can be shown from the results of the drag variation with the Reynolds number that only some regions of the Reynolds number are prone to having turning points.

4). Results from the dynamic testing have shown that effects of an individual vortex is prevalent over the sphere for a period which can be determined from vortex size and velocity. This showed that individual vortices can be identified as they passed the sphere, which further enhances the assertion that an oscillating wake is formed by vortices and that a non-interactive model of the free-stream vortices (such as that discussed in chapter 4) fully described the actual situation.

FURTHER WORK.

Work to be carried out as an extension of the present project is suggested to proceed in the following direction, with the aim of achieving the results discussed below.

1). Further statistical analysis of the dynamic results obtained is likely to give a greater insight into the dynamic behaviour of the boundary layers and the wake. Because of the way that these results were taken - individual tapping holes recorded totally independently - the data will have to be analysed in such a manner that: either the starting point of the individual results is determined; or the time positions of the individual results can be identified. This will involve a lot of statistical analysis, but will give a clear picture of the dynamic behaviour of the pressure distribution. An alternative to this method is to conduct another set of experiments using a single hollow sphere with 33 pressure transducers positioned as follows: One at the front stagnation point, four at 45^{o} from the front stagnation point but at 90^{o} to each other, and this repeated at the 60^{o}, 90^{o}, 100^{o}, 110^{o}, 125^{o}, 140^{o} and 155^{o} positions. Using pressure transducers with connecting leads small enough to enable the leads from all 33 transducers to pass through the hollow sting whilst still maintaining the required

sting/sphere diameter ratio, will enable the pressure transducers to be scanned simultaneously using the data logger. This will give an accurate picture of the instanteneous pressure distributions and the corresponding drag.

Amongst the observations expected from these results is a confirmation of an assertion made by Achenbach [1974] that vortex shedding from a sphere occurs a point which itself rotates around the sphere. These results are also expected to show more conclusively the dynamic behaviour of the wake and the distinct link between the instantaneous pressure distribution and the instantaneous drag.

2). In the development of methods for the prediction of the prevailing drag coefficients for known turbulence characteristic combinations, there are two main ways to proceed: firstly, to further develop a chart such as the sphere drag chart shown in figure F1; and secondly, to develop a similar chart to figure F1 but with variables based on the frequency spectrum and not grid dimensions.

Sphere drag chart.

The sphere drag chart of figure F1, shows the drag variation with the turbulence characteristics based on the grid dimensions. These variations on the four axes are:

a). The drag coefficient, Cd [left Y-axis].

b). The intensity function, $I(MH/b^2)$ [bottom X-axis].

c). The velocity function, (Re_b) [right Y-axis].

d). The scale function, (Lx/b) [top X-axis].

Where I is the turbulence intensity as a percentage

M is the grid mesh length

H is the wind tunnel width

b is the grid slat width

and Re_b is the Reynolds number based on the grid slat width.

The aim of this drag chart is to predict the drag coefficient values to be expected from a test rig of known wind tunnel and grid dimensions. Further additions to this chart are still required, to include results from experiments conducted in wind tunnels and grids of varying dimension combinations so that a more generalised chart may be obtained. The curves shown are of constant scale and velocity functions as obtained from the present results. Although the actual data points are not shown, errors of up to 15% were obtained.

A similar chart based on the spectrum of the turbulence field would assist those researchers using turbulence flow fields that are generated in means other than by grids in the drag coefficient predictions of their various applications.

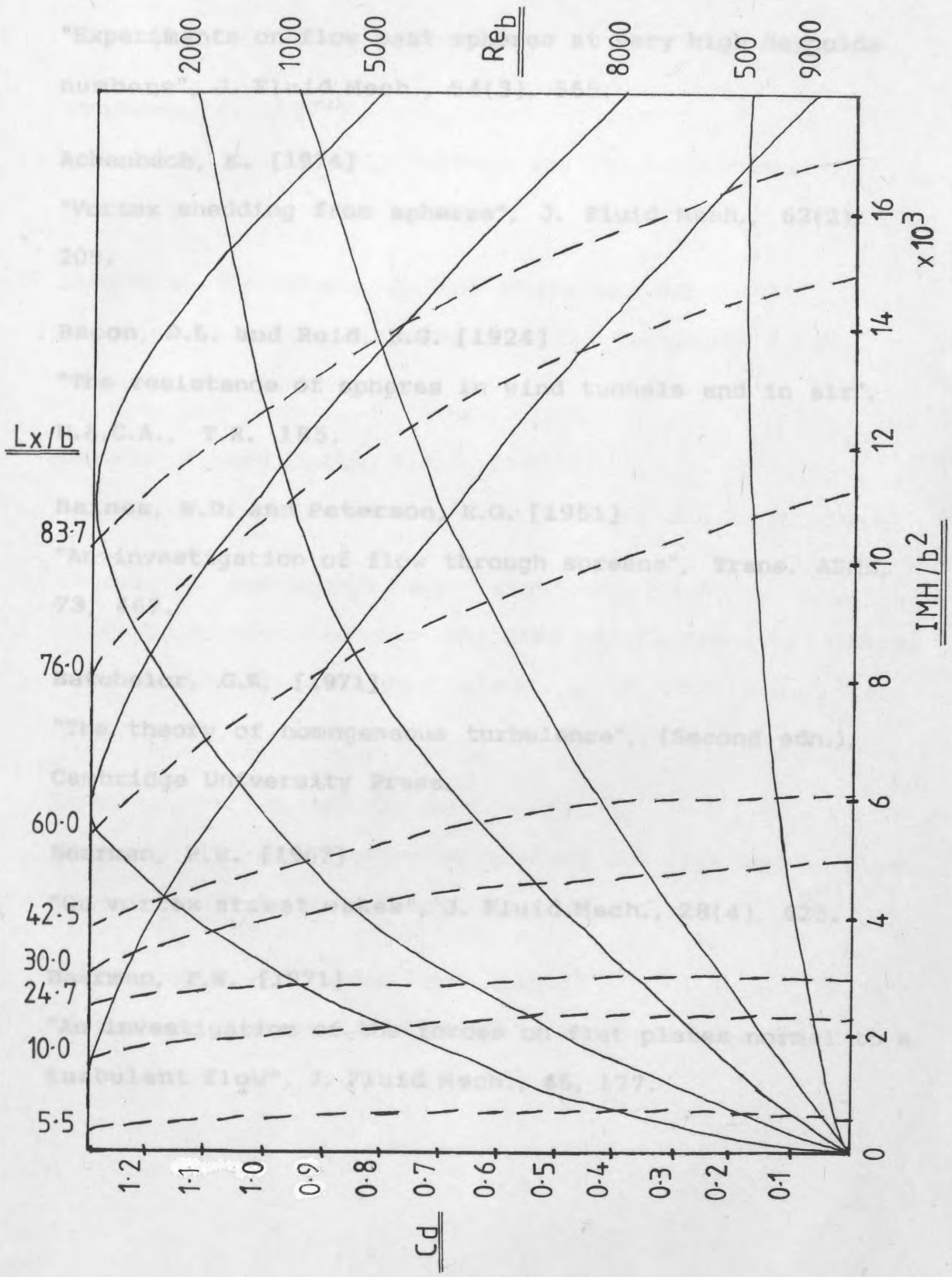

Fig. F1 Sphere drag chart

REFERENCES AND BIBLIOGRAPHY

Achenbach, E. [1972]

"Experiments on flow past spheres at very high Reynolds numbers", J. Fluid Mech., **54**(3), 565.

Achenbach, E. [1974]

"Vortex shedding from spheres", J. Fluid Mech., **62**(2), 208.

Bacon, D.L. and Reid, E.G. [1924]

"The resistance of spheres in wind tunnels and in air", N.A.C.A., T.R. **185**.

Baines, W.D. and Peterson, E.G. [1951]

"An investigation of flow through screens", Trans. ASME, **73**, 467.

Batchelor, G.K. [1971]

"The theory of homogeneous turbulence", (Second edn.), Cambridge University Press.

Bearman, P.W. [1967]

"On vortex street wakes", J. Fluid Mech., **28**(4), 625.

Bearman, P.W. [1971]

"An investigation of the forces on flat plates normal to a turbulent flow", J. Fluid Mech., **46**, 177.

Boltze, E. [1908]

"Grenzschicht an rotationskörpern in flussigkeiten mit kleiner reibung", Göttingen Dissertation.

(Quoted by Goldstein, S. [1938])

Bradshaw, P. [1971]

"An introduction to turbulence and its measurement", Pergamon Press.

Bradshaw, P.; Cebeci, T. and Whitelaw, J.H. [1981]

"Engineering calculation methods for turbulent flow", Academic Press.

Cebeci, T. and Smith, A.M.O. [1974]

"Analysis of turbulent boundary layers", Academic Press.

Clamen, A. and Gauvin, W.H. [1969]

"Effects of turbulence on the drag coefficients of spheres in a supercritical flow regime", J. Am. Inst. Chem. E., 15(2), 184.

Comte-Bellot, G. and Corrsin, S. [1966]

"The use of a contraction to improve the isotropy of grid turbulence", J. Fluid Mech., 25, 657.

Cooper, R.D. and Tuplin, M.P. [1955]

"Turbulence measurements with the hot-wire anemometer", AGARDograph, 12.

Davies, P.O.A.L.; Fisher, M.J. and Barratt, M.J. [1963]
"The characteristics of the turbulence in the mixing region of a round jet", J. Fluid Mech., 15, 337.

Dryden, H.L. [1941]
"Isotropic turbulence in theory and experiment", T. von Karman Anniv. Vol., 85.

Dryden, H.L. [1943]
"A review of the statistical theory of turbulence", Quart. Appl. Math., 1, 7.

Dryden, H.L. and Kuethe, A.M. [1930]
"The effect of turbulence in wind tunnel measurements", N.A.C.A., T.R. 342.

Dryden,H.L.;Schubauer,G.B.;Mock,Jr.,W.C.;Skramstad,H.K. [1937]
"Measurements of intensity and scale of wind-tunnel turbulence and their relation to the critical Reynolds number of spheres", N.A.C.A., T.R. 581, 109.

Duncan, W.J.; Thom, A.S. and Young, A.D. [1970]
"Mechanics of fluids", (Second edn.), Edward Arnold.

Eiffel, G. [1912]
"Sur la resistance des spheres dans l'air en mouvement", Comptes Rendus, 155, 1597.
(Quoted by Goldstein, S. [1938])

Emmons, H.W. and Bryson, A.E. [1951]

"The laminar-turbulent transition in a boundary layer. - Part 1", J. Aeronaut. Sci., **18**, 490.

Fage, A. [1937]

"Experiments on a sphere at critical Reynolds numbers", A.R.C., R.& M. **1766**, 83.

Fage, A. and Johansen, F.C. [1927]

"The structure of vortex streets", A.R.C., R.& M. **1143**.

Goldstein, S. [1938a]

"Modern developments in fluid dynamics", Vol 1, Oxford University Press.

Goldstein, S. [1938b]

"Modern developments in fluid dynamics", Vol 2, Oxford University Press.

Grant, H.L. [1958]

"The large eddies of turbulent motion", J. Fluid Mech., **4**, 149.

Hancock, P.E. [1980]

"The effect of free-stream turbulence on turbulent boundary layers", Ph.D. Thesis, Imperial College, London.

Hinze, J.O. [1959]

"Turbulence : An introduction to its mechanism and theory", McGraw-Hill, New York.

Ho, C.M. and Nosseir, N.S. [1981]

"Dynamics of an impinging jet, Part 1: The feedback phenomenon", J. Fluid Mech., **105**, 119.

Hoerner, S. [1934]

"Versuhe mit kugeln betreffend kennzahl, turbulenz und oberflachenbeschaffenheit", Luftfahrtforschung, **12**, 42.

Hoerner, S. [1935]

"Tests of spheres with reference to Reynolds number, turbulence and surface roughness", N.A.C.A., T.M. 777.

Holstein, H. and Bohlsen, T. [1940]

Lilienthal-Bericht, **s-10**, 5.

(**Quoted** by Schlichting, H. [1968])

von Karman, T. [1911]

"Uber den mechanismus des widerstandes, den ein bewegter korper in einer flussigkeit erzeugt", Nachr. Ges. Wiss. Göttingen, Math. Phys. Klasse, 509.

von Karman, T. [1912]

"Uber laminare und turbulente reibung", Z. angew. Math. Mech., **1**, 233.

von Karman, T. [1930]

"Mechanische ahnlichhkeit und turbulenz", Proc. 3rd Int. Cong. Appl. Mech., Stockholm, **1**, 85.

von Karman, T. [1937a]

"Turbulence", J. Roy. Aeronaut. Soc., **41**, 1109.

von Karman, T. [1937b]

"On the statistical theory of turbulence", Proc. Nat. Acad. Sci., Wash., **23**, 98.

von Karman, T. and Howarth, L. [1938]

"On the statistical theory of isotropic turbulence", Proc. Roy. Soc. London, **A164**, 192.

von Karman, T. and Lin, C.C. [1951]

"On the concept of similarity in the theory of isotropic turbulence", Adv. Appl. Mech., **2**, 1.

Kinsler, L.E. and Frey, A.R. [1962]

"Fundamentals of acoustics", (Second edn.), John Wiley and Sons Inc., Chapter 7.

Laurence, J.C. [1956]

"Intensity, scale and spectra of turbulence in mixing region of free subsonic jet", N.A.C.A., Rep. **1292**, 891.

Lee, B.E. [1975/6]

"Some effects of turbulence scale on the mean forces on a bluff body", J. Ind. Aero., 1,361.

Lin, C.C. [1955]

"The theory of hydrodynamic stability", Cambridge University Press.

Lin, C.C. [1957]

"Motion in the boundary layer with a rapidly oscillating external flow", Proc. 9th. Int. Cong. Appl. Mech. Brussels, 4, 155.

Millikan, C.B. and Klein, A.L. [1933]

"The effect of turbulence", Aircraft Engineering, 5, 169.

Mujumdar, A.S. and Douglas, W.J.M. [1970]

"Eddy-shedding from a sphere in turbulent free-streams", Int. J. Heat & Mass Transfer, 13, 1627.

Neve, R.S. [1986]

"The importance of turbulence macroscale in determining the drag coefficient of spheres", Int. J. Heat & Fluid Flow, 7(1), 28.

Neve, R.S. and Jaafar F.B. [1982]

"The effect of turbulence and surface roughness on the drag of spheres in thin jets", The Aeronautical Journal, 86, 331.

Owen, P.R. [1945]

"Note on the apparatus and work of the W.V.A. Supersonic Institute at Kochel, Part 3", A.R.C.,9361.

Owen, P.R. and Zienkiewicz, H.K. [1957]

"The production of uniform shear flow in a wind tunnel", J. Fluid Mech., 2, 521.

Ower, F. and Warden, R. [1934]

"Note on the use of networks to introduce turbulence into a wind tunnel", A.R.C., R.& M. **1559.**

Platt, R.C. [1936]

"Turbulence factors of N.A.C.A. wind tunnels as determined by spheres tests", N.A.C.A., T.R. **558**, 13.

Pohlhausen, K. [1921]

"Zur naherungsweisen integration der differentialgleichung der laminaren reibungsschicht", Z. angew. Math. Mech., **1**, 252.

(**Quoted** by Schlichting, H. [1968])

Pope, A. and Harper, J.J. [1966]

"Low-speed wind tunnel testing", John Wiley and Sons Inc., New York.

Prandtl, L. [1904]

"Uber flussigkeits bewegung bei sehr kleir reibung", Proc. 3rd. Int. Math. Cong., Heidelberg.

Prandtl, L. [1914]

"Der luftwiderstand von kugeln", Nachr. D. K. Ges. D. Wissensch., Göttingen, Math. Phys. Klasse, 177.

Prandtl, L. [1926]

"Ueber die ausgebildete turbulenz", Proc. 2nd. Int. Cong. Appl. Mech., Zurich.

Reynolds, O. [1883]

"An experimental determination of the circumstances which determine whether the motion of water shall be direct or sinuous, and the law of resistance in parallel channels", Phil. Trans. Roy. Soc. London, **A174**, 935.

Reynolds, O. [1895]

"On the dynamical theory of incompressible viscous fluids and the determination of the criterion", Phil. Trans. Roy. Soc. London, **A186**, 123.

Rose, W.G. [1970]

"Interaction of grid turbulence with a uniform shear", J. Fluid Mech., **44**, 767.

Roshko, A. [1954]

"On the development of turbulent wakes from vortex streets", N.A.C.A., Rep. **1191**.

Schlichting, H. [1968]

"Boundary-layer theory", (Sixth edn.), McGraw-Hill.

Schmidt, E. and Wenner, K. [1941]

"Wärmeabgabe über den umfang eines angeblasenen geheizten zylinders", Forschg. Ing.- Wes. **12**, 65.

Schubauer, G.B. and Skramstad, H.K. [1947]

"Laminar boundary layer oscillations and stability of laminar flow", J. Aero. Soc., **14**, 69.

Serby, J.E. and Morgan, M.B. [1936]
"Turbulence measurements in flight", A.R.C., R.& M. **1725**, 75.

Stewart, R.W. and Townsend, A.A. [1951]
"Similarity and self-preservation in isotropic turbulence", Phil. Trans. Roy. Soc. London, **243A**, 359.

Strouhal, V. [1878]
"Uber eine besondere art der tonerregung", Ann. Phys. und chemie. New Series **5**, 216.
(**Quoted** by Hinze [1959])

Tan-Atichat, J.; Nagib, H.M. and Loehrke, R.I. [1982]
"Interaction of free-stream turbulence with screens and grids: A balance between turbulence scales", J. Fluid Mech., **114**, 501.

Taylor, G.I. [1921]
"Diffusion by continuous movements", Proc. Lond. Math. Soc., **20**, 196.

Taylor, G.I. [1932]
"Transport of vorticity and heat through fluids in turbulent motion", Proc. Roy. Soc. London, **A135**.

Taylor, G.I. [1935]
"Statistical theory of turbulence. Parts 1-4", Proc. Roy. Soc. London, **A151**, 421.

Taylor, G.I. [1936]
"Statistical theory of turbulence. Part 5", Proc. Roy. Soc. London, **A156**, 307.

Taylor, G.I. [1938]
"The spectrum of turbulence", Proc. Roy. Soc. London, **A164**, 476.

Thomson, W. [1981]
"Theory of vibration with applications", (Second edn.), George Allen and Unwin.

Thwaites, B. [1949]
"Approximate calculation of the laminar boundary layer", Aero. Qtly., **I**, 245.
(**Quoted** by Schlichting, H. [1968])

Torobin, L.B. and Gauvin, W.H. [1961]
"The drag coefficients of single spheres moving in steady and accelerated motion in a turbulent field", J. Am. Inst. Chem. E., **7**(4), 615.

Townsend, A.A. [1956]
"The structure of turbulent shear flow", Cambridge University Press.

Wygnanski, I. and Fiedler, H. [1969]
"Some measurements in the self-preserving jet", J. Fluid Mech., **38**(3), 577.

Wygnanski, I. and Fiedler, H. [1970]

"The two-dimensional mixing region", J. Fluid Mech., **41**(2), 327.

Young, A.D. and Winterbottom, N.E. [1940]

A.R.C., R.& M. **2400.**

(**Quoted** by Schlichting, H. [1968])

van der Hegge Zijnen, B.G. [1958]

"Heat transfer from horizontal cylinders to a turbulent air flow", Appl. Sci. Res., **A7**, 205.

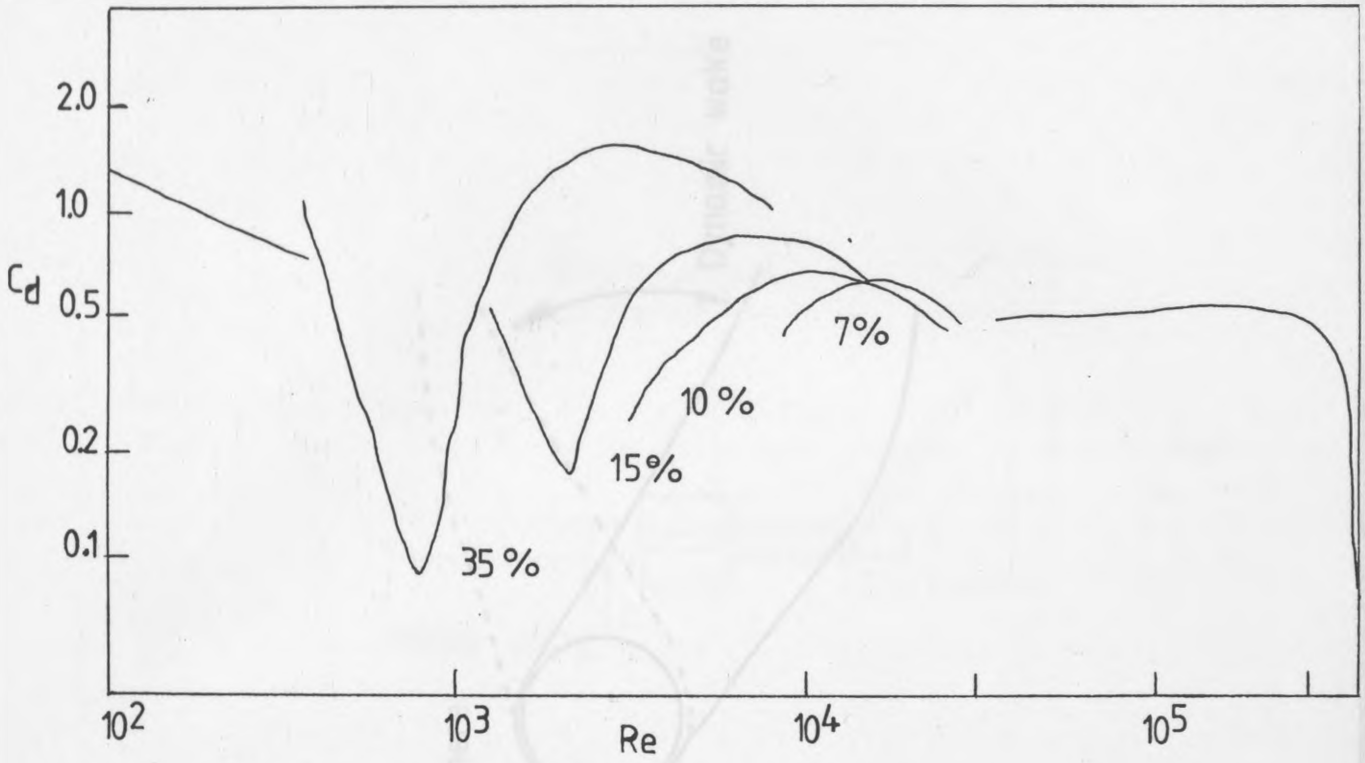

Figure 1.1 Standard drag coefficient variation with Reynolds number.

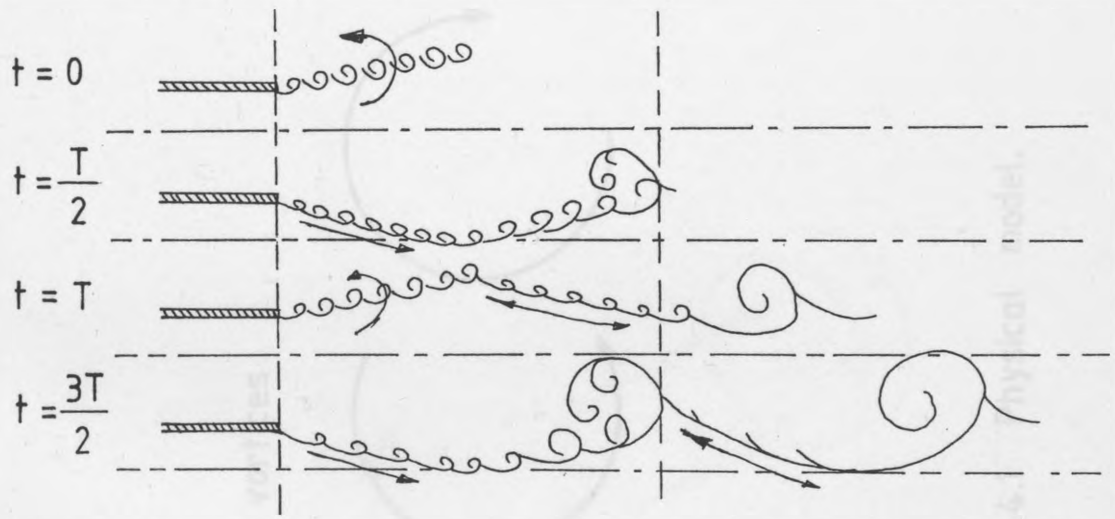

Fig. 2.1 Early development of vortical structures. (Laufer [1971])

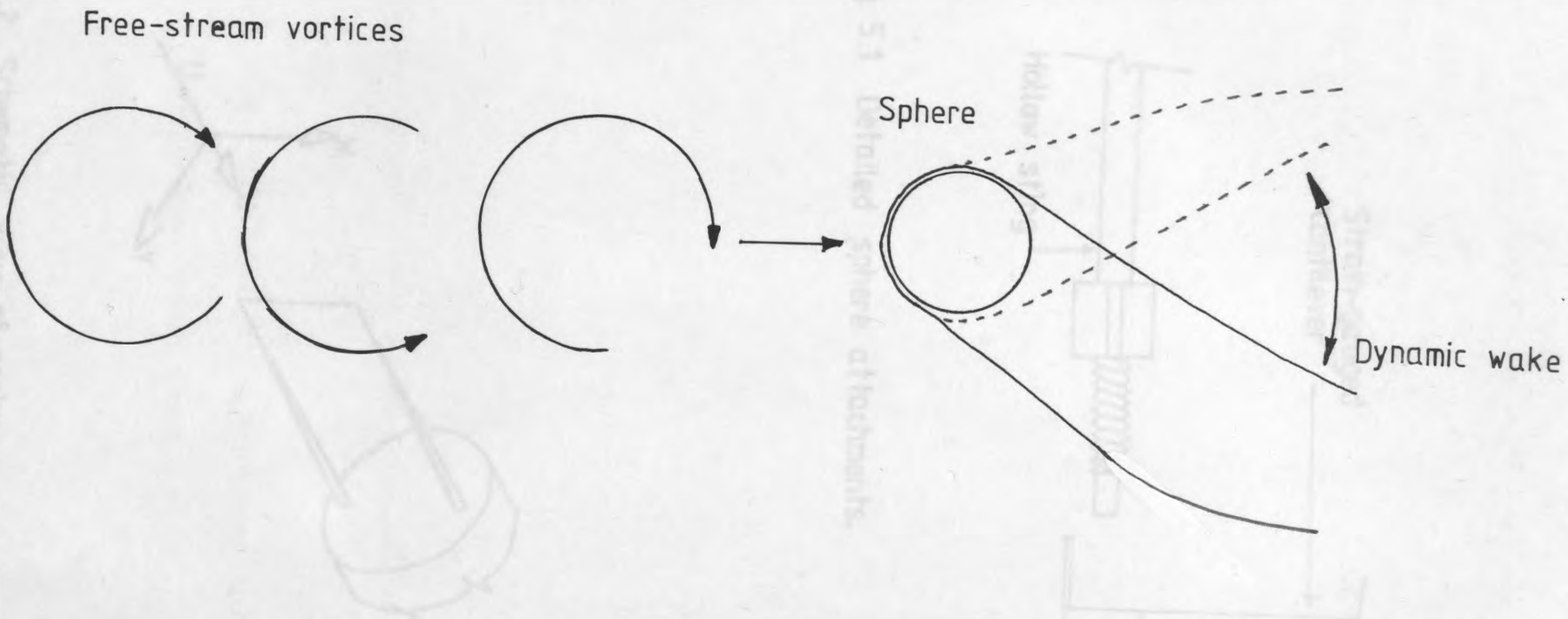

Fig. 4.1 Physical model.

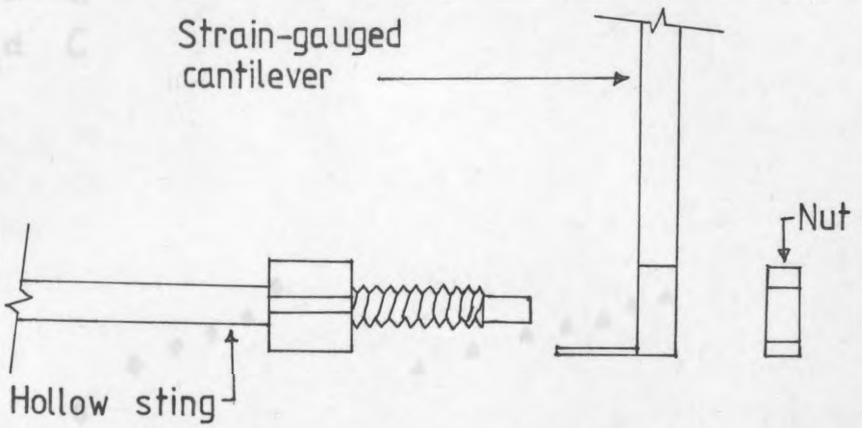

Fig. 5.1 Detailed sphere attachments.

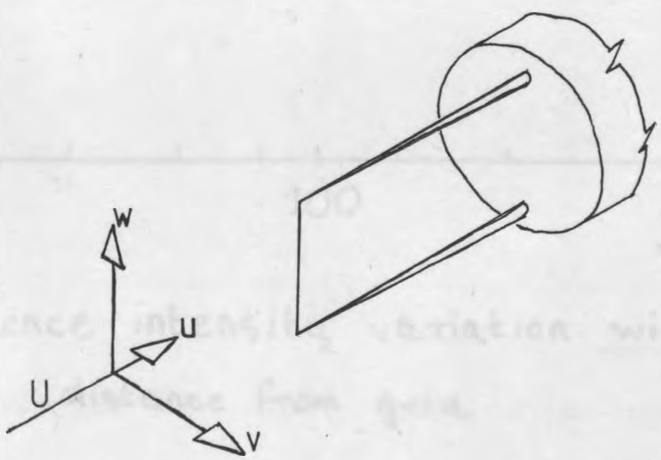

Fig. 5.2 Schematic view of probe.

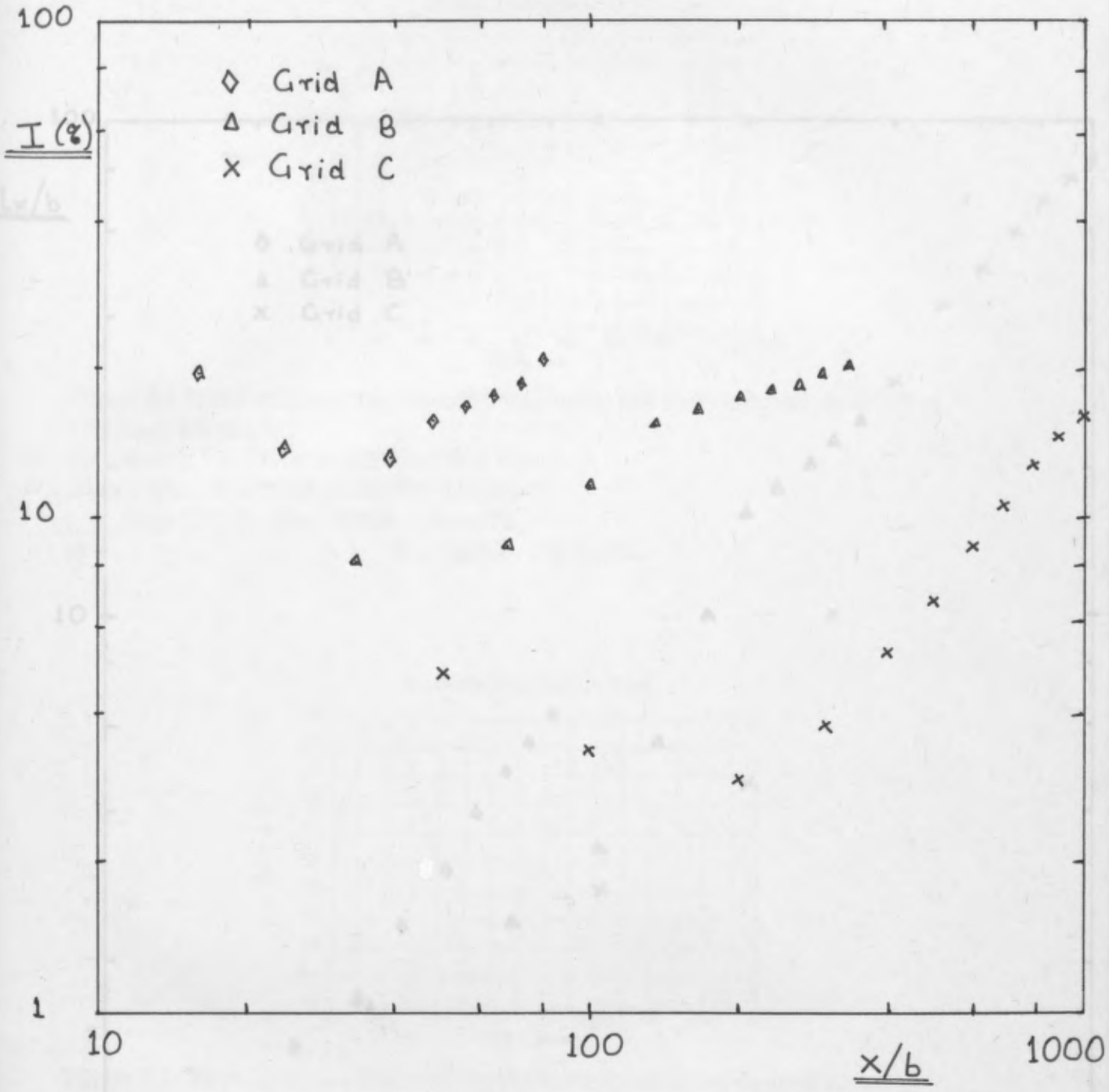

Fig. 6.1. Turbulence intensity variation with distance from grid.

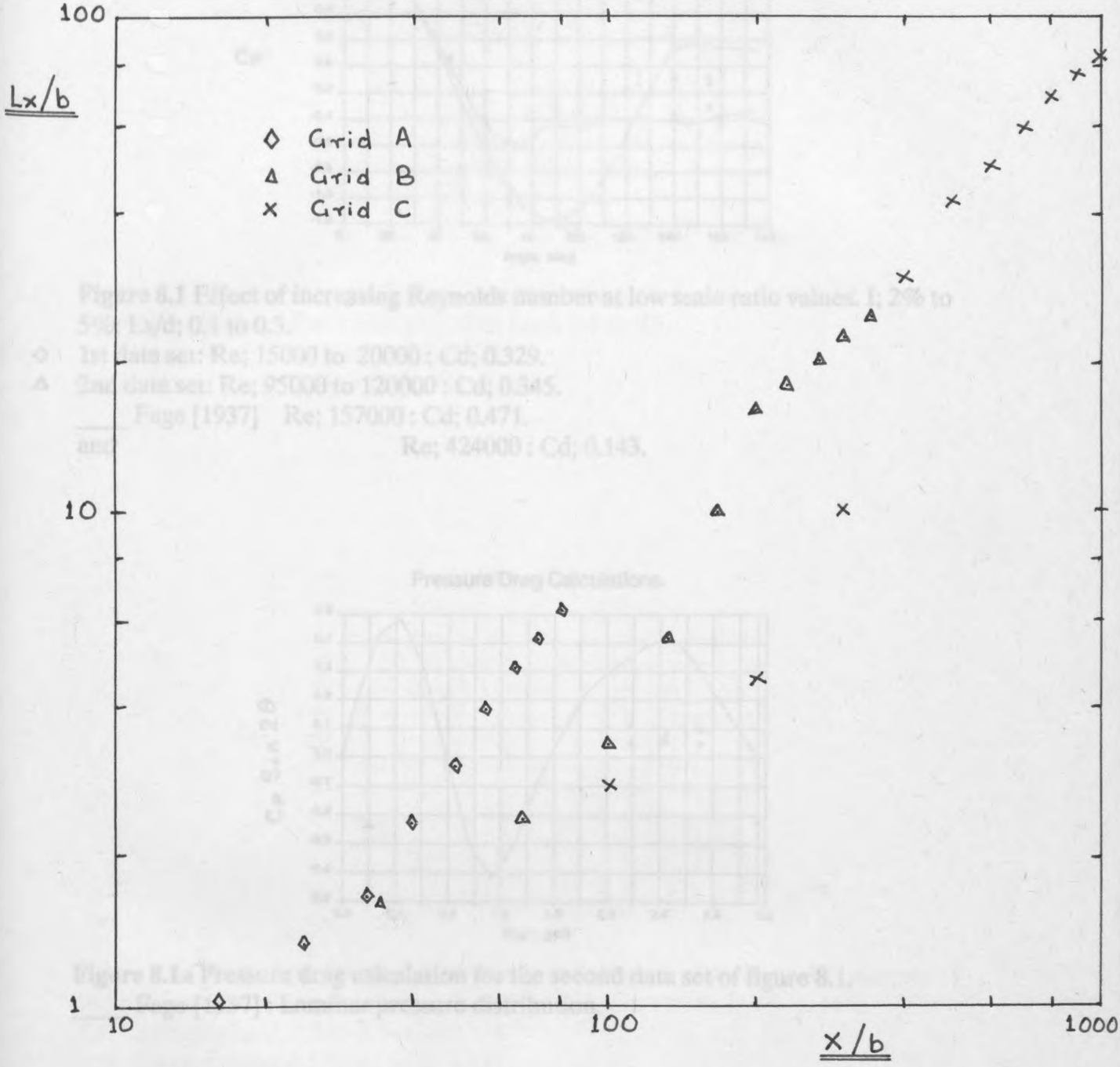

Fig. 6.2. Macroscale variation with distance from grid.

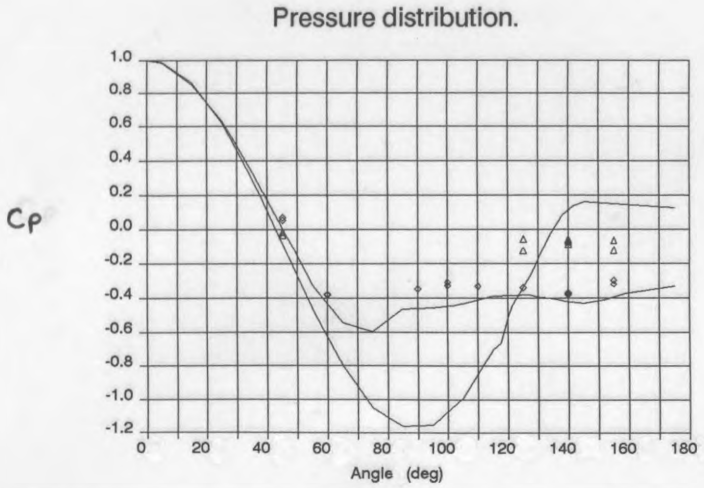

Figure 8.1 Effect of increasing Reynolds number at low scale ratio values. I; 2% to 5%: Lx/d; 0.1 to 0.3.

◇ 1st data set: Re; 15000 to 20000 : Cd; 0.329.

△ 2nd data set: Re; 95000 to 120000 : Cd; 0.345.

____ Fage [1937] Re; 157000 : Cd; 0.471.

and Re; 424000 : Cd; 0.143.

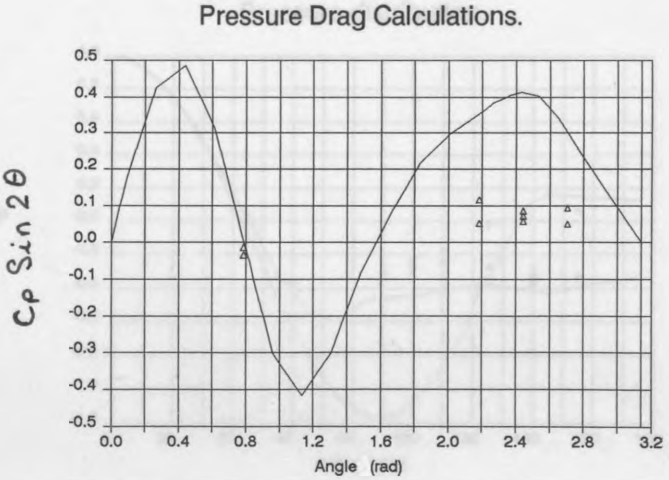

Figure 8.1a Pressure drag calculation for the second data set of figure 8.1.

____ Fage [1937] : Laminar pressure distribution.

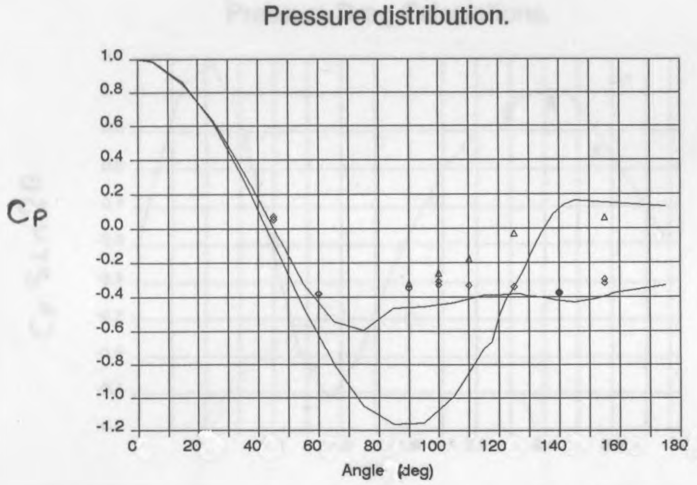

Figure 8.2 Effect of increasing turbulence intensity at low scale ratios and Reynolds numbers. Re; 15000 to 20000: Lx/d; 0.1 to 0.3.

◊ 1st data set: I; 2% to 5% : Cd; 0.329.

△ 2nd data set: I; 12% to 14% : Cd; 0.328.

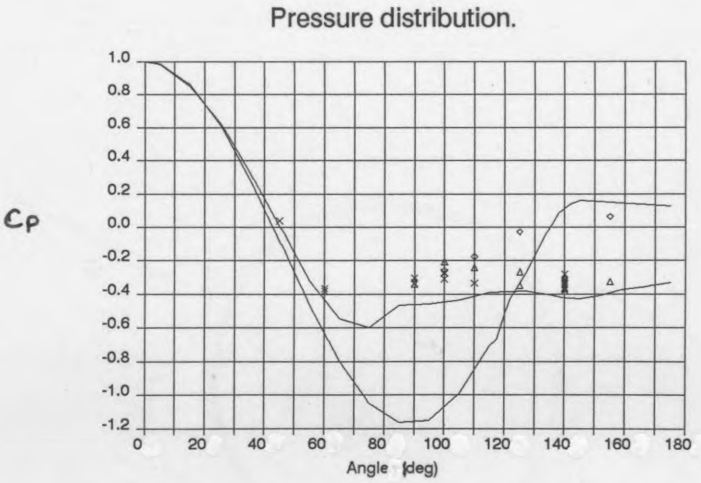

Figure 8.3 Effect of progressively increasing scale ratio for low Reynolds number and medium turbulence intensity values. Re; 15000 to 20000: I; 9% to 15%.

◊ 1st data set: Lx/d; 0.1 to 0.3 : Cd; 0.328.

△ 2nd data set: Lx/d; 0.5 to 0.6 : Cd; 0.353.

× 3rd data set: Lx/d; 1.5 to 3.0 : Cd; 0.486.

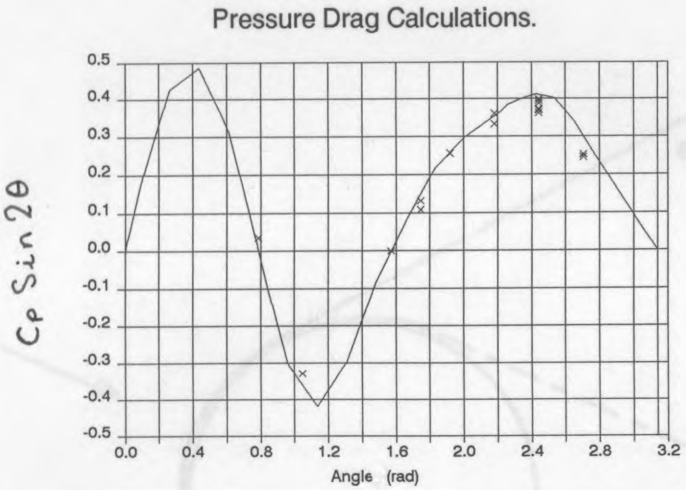

Figure 8.3a Pressure drag calculation for the third data set of figure 8.3.
____ Fage [1937] : Laminar pressure distribution.

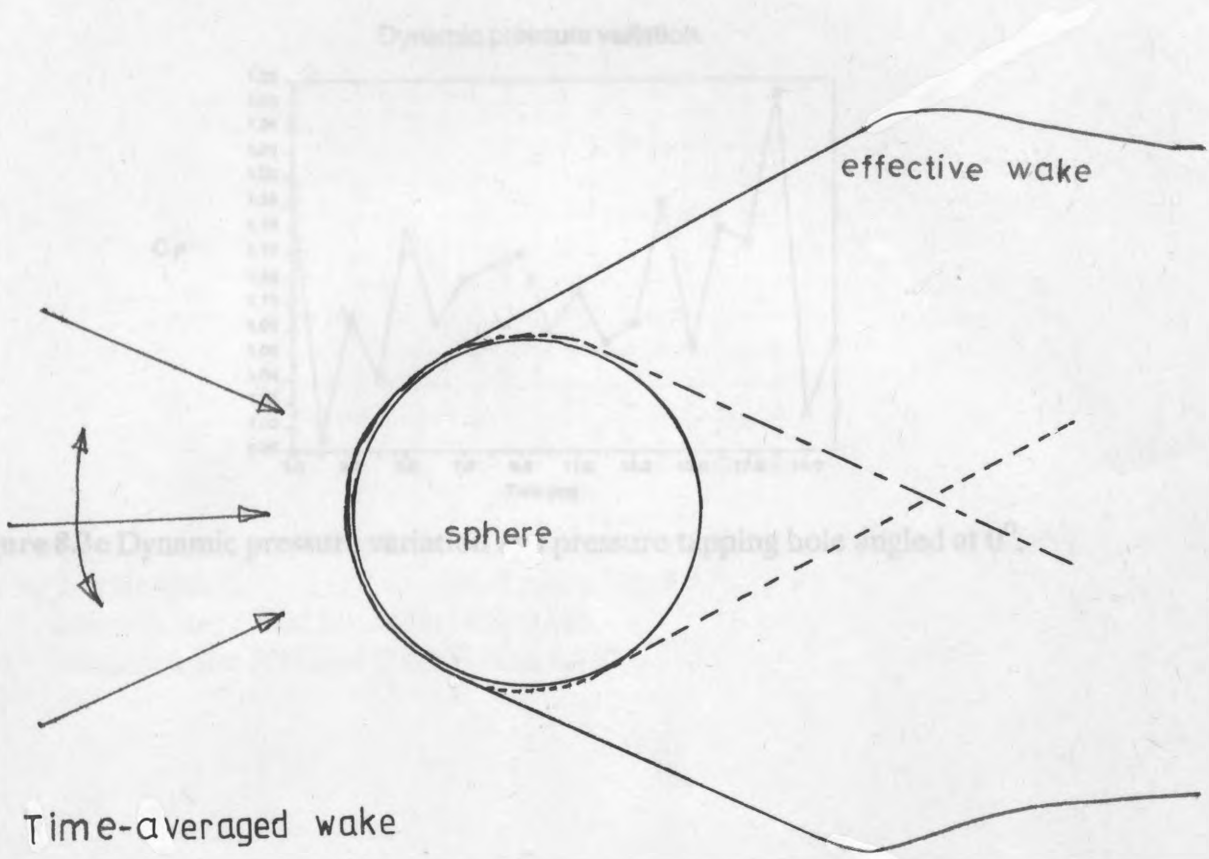

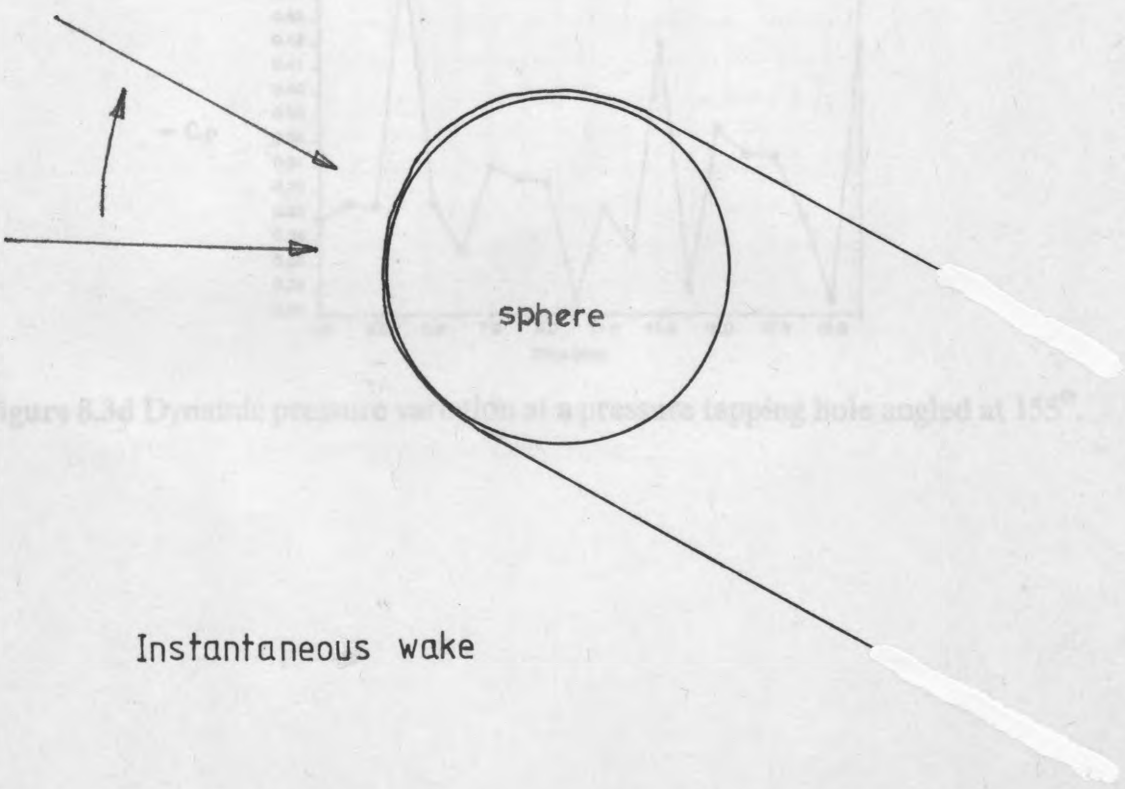

Fig. 8.3b Suggested wake development.

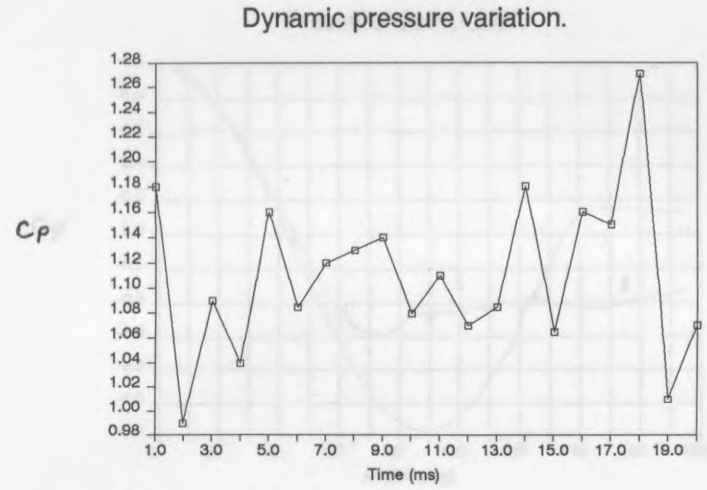

Figure 8.3c Dynamic pressure variation at a pressure tapping hole angled at 0^{o}.

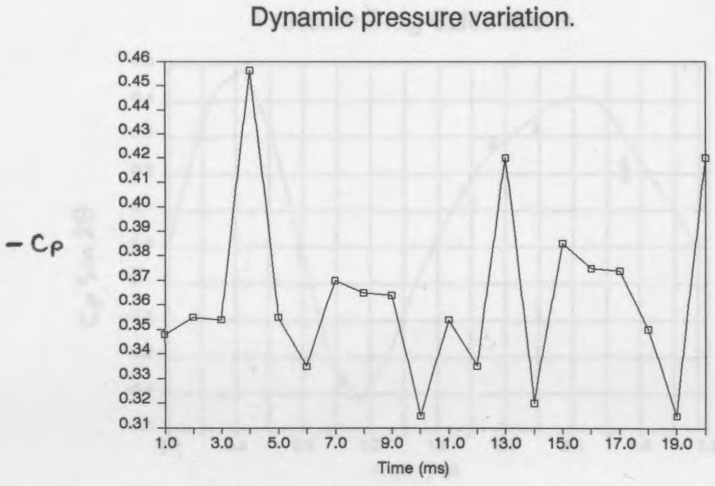

Figure 8.3d Dynamic pressure variation at a pressure tapping hole angled at 155^{o}.

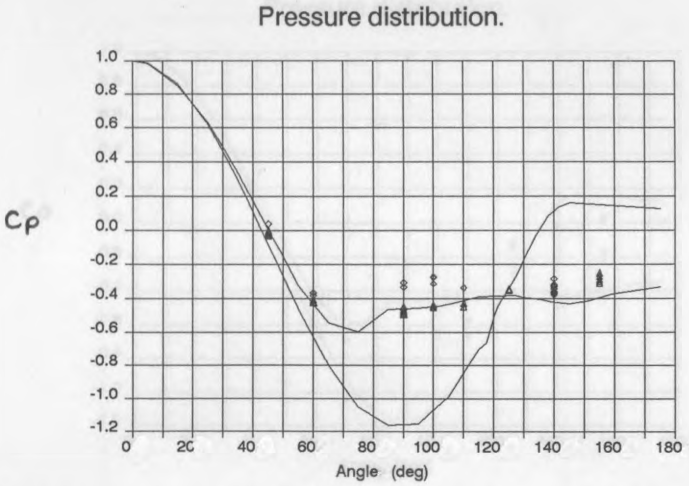

Figure 8.4 Effect of increasing Reynolds numbers for medium turbulence intensity and high scale ratios. I; 8% to 10%: Lx/d; 1.5 to 3.0.

◇ 1st data set: Re; 15000 to 20000 : Cd; 0.486.

△ 2nd data set: Re; 50000 to 100000 : Cd; 0.782.

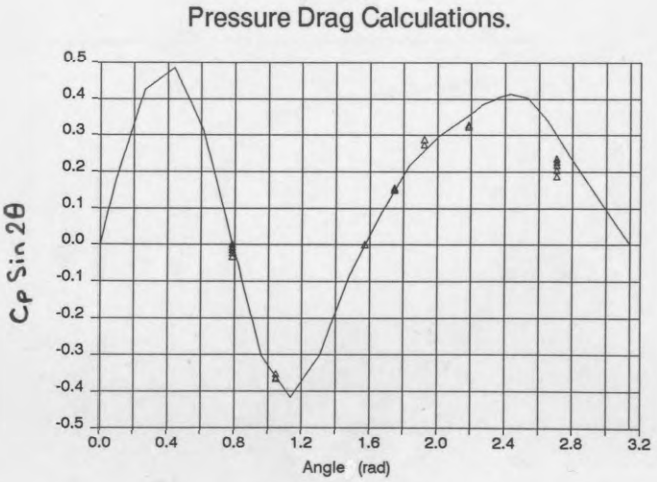

Figure 8.4a Pressure drag calculation for the second data set of figure 8.4.

____ Fage [1937] : Laminar pressure distribution.

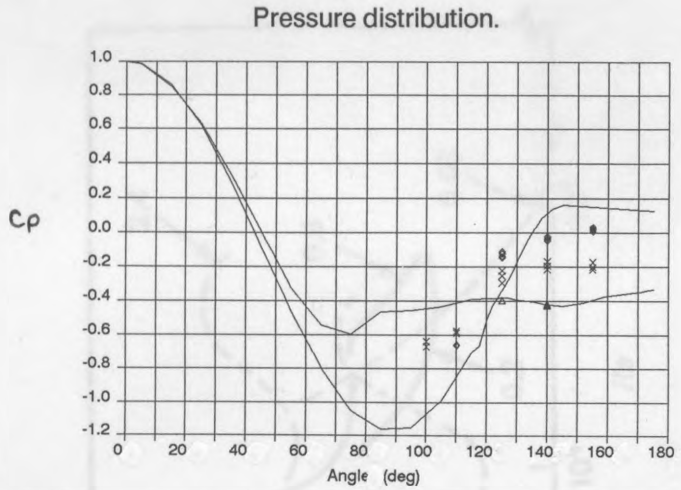

Figure 8.5 Effect of progressively increasing scale ratio at high turbulence intensity and Reynolds numbers. Re; 50000 to 80000: I;14% to 19%.

◇ 1st data set: Lx/d; 0.6 to 0.7: Cd; 0.576.

△ 2nd data set: Lx/d; 1.4 to 1.6: Cd; 0.636.

× 3rd data set: Lx/d; 2.0 to 2.1: Cd; 0.606.

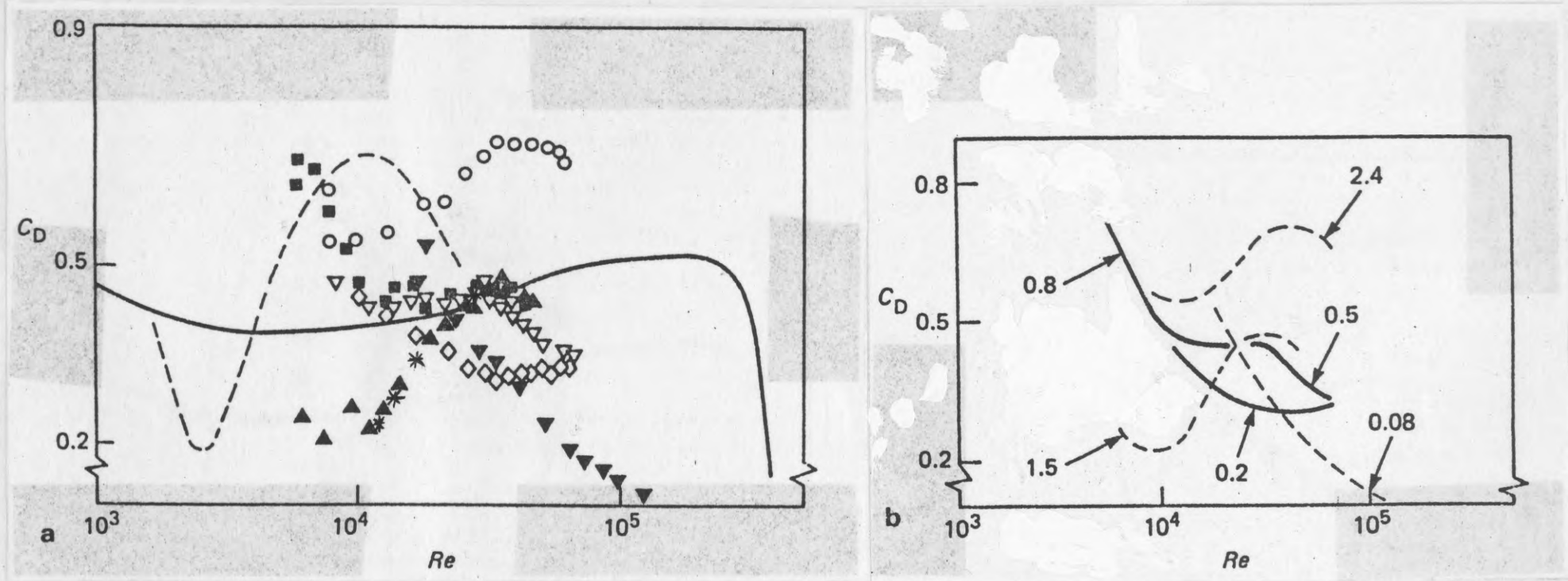

Fig. 8.6 Effect of scale ratio on the drag coefficient for turbulence intensities of 10% ± 2% (Neve[1986])

* Present results: I;11% , Lx/d;1·5

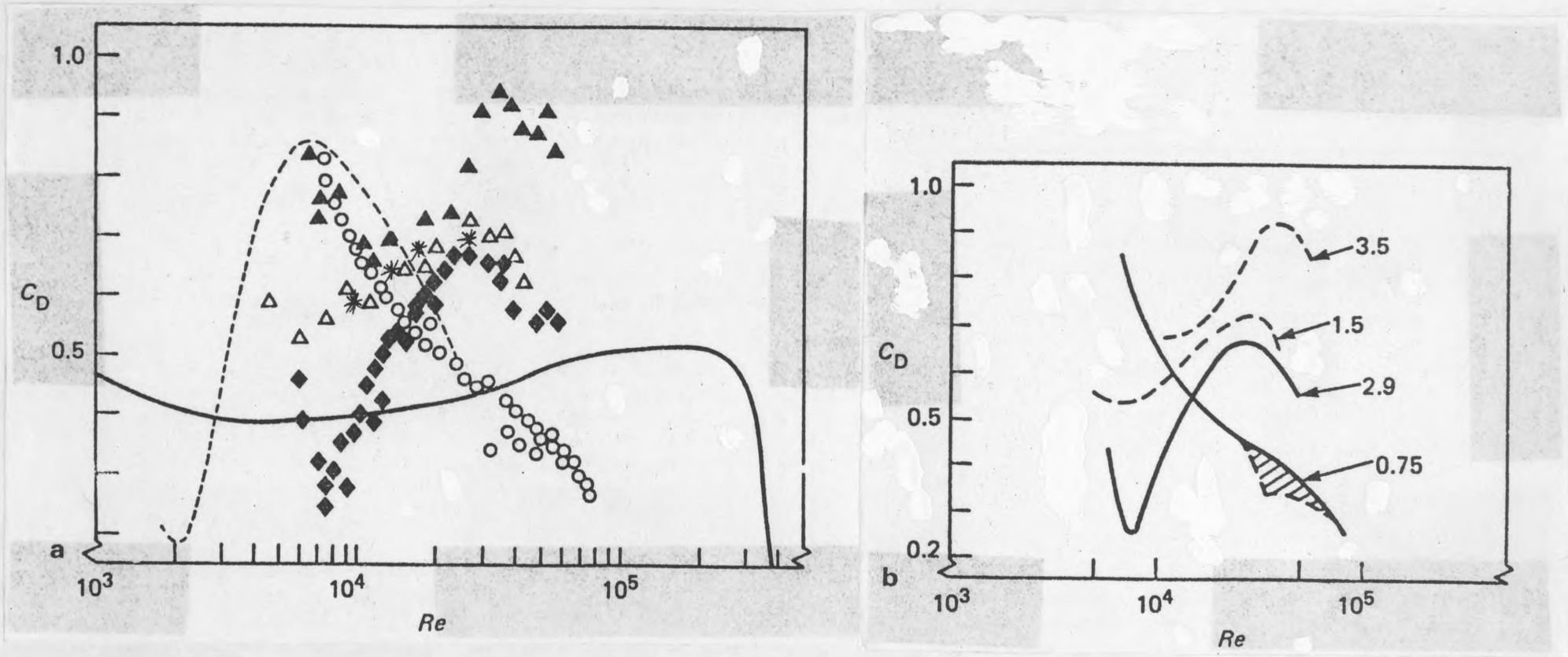

Fig. 8.7 Effect of scale ratio on the drag coefficient for turbulence intensities of 16% ± 2% (Neve[1986])

✳ Present results: I; 16%, Lx/d; 1·5

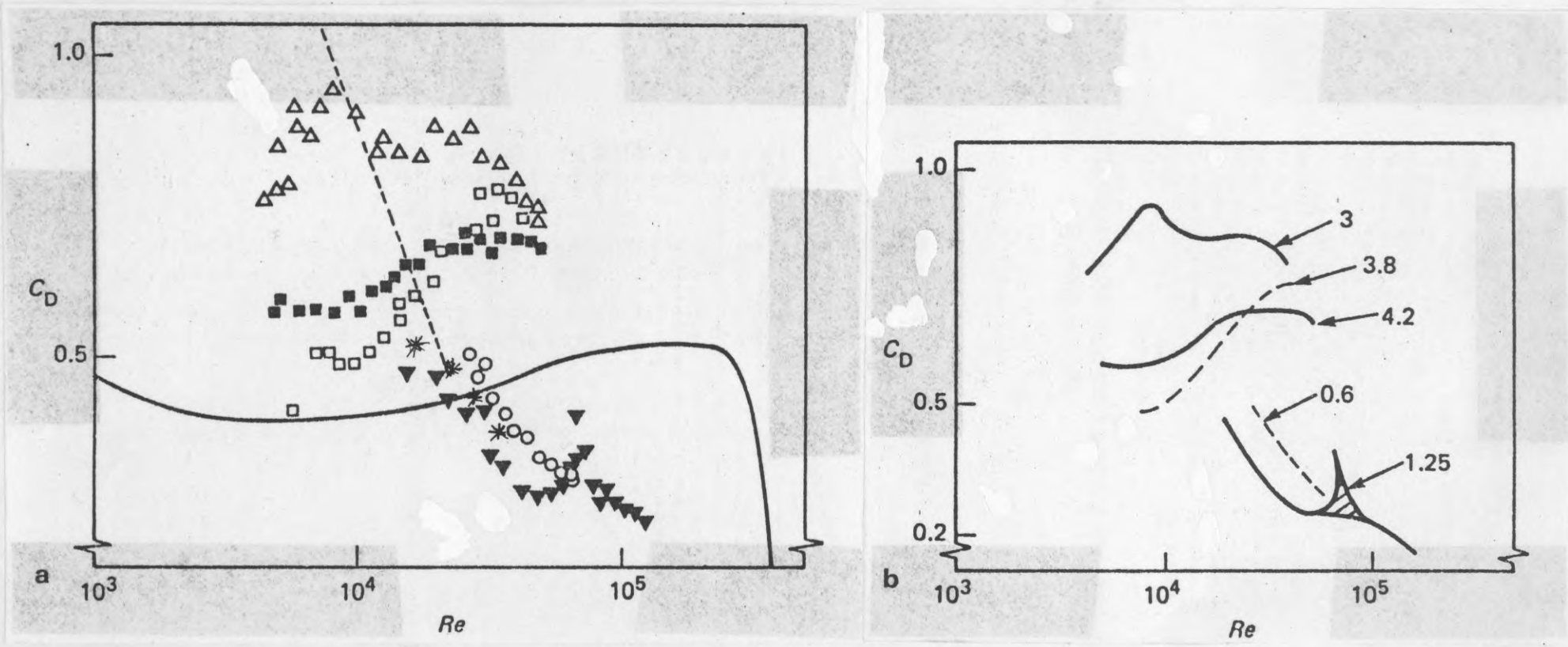

Fig. 8.8 Effect of scale ratio on the drag coefficient for turbulence intensities of 22% ± 2% (Neve [1986])

✱ Present results: I; 20%, Lx/d; 1·5

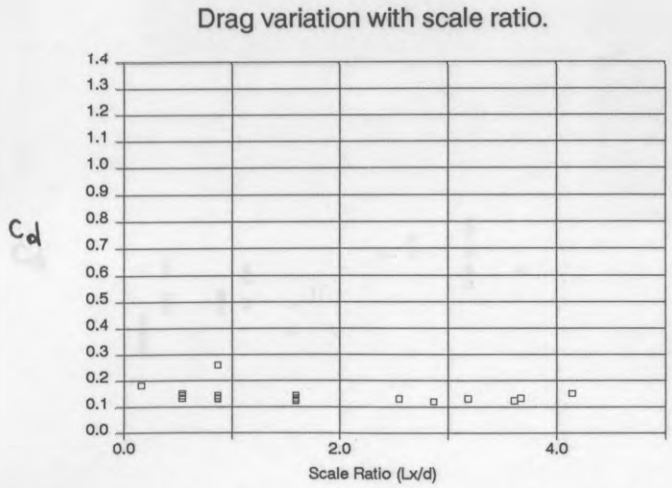

Figure 8.9 Effect of scale ratio on the drag coefficient for turbulence intensities of between 13% and 20%. Re; 5000 to 6300.

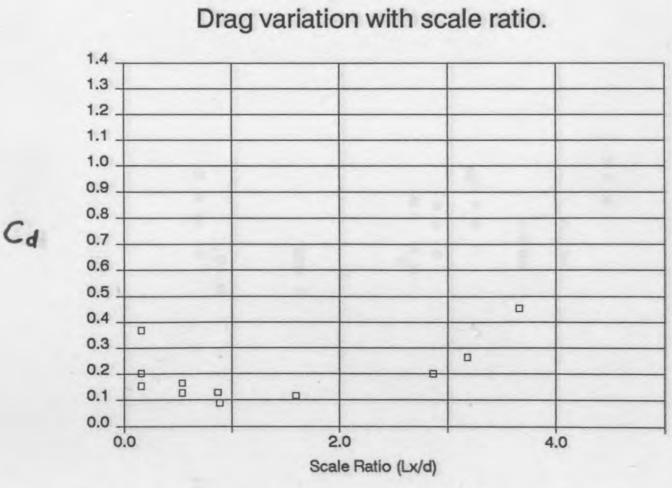

Figure 8.10 Effect of scale ratio on the drag coefficient for Reynolds numbers of between 10000 and 11000. I; 11% to 17%.

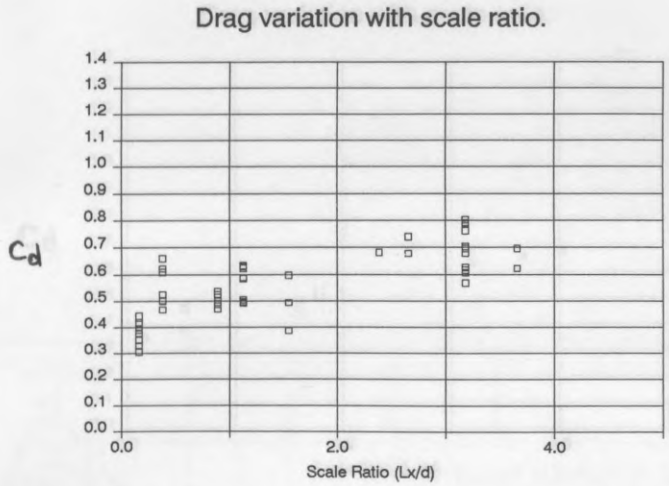

Figure 8.11 Effect of scale ratio on the drag coefficient for Reynolds numbers of between 21000 and 30000. I; 11% to 14%.

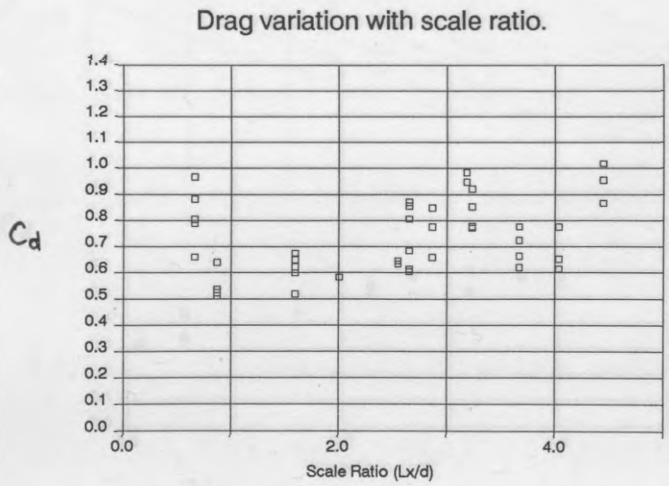

Figure 8.12 Effect of scale ratio on the drag coefficient for Reynolds numbers of between 21000 and 30000. I; 18% to 20%.

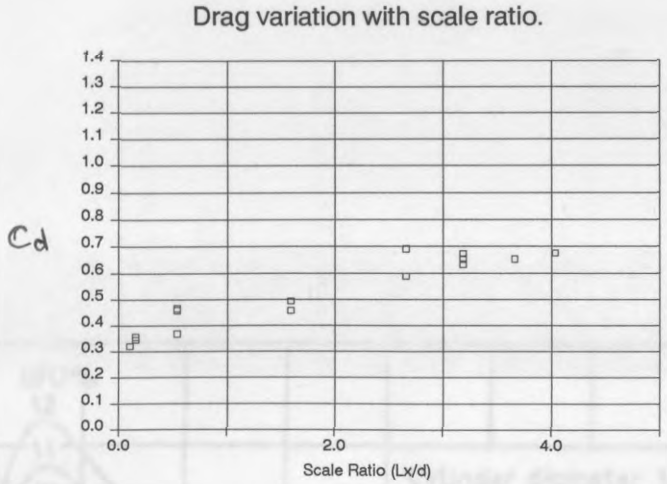

Figure 8.13 Effect of scale ratio on the drag coefficient for Reynolds numbers of between 80000 and 85000. I; 3.5% to 15%.

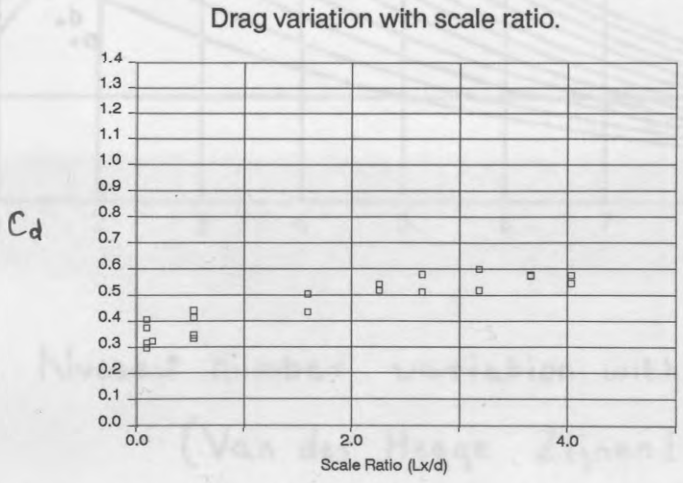

Figure 8.14 Effect of scale ratio on the drag coefficient for Reynolds numbers of between 90000 and 100000. I; 3.5% to 15%.

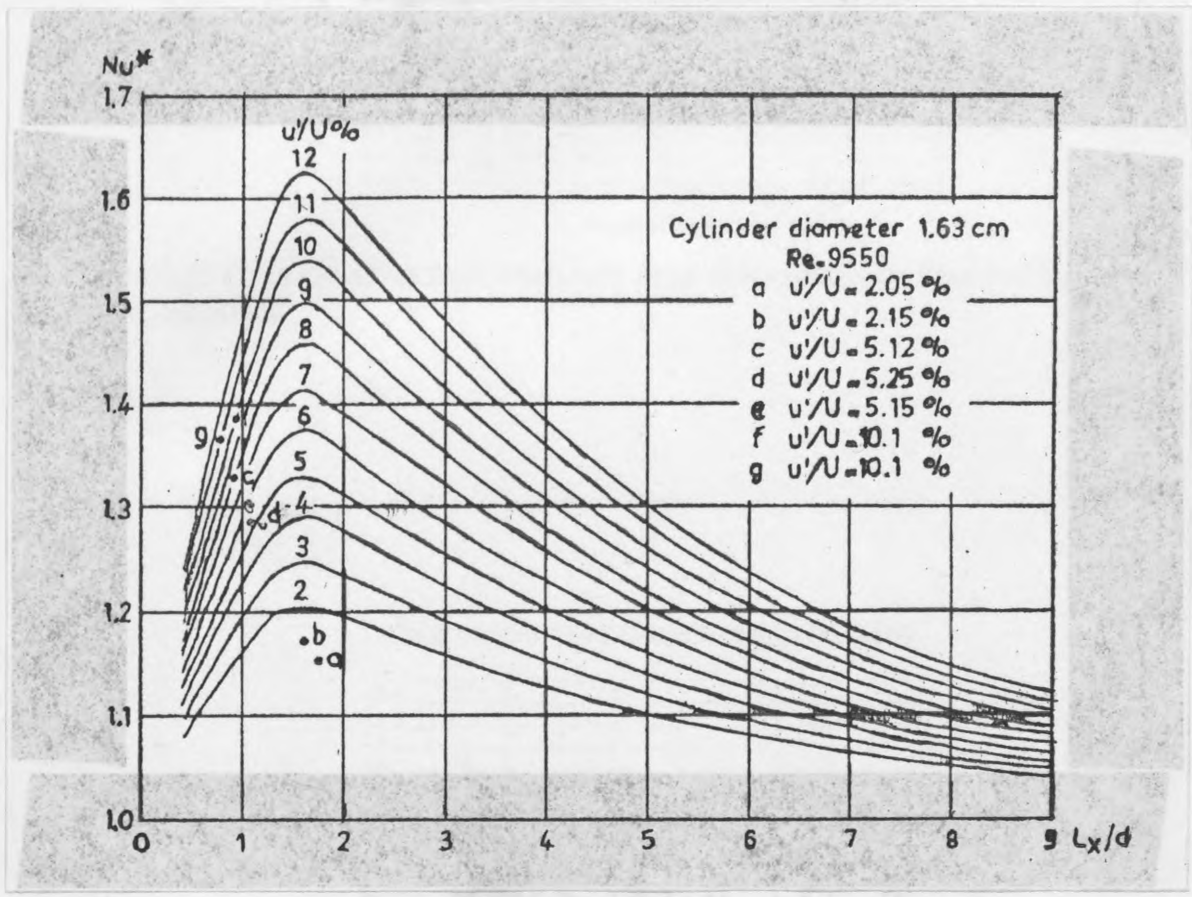

Fig. 8.14 a. Nusselt number variation with scale ratio

(Van der Hegge Zijnen [1958])

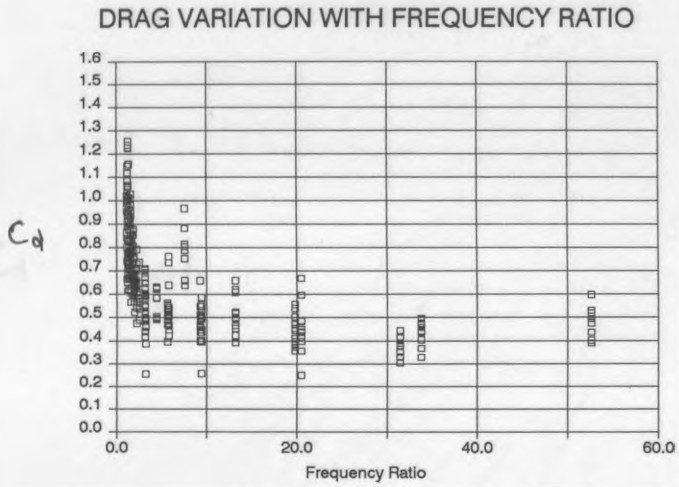

Figure 8.15 Drag variation with frequency ratio at Reynolds numbers of between 21000 and 30000.

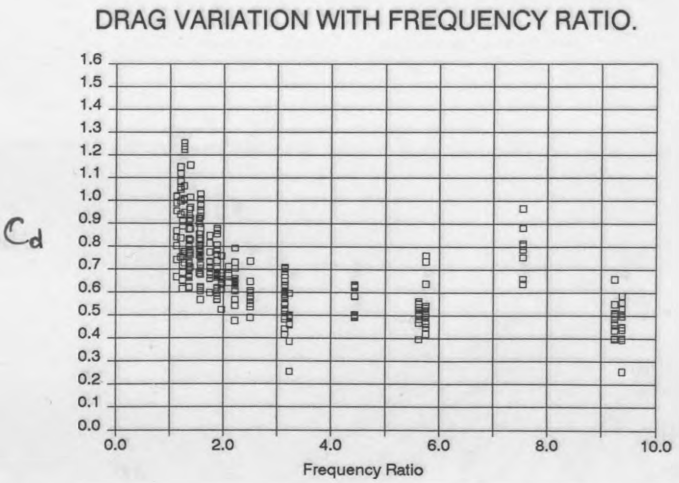

Figure 8.15(a) Expanded view of figure 8.15, showing the resonance position.

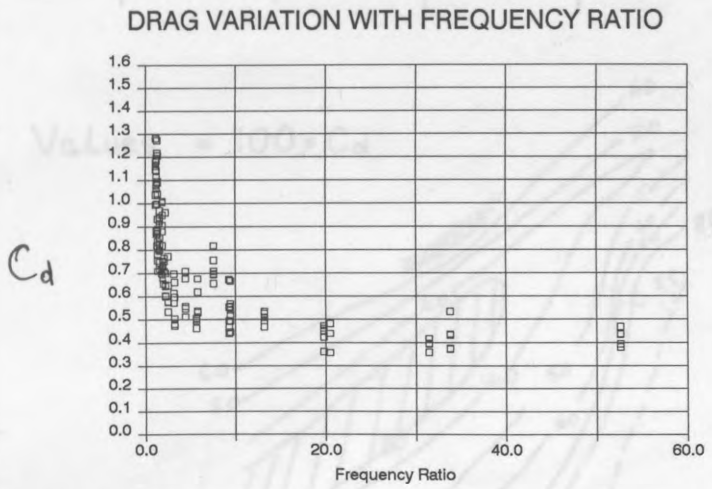

Figure 8.16 Drag variation with frequency ratio at Reynolds numbers of between 41000 and 45000.

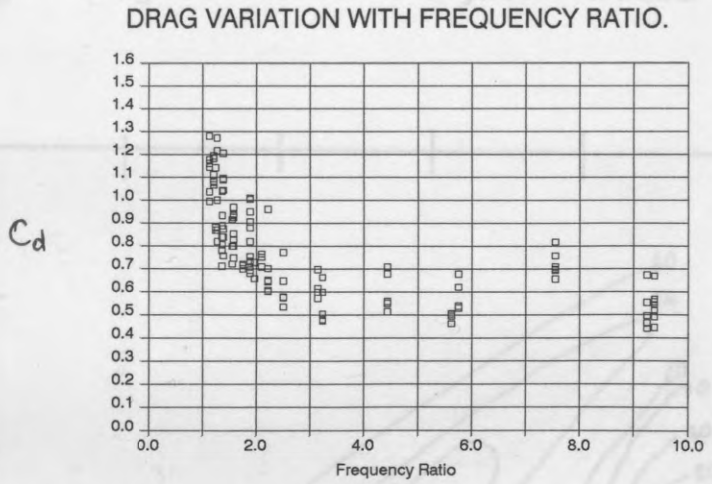

Figure 8.16(a) Expanded view of figure 8.16, showing a reduced amplitude resonance position.

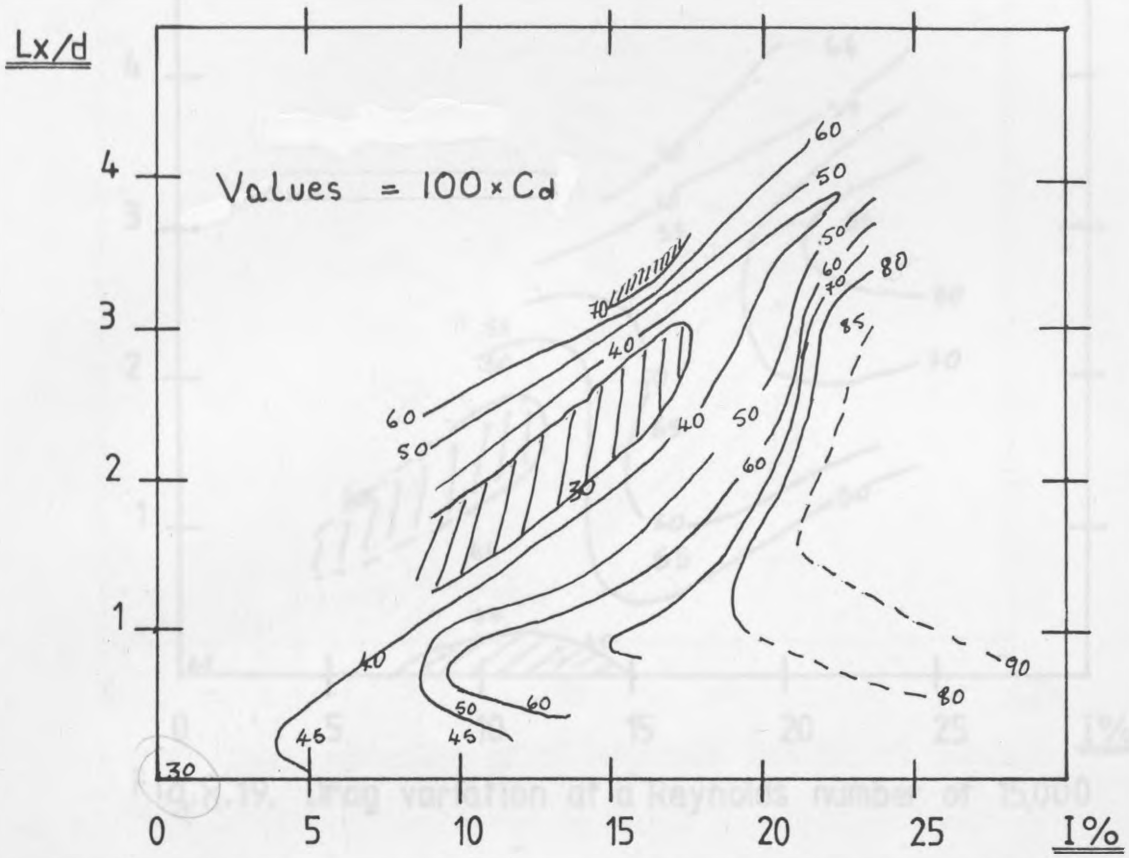

Fig. 8.17. Drag variation at a Reynolds number of 6,000

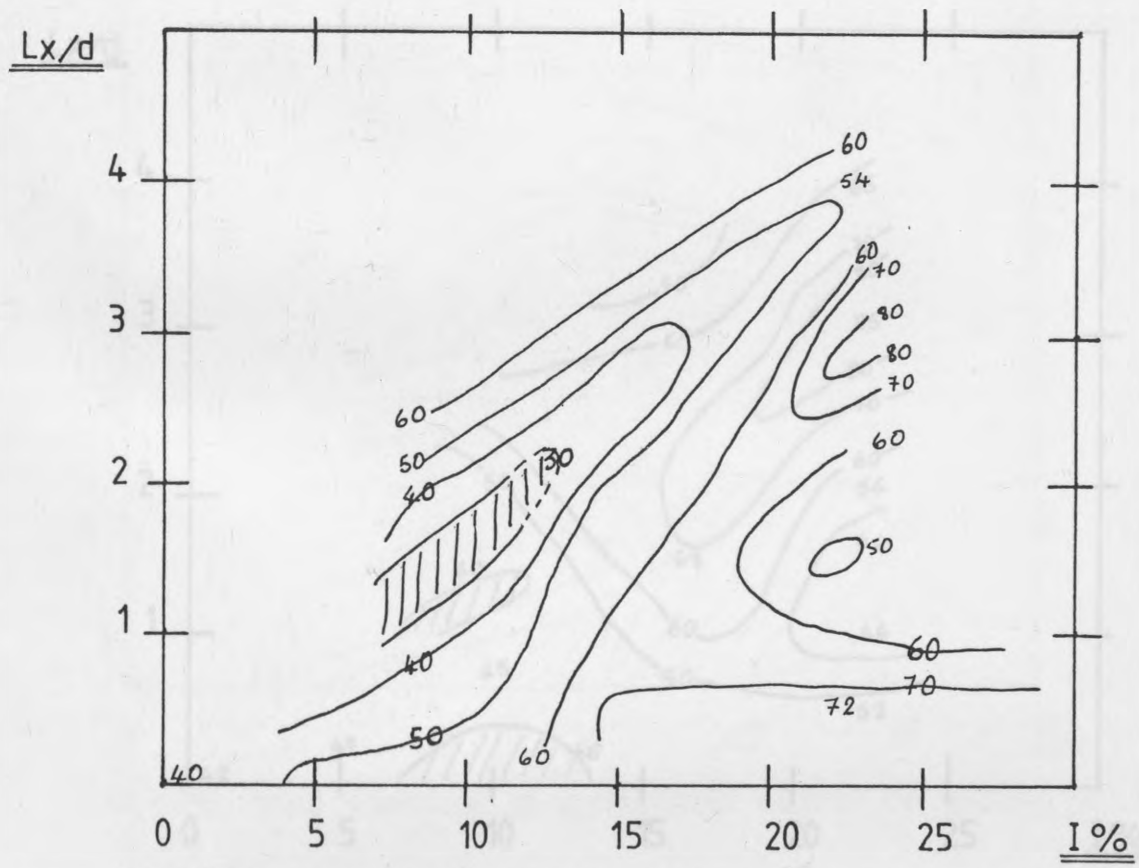

Fig. 8.18. Drag variation at a Reynolds number of 10,000

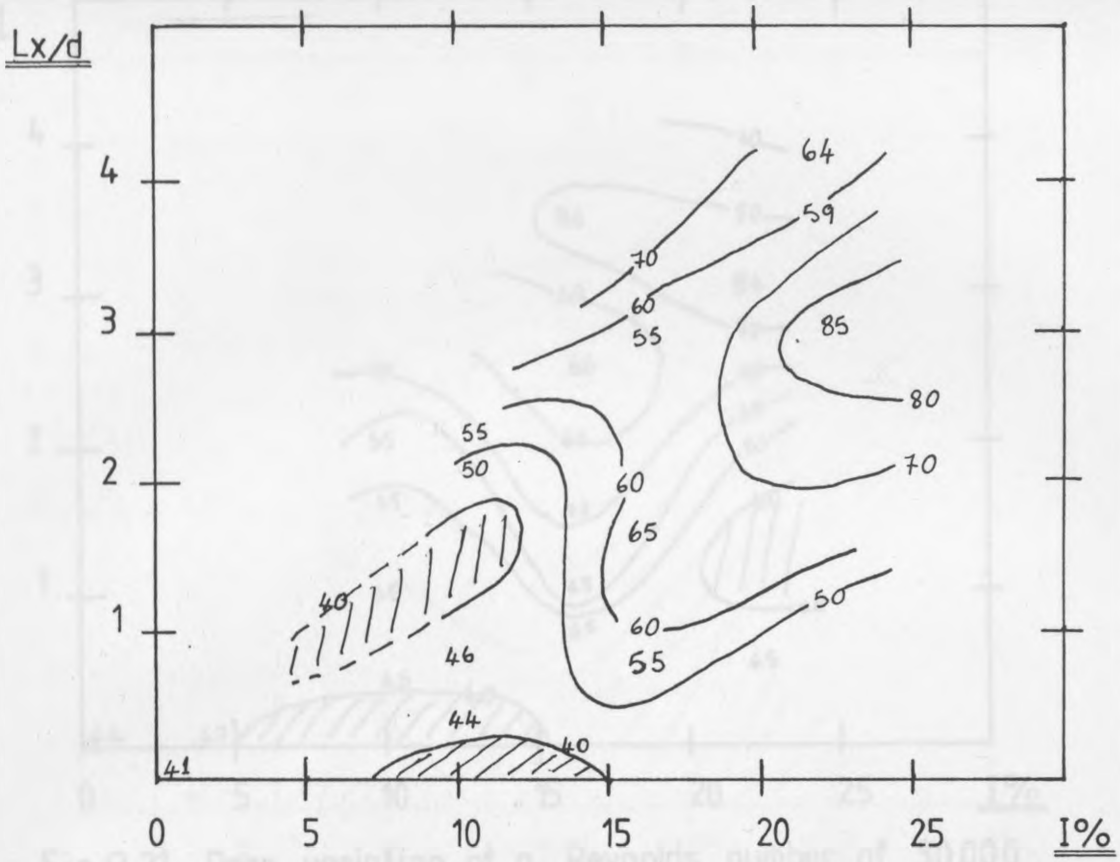

Fig.8.19. Drag variation at a Reynolds number of 15,000

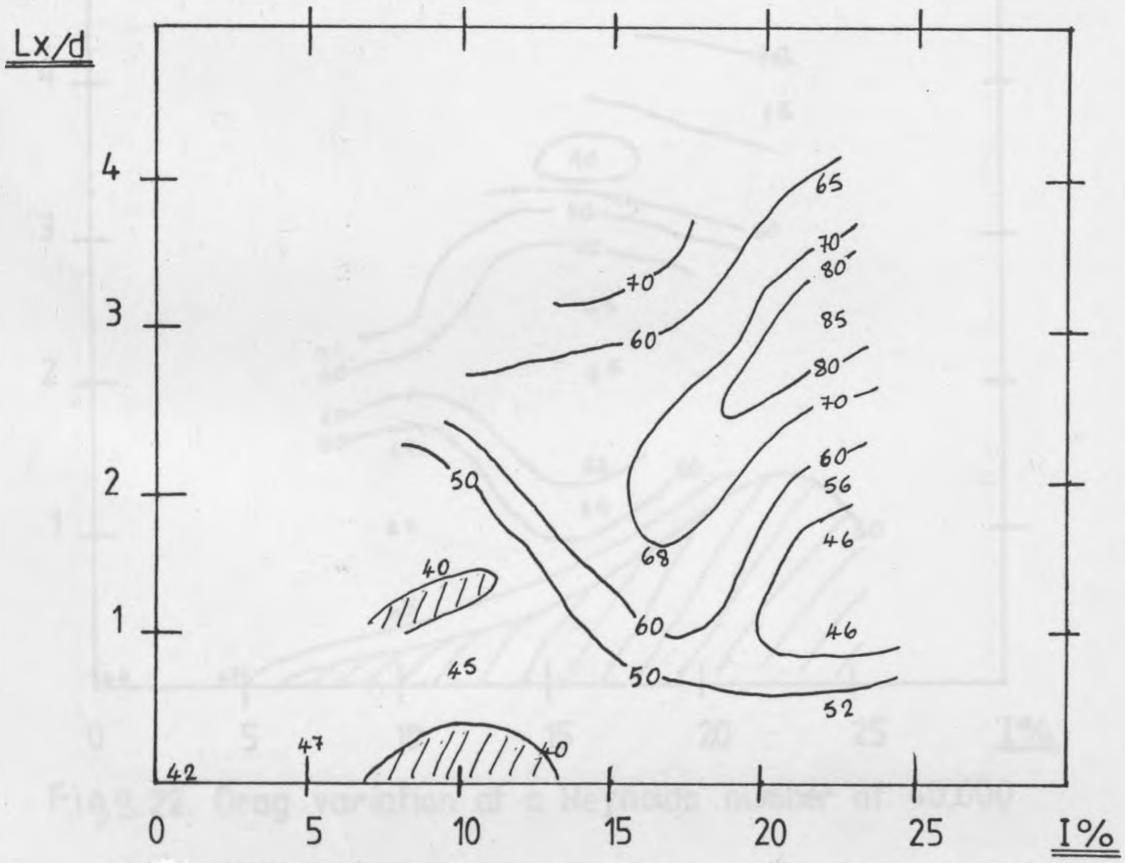

Fig.8.20. Drag variation at a Reynolds number of 20,000

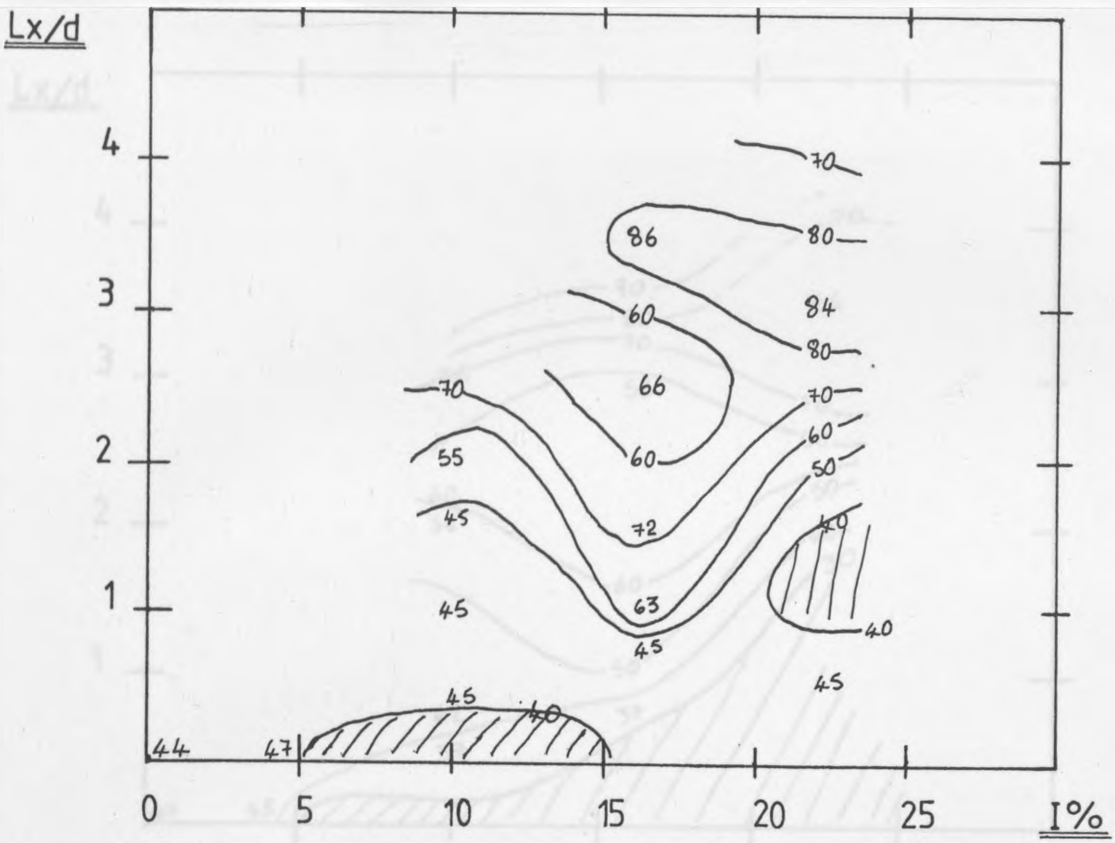

Fig.8.21. Drag variation at a Reynolds number of 30,000

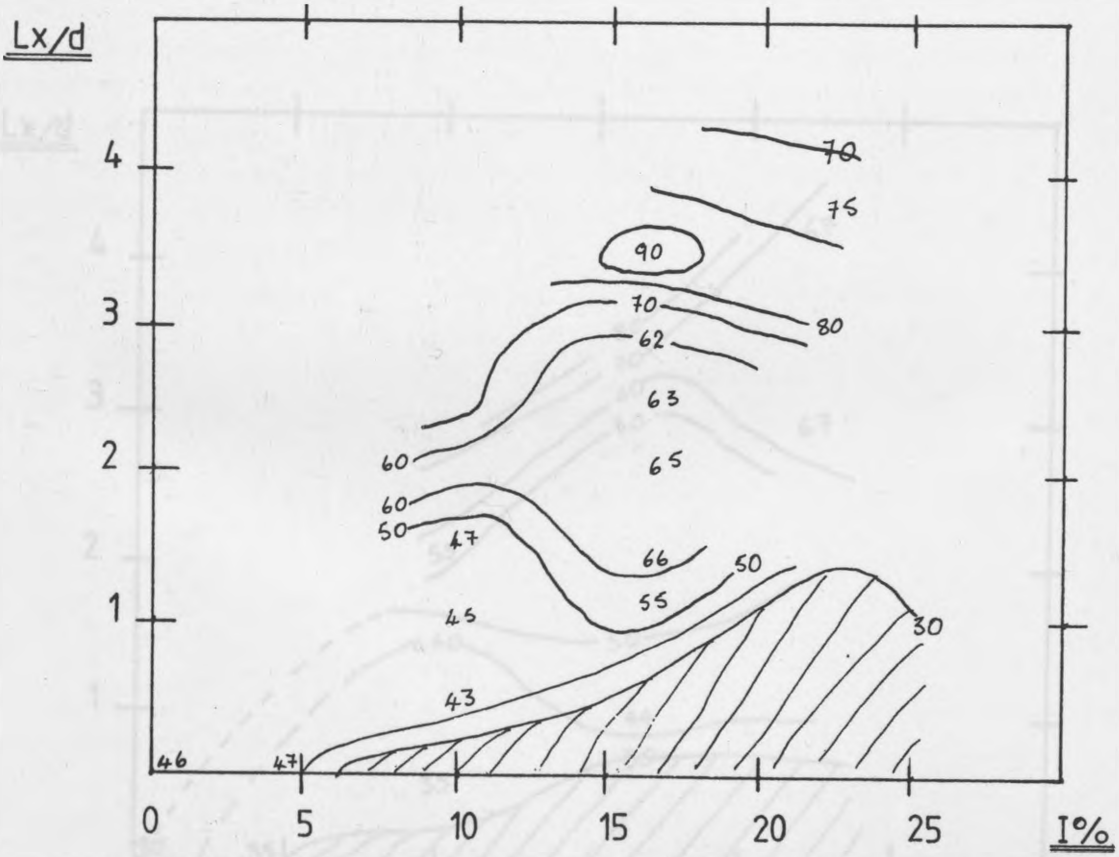

Fig.8.22. Drag variation at a Reynolds number of 40,000

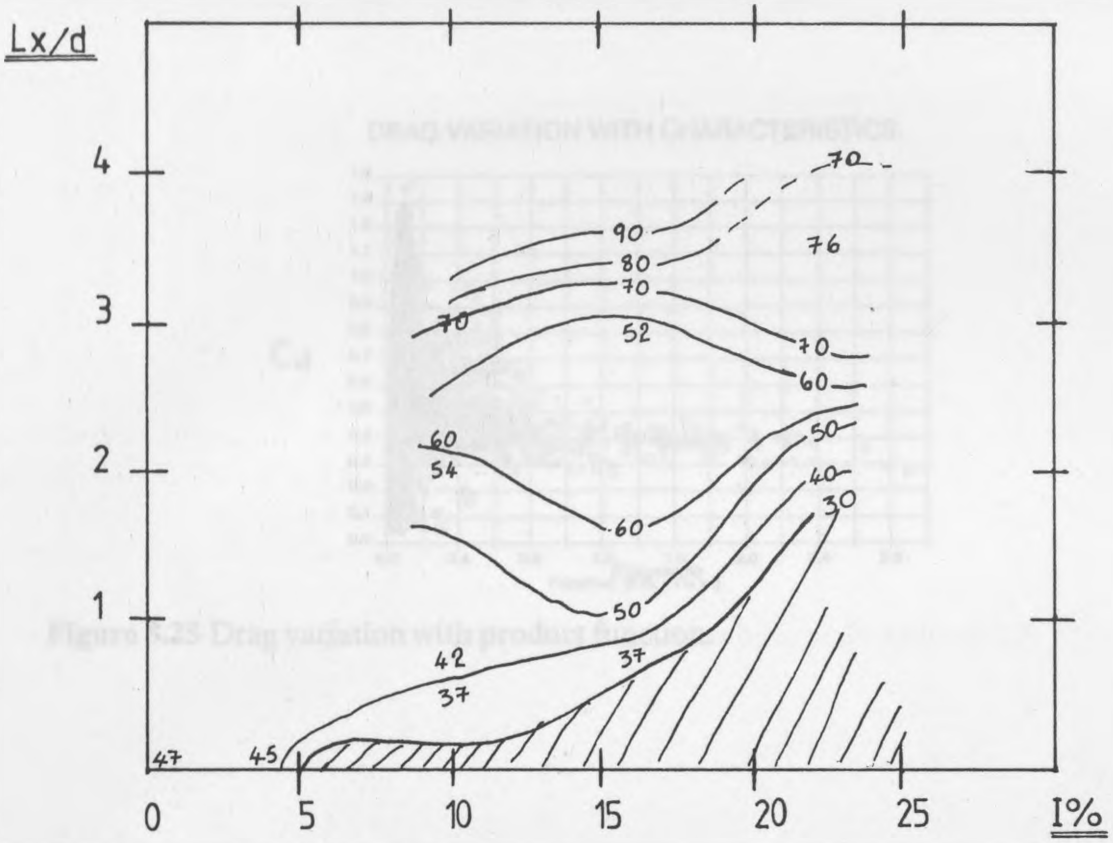

Fig. 8.23. Drag variation at a Reynolds number of 50,000

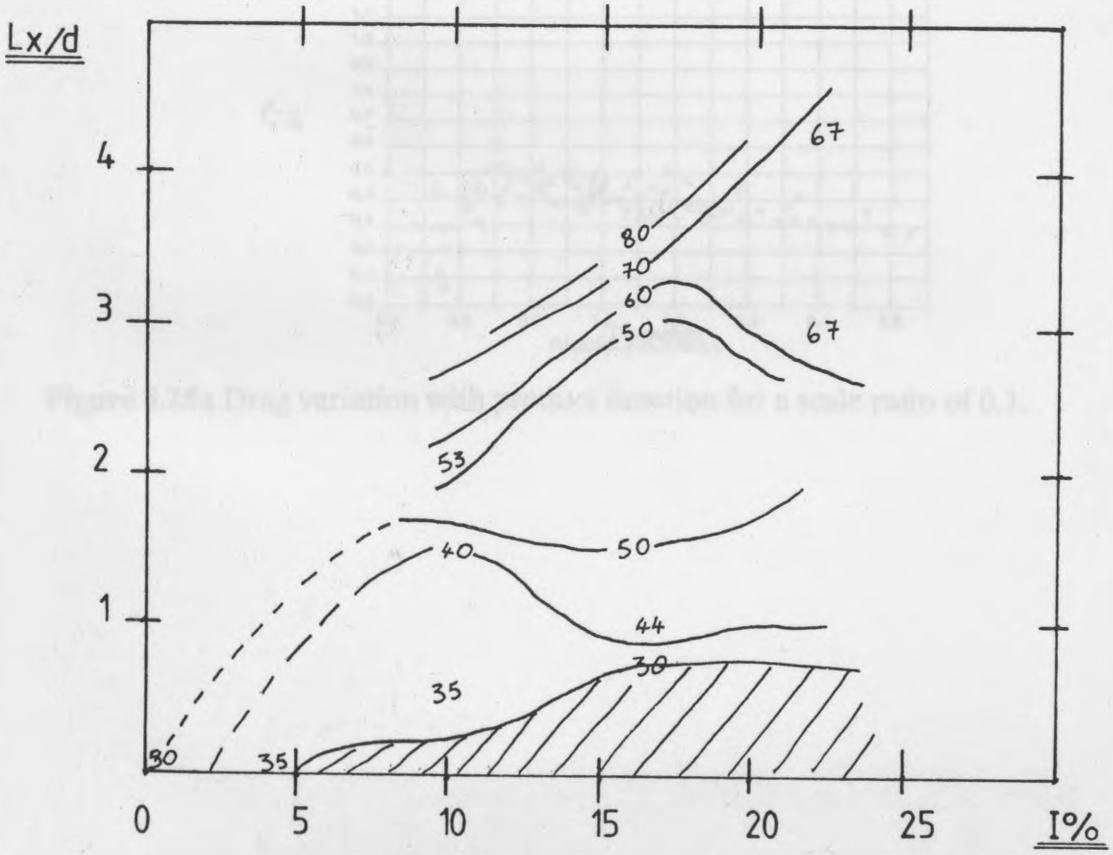

Fig.8.24. Drag variation at a Reynolds number of 70,000

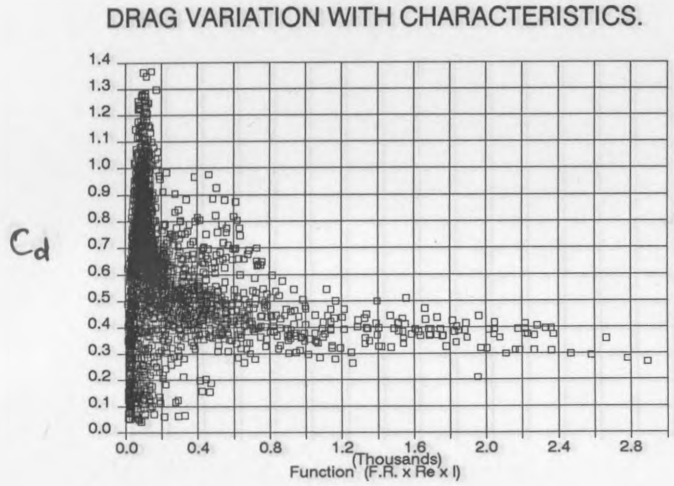

Figure 8.25 Drag variation with product function.

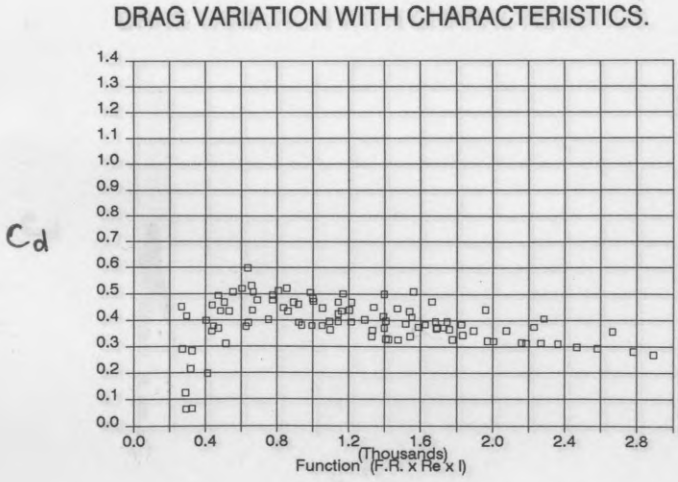

Figure 8.25a Drag variation with product function for a scale ratio of 0.1.

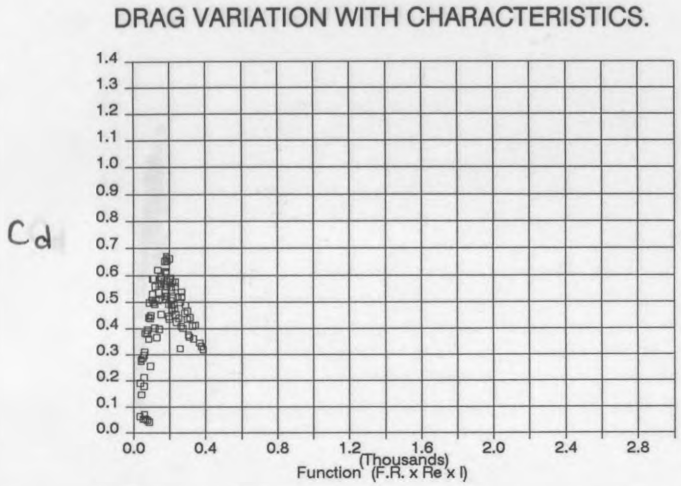

Figure 8.25b Drag variation with product function for a scale ratio of 0.5.

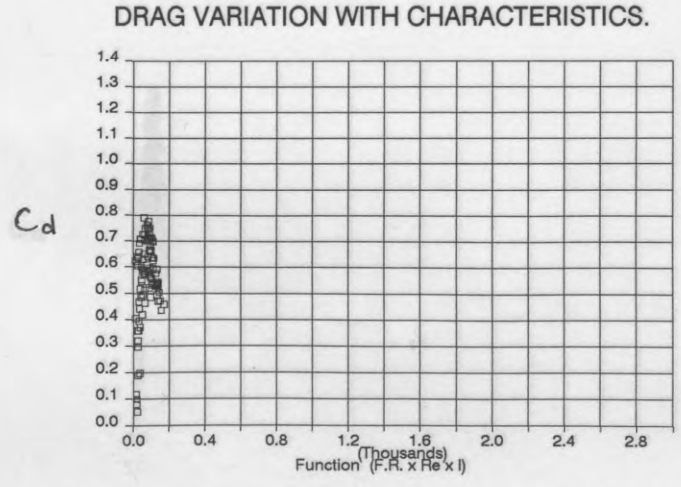

Figure 8.25c Drag variation with product function for a scale ratio of 1.5.

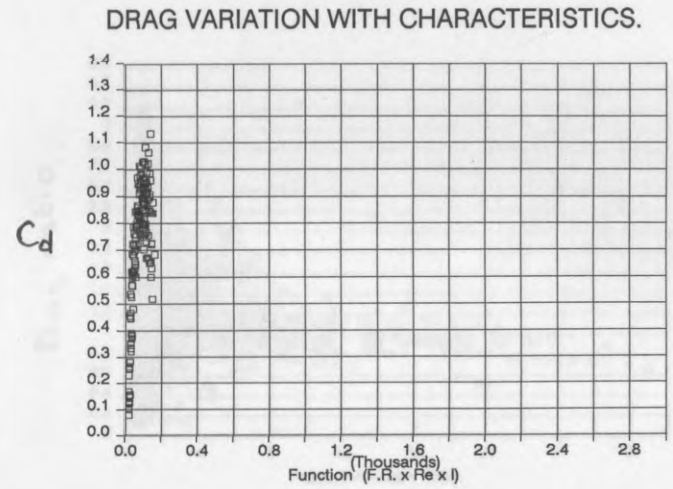

Figure 8.25d Drag variation with product function for a scale ratio of 3.2.

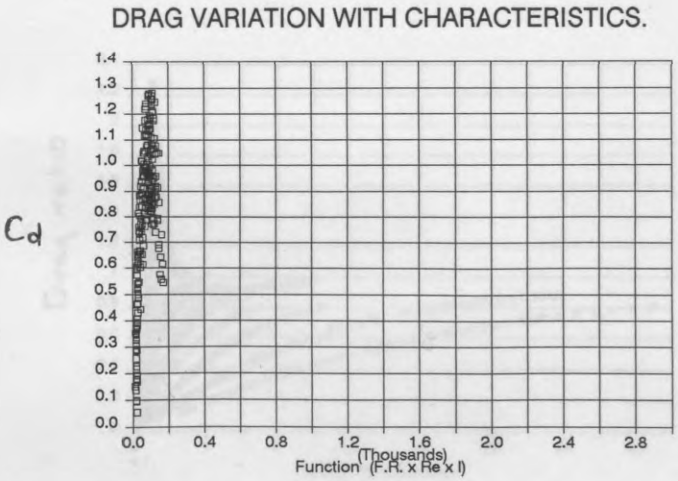

Figure 8.25e Drag variation with product function for a scale ratio greater than 4.0.

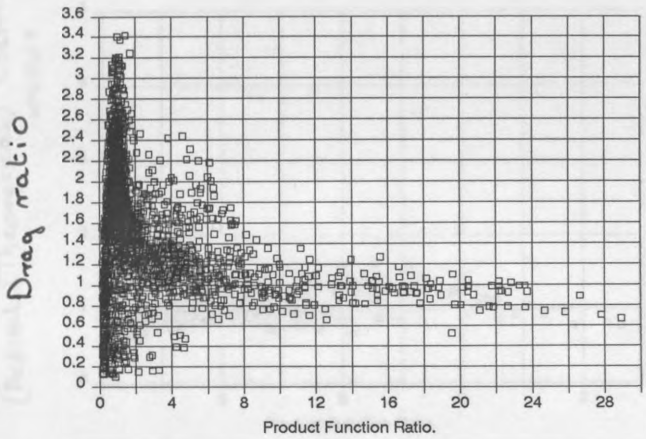

Figure 8.26 Drag ratio variation with function ratio.

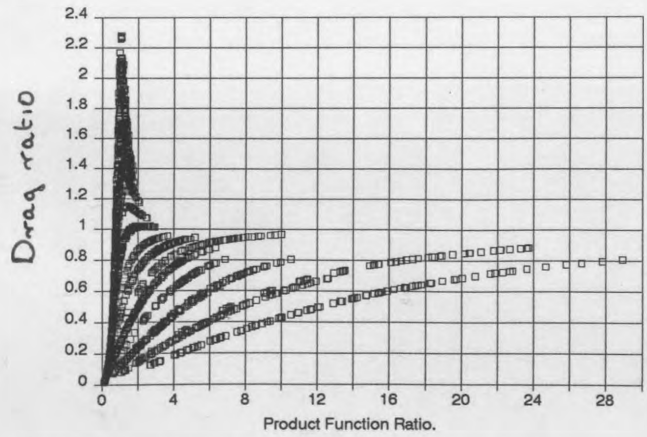

Figure 8.26a Theoretical drag ratio variation with function ratio.

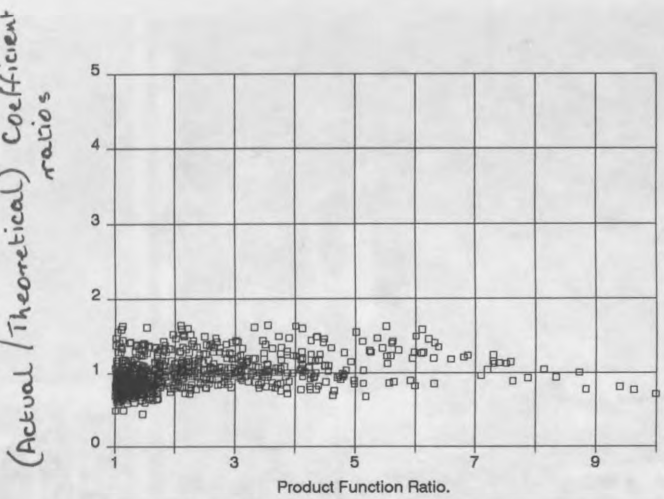

Figure 8.26b Comparison of the actual against the theoretical drag coefficient ratios for scale ratios greater than 0.6.

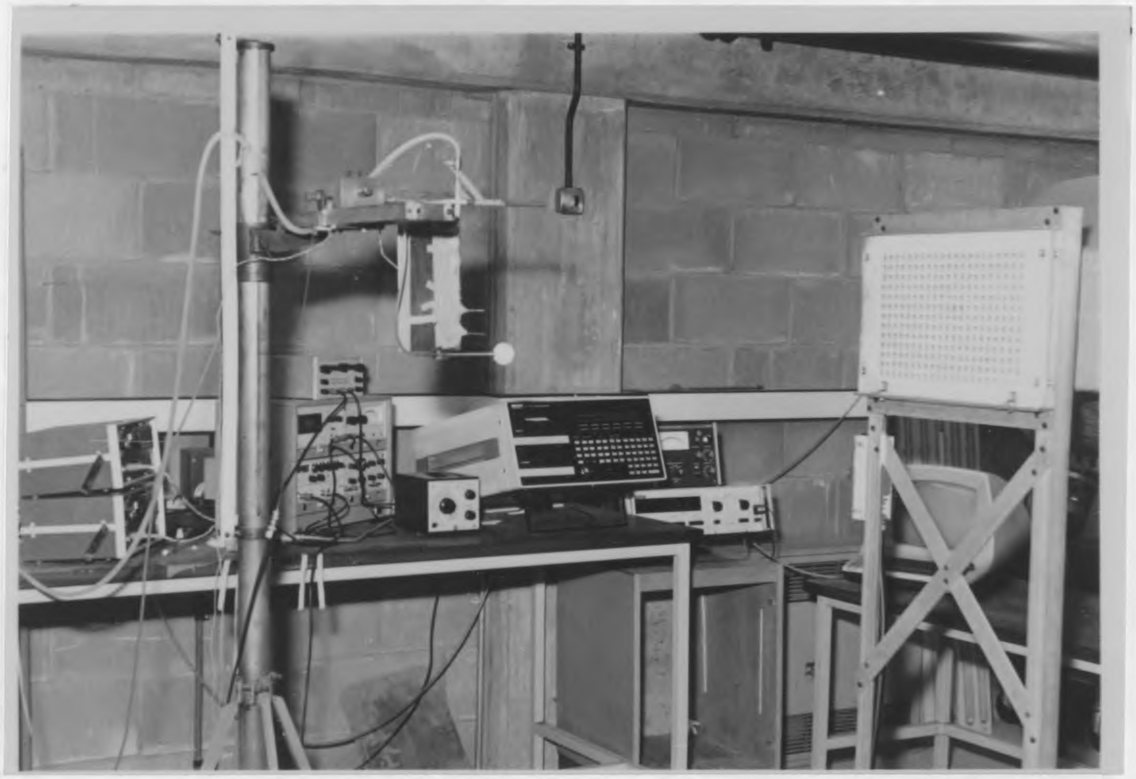

Plate 1. Experimental arrangement.

Plate 2. Wind tunnel.

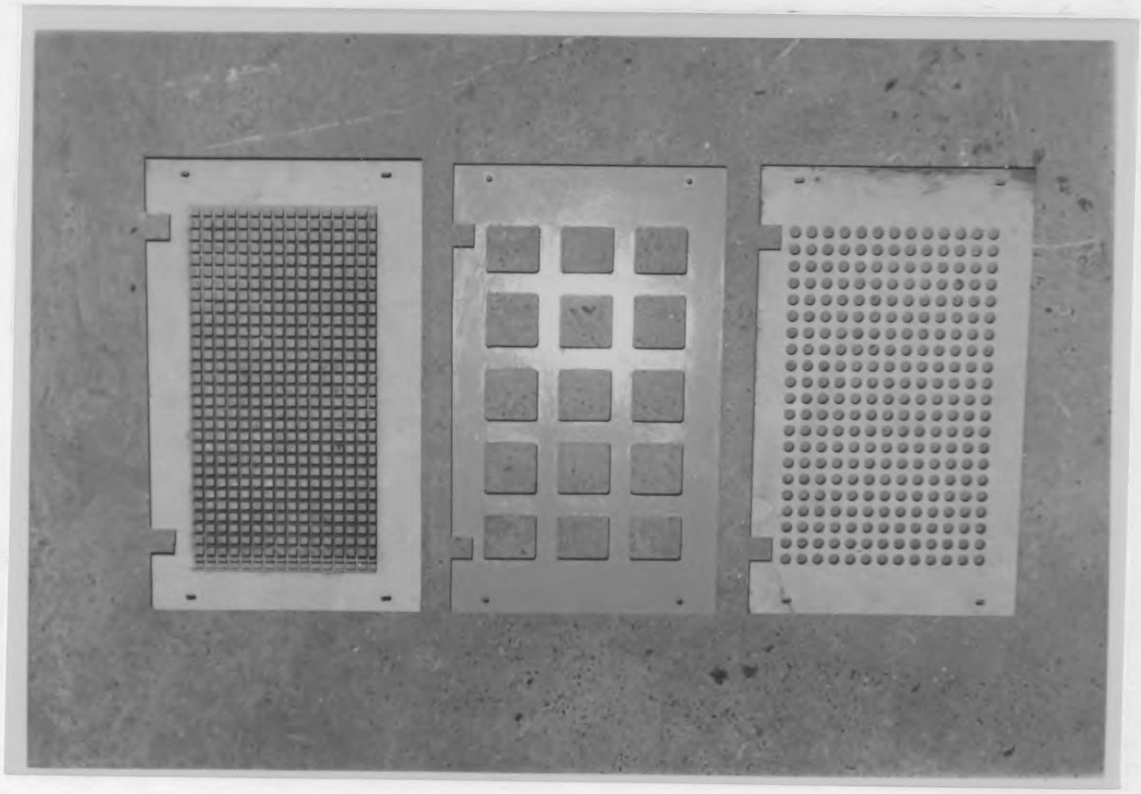

Plate 3. Grids C, B & A respectively.

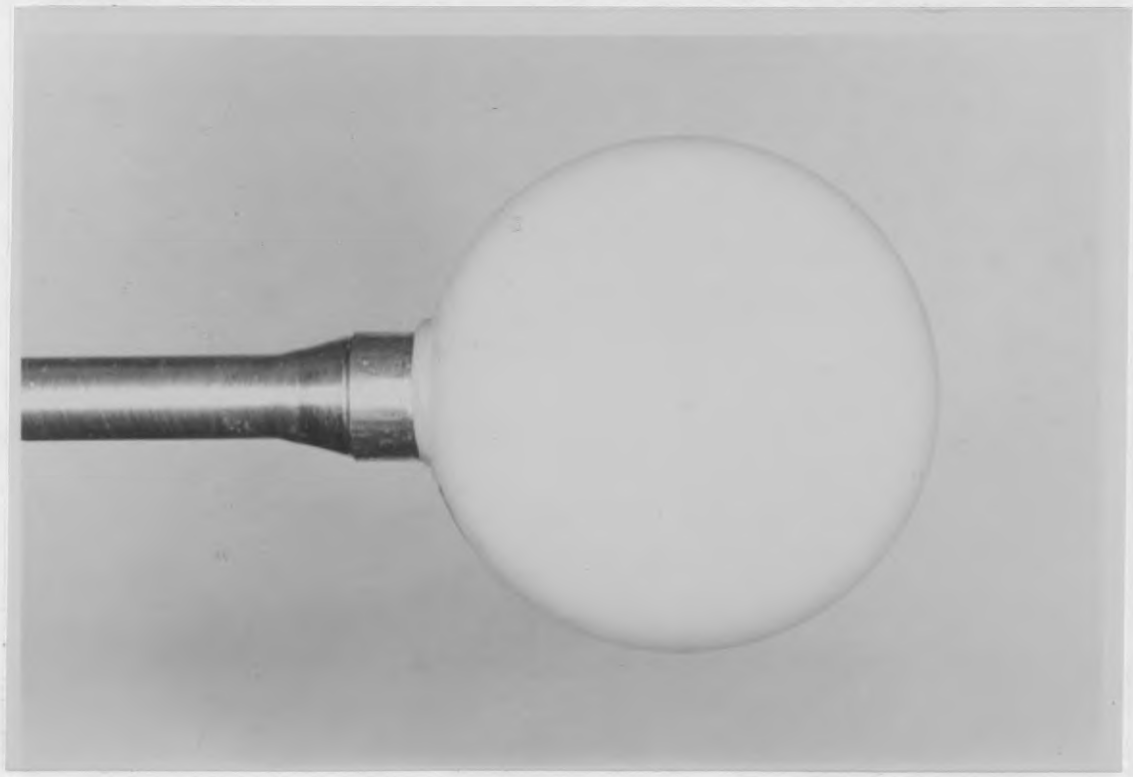

Plate 4. Sphere and sting.

Plate 5. Probe arrangement on traversing mechanism.

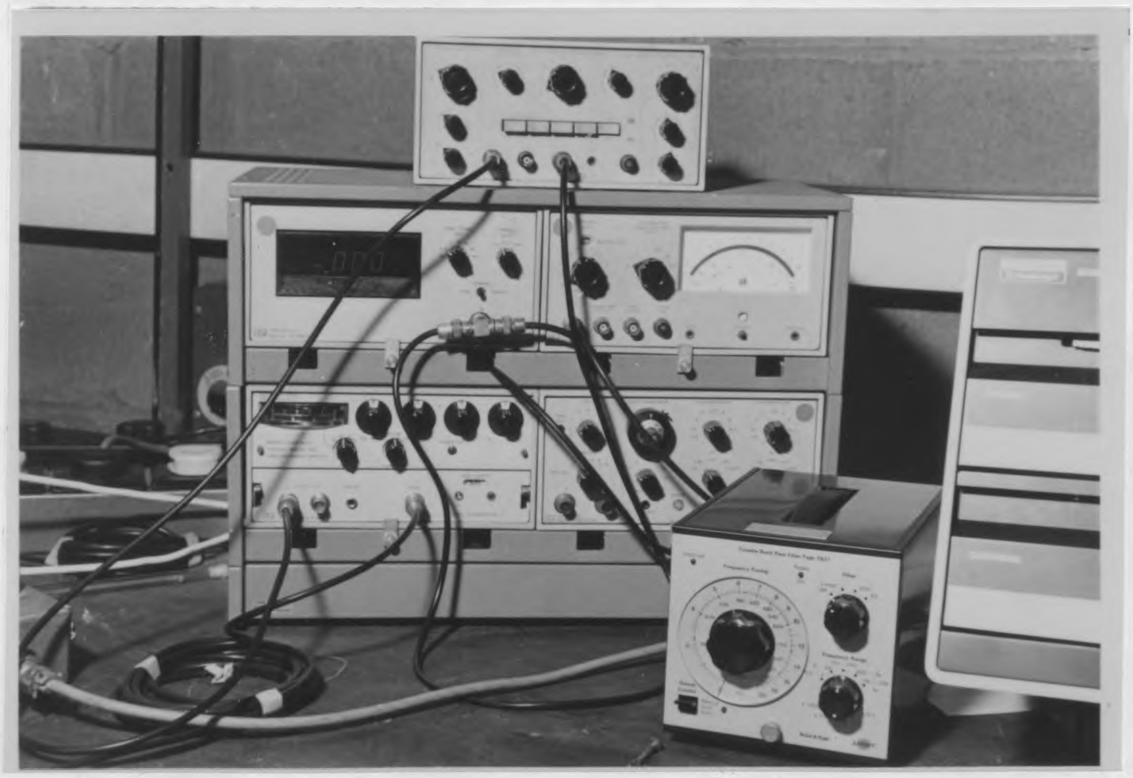

Plate 6. Anemometry.

APPENDIX A.

Calibration of the Wheatstone bridge.

To determine the drag force exerted on the sphere, a strain-gauged cantilever is used. Figure A1 shows an exploded view of this system. The wedge-shaped guard is positioned upstream of the strain-gauges so as to ensure that all the strain on the strain-gauges is caused purely by the forces exerted on the sphere. To calibrate the force balance system, the procedure used was as follows:

1). The distance between the strain-gauges and the horizontal centreline of the sting (150 mm) together with the distance between the sting and the vertical support (100 mm) are determined.

2). Known masses are hang at the position where the sting is attached to the sphere. The strains caused by these masses are noted from the Solartron true time averager which is connected to the Wheatstone bridge for which the strain-gauges form one of the arms.

3). The force which causes the above mentioned force is determined by taking moments about the sting and vertical arm connection. A graph of the applied force against the Solartron reading is shown in figure A2 from which the calibration factor of 2.206 N/volt was determined.

Taking moments about the sting and vertical arm connection:

$$100\ mg = 150\ F$$

from which

$$F = \frac{100}{150}\ mg \qquad (1)$$

From the slope of figure A2

$$mg = 3.31 \times 10^{-3}\ DR \qquad (2)$$

where mg is the weight of the known masses hang

F is the force on the strain-gauges

and DR is the solartron reading of the strain on the gauges.

Combining equations (1) and (2),

$$F = 2.206 \times 10^{-3}\ DR$$

which relates the force applied on the sphere and thus the strain-gauges to the Solartron reading.

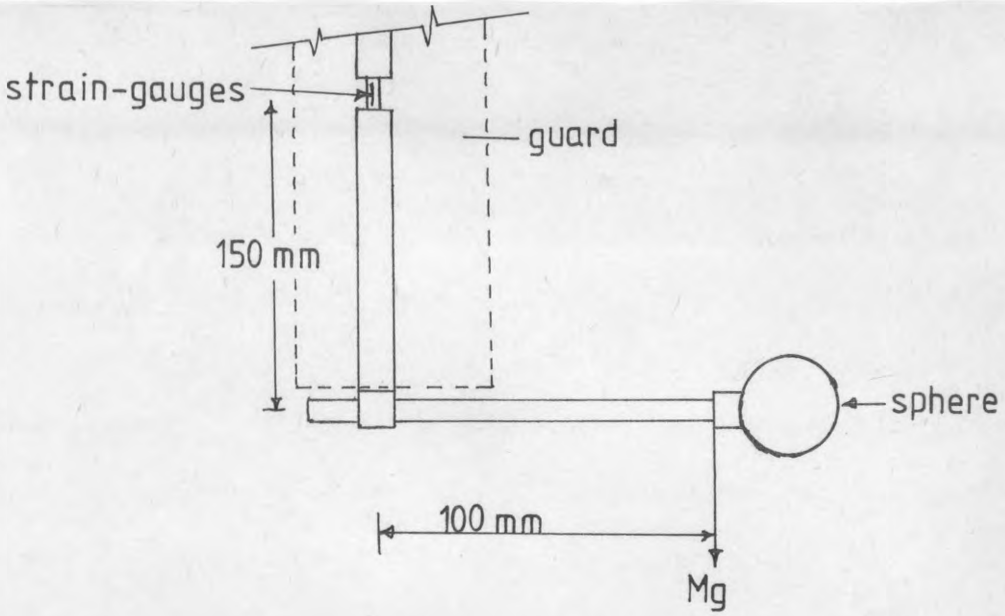

Fig. A1 Force balance system

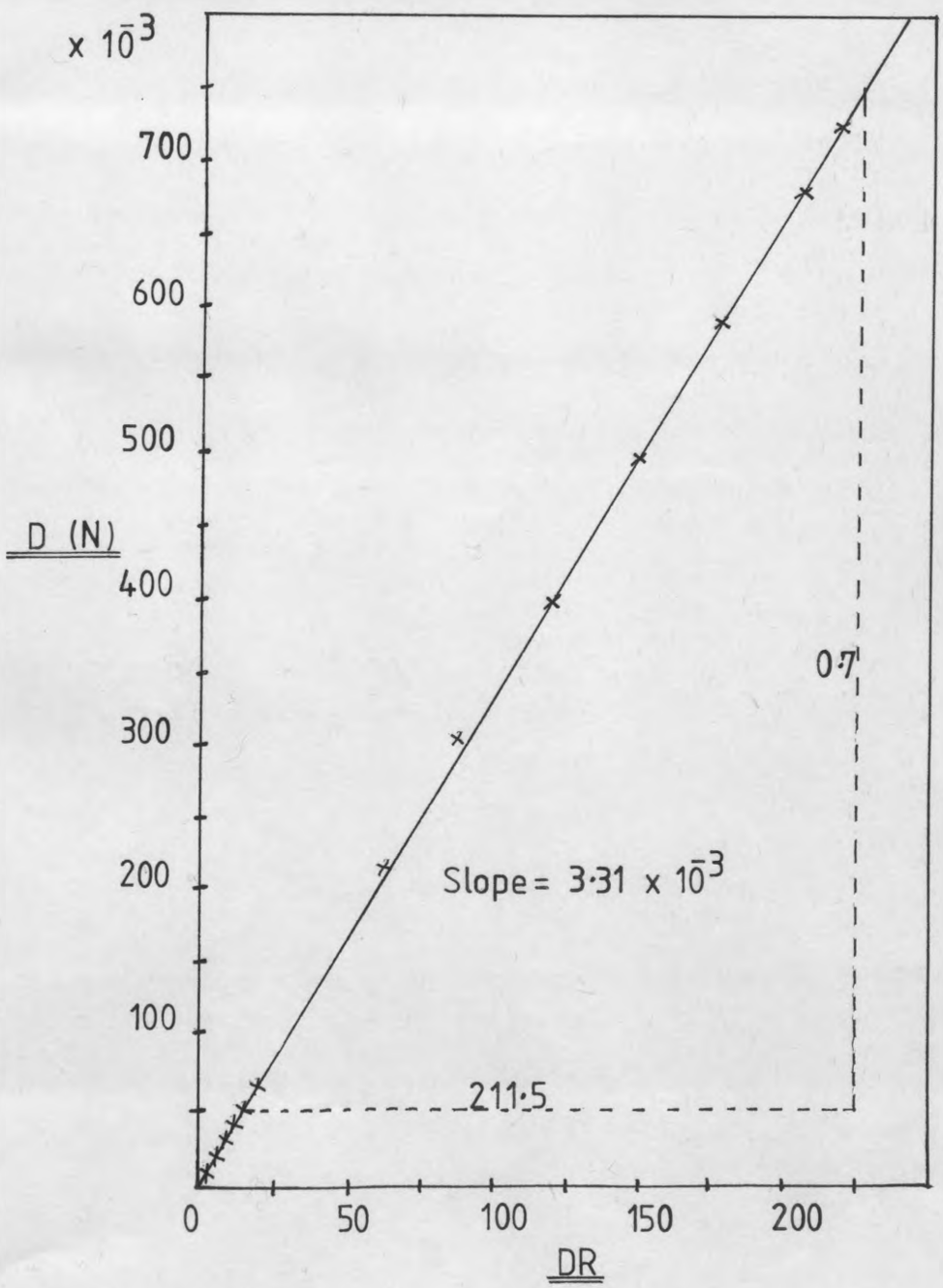

Fig. A2 Solartron calibration

APPENDIX B.

Determination of the longitudinal macroscale

The method used to determine the longitudinal macroscale of turbulence, as discussed in chapter 6, was found to produce inaccuracies when the peak position for the curve was not distinctly defined. This is because of the direct dependence of the macroscale of turbulence on the peak position. Well defined peaks, as illustrated in figures B1 and B2, are not always obtained in which case the method discussed in chapter 6 is rendered inoperative. A method using results from both the high and low frequency ranges to determine the macroscale of turbulence is therefore a better means of solving the problem. Such a method has been developed and is discussed below.

From E.S.D.U. Data Sheet 74031 (superseded by 85020), the von Karman spectral density equation which is generally accepted as the best analytical representation of atmospheric turbulence is given as:

$$S(n) = \frac{4\,c^2\,(L/U)}{[1 + 70.8\,(Ln/U)^2]^{5/6}}$$

where $S(n)$ is the power spectral density

n is the frequency

c^2 is the variance (or total energy)

L is the macroscale of turbulence

& U is the time-averaged free-stream velocity.

If this equation is assumed to be equally applicable to free-stream grid generated turbulence, then the new method can be developed as follows:

Because the power spectral density of turbulence is also defined as the energy in the waveband per unit bandwidth

$$\text{i.e.} \qquad S(n) = \frac{\text{energy in waveband}}{\text{bandwidth}}$$

$$= \frac{e^2}{dn}$$

where e^2 is the energy in a waveband

& dn is the bandwidth

then using a bandpass filter set at 1/3 octave, (i.e. $dn = 0.231n$) the spectral density of the turbulence flow field can therefore also be defined as

$$S(n) = \frac{e^2}{0.231n}$$

Equating the two equations which both define the spectral density of the turbulence flow field gives the following equation.

$$\frac{4\,c^2\,(L/U)}{[1 + 70.8\,(Ln/U)^2]^{5/6}} = \frac{e^2}{0.231n}$$

The total energy in the full frequency range is therefore given by

$$c^2 = \frac{e^2\,[1 + 70.8\,(Ln/U)^2]^{5/6}}{0.924\,(Ln/U)}$$

This equation can be simplified accordingly at the high and low frequencies using the following approximations:

At very high frequency values, $70.8\,(Ln/U)^2 >> 1$.

Therefore the total energy is given by

$$c^2 = \frac{e_H^{\,2}\,[70.8\,(Ln_H/U)^2]^{5/6}}{0.924\,(Ln_H/U)}$$

$$= 37.67\,e_H^{\,2}\,(Ln_H/U)^{2/3}$$

And at very low frequency values, $70.8\,(Ln/U)^2 << 1$.

Therefore the total energy is given by

$$c^2 = \frac{e_L^{\,2}}{0.924\,(Ln_L/U)}$$

Equating these equations which give the total energy of the full frequency range defines the longitudinal macroscale of turbulence as follows:

$$Lx = \frac{0.1188\,U(e_L/e_H)^{6/5}}{n_L^{\,3/5}\,n_H^{\,2/5}}$$

To determine the accuracy of this equation, the following table which gives a comparison of the actual macroscales of turbulence taken from curves and calculated macroscales

of turbulence from the equation are taken. The first two results are taken from figures B1 and B2 respectively.

Velocity (m/s)	e_L	e_H	n_L	n_H	$\langle v \rangle$	L_x (calculated)	L_x (actual)	Difference (%)
13.70	0.0092	0.0052	2	2000	12.0	0.102	0.167	39
21.60	0.0040	0.0038	2	2000	24.5	0.086	0.129	33
17.70	0.0095	0.0060	2	2000	17.5	0.115	0.148	22
20.19	0.0053	0.0048	2	2000	22.0	0.085	0.134	37
16.03	0.0062	0.0045	2	2000	15.0	0.088	0.156	44

From this table it is shown that the calculated macroscale of turbulence is greater than the actual macroscale of turbulence by an average of 35%. Its consistancy suggests that there is be a spectral phase difference between the atmospheric turbulence for which the von Karman equation was developed and the grid generated turbulence.

The equation obtained can therefore be used to determine the macroscale of turbulence using the results at both the high and low frequency ranges. Adjusting the determined macroscale of turbulence to account for the spectral phase difference, an accuracy of up to 15% can be achieved.

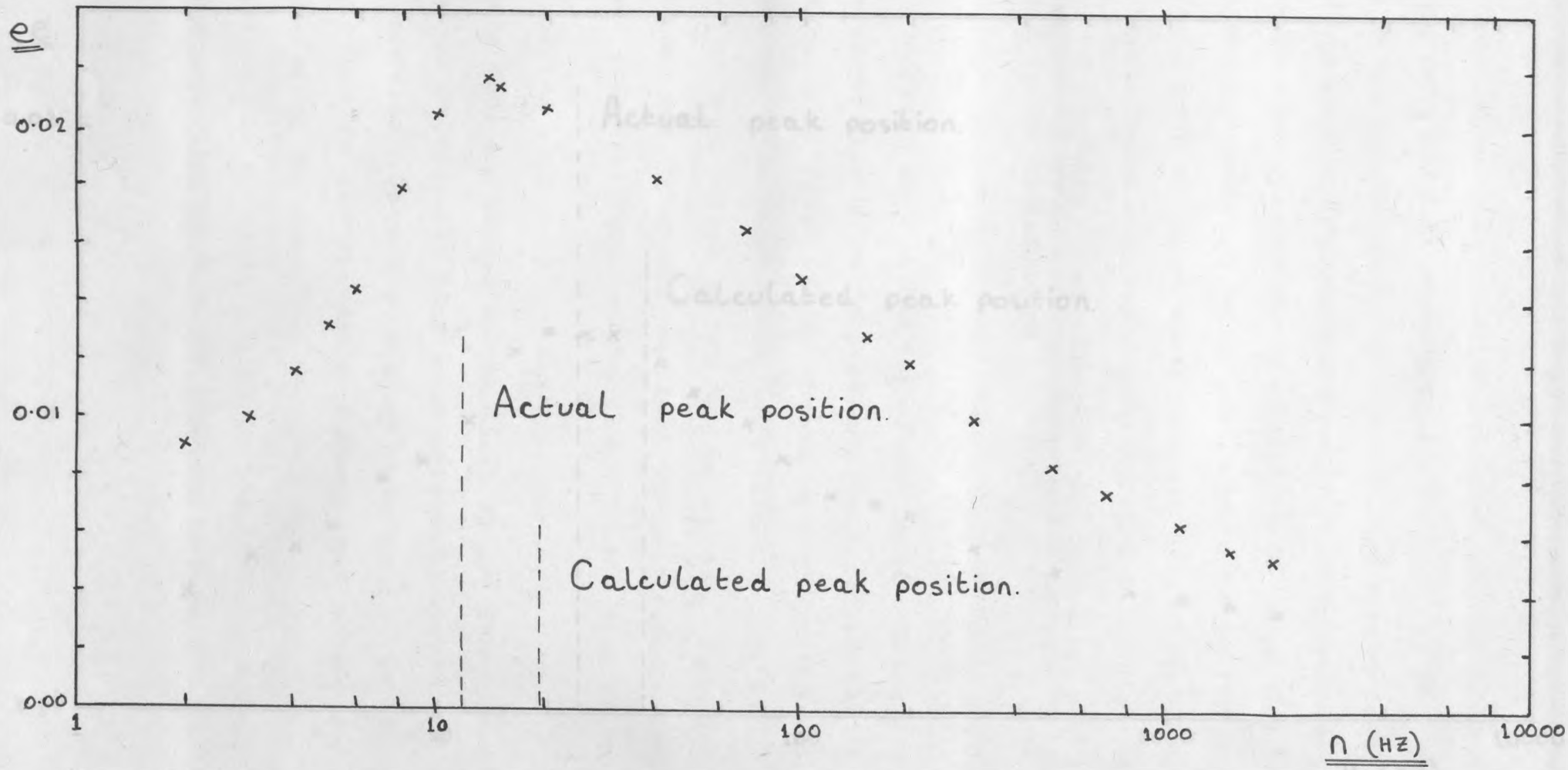

Fig. B1 Frequency spectrum at x = 2000 mm

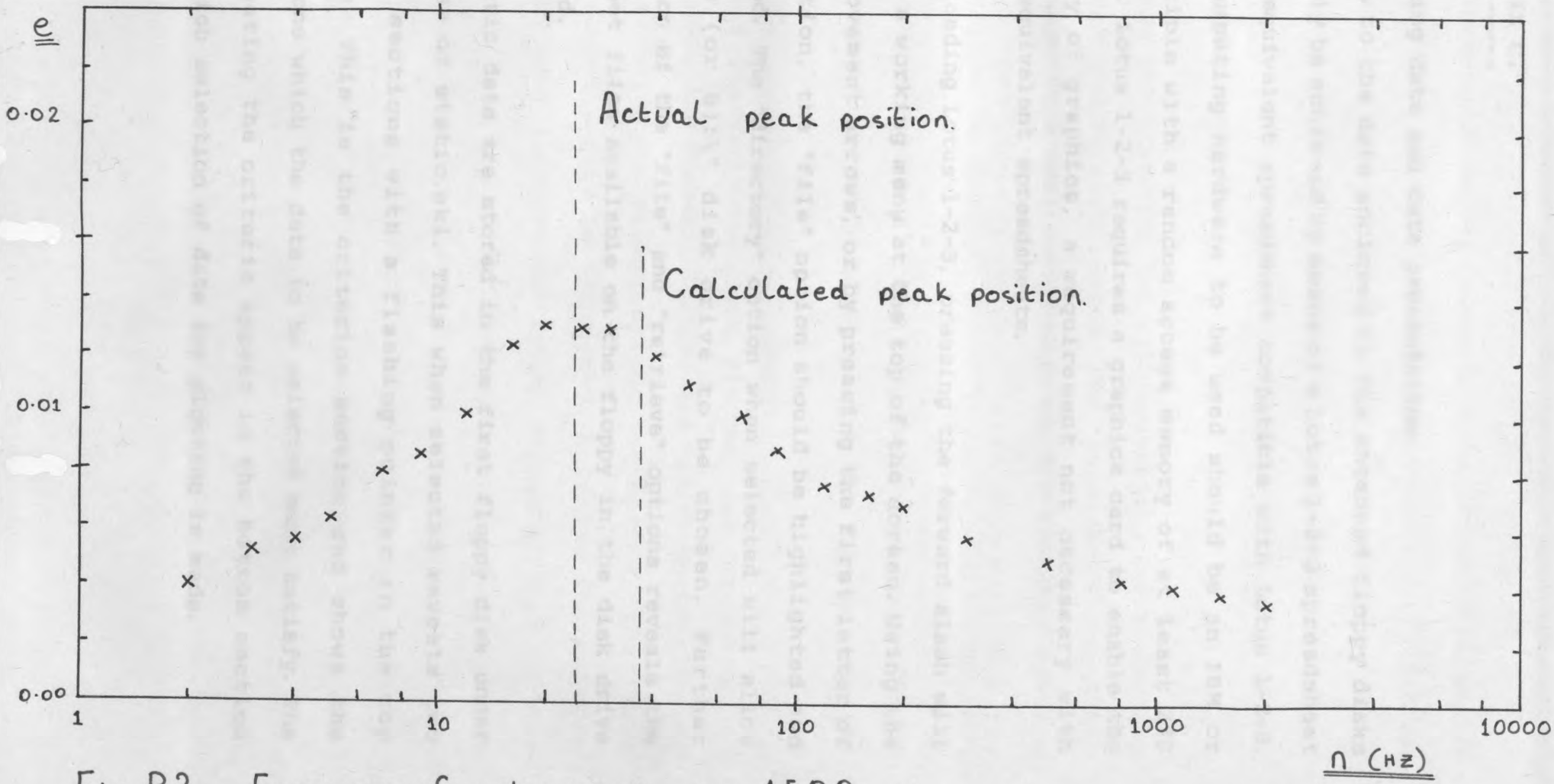

Fig. B2 Frequency Spectrum at $x = 1500$ mm.

APPENDIX C.

Accessing data and data presentation.

Access to the data enclosed in the attached floppy disks can only be achieved by means of a Lotus 1-2-3 spreadsheet or an equivalent spreadsheet compatible with Lotus 1-2-3. The computing hardware to be used should be an IBM or compatible with a random access memory of at least 253 kbytes. Lotus 1-2-3 requires a graphics card to enable the display of graphics, a requirement not necessary with other equivalent spreadsheets.

After loading Lotus 1-2-3, pressing the forward slash will reveal a working menu at the top of the screen. Using the side movement arrows, or by pressing the first letter of the option, the "file" option should be highlighted and selected. The "directory" option when selected will allow the "a (or b):\" disk drive to be chosen. Further selection of the "file" and "retrieve" options reveals the worksheet files available on the floppy in the disk drive selected.

The static data are stored in the first floppy disk under the name of static.wk1. This when selected reveals two titled sections with a flashing pointer in the top section. This is the criterion section and shows the conditions which the data to be selected must satisfy. The data meeting the criteria appear in the bottom section from which selection of data for plotting is made.

The "function 7" key begins selection of data satisfying the conditions given in the criterion section. To extract data for plotting graphs, a macro is evoked by the "alt a" keys. Display of the graphs is by use of the "function 10" key. The "return" key removes the graphic display and returns the spreadsheet.

To change the criteria, the cell containing the conditions to be changed is highlighted. The "function 2" key makes editing of this cell possible using the standard editing keys of "del", "back space", "side arrows", and the "return" key to end editing. The same procedure of "function 7", "alt a", and "function 10" keys can be repeated to display the graph of results that satisfy the new criteria.

To change the variables being plotted, the "graph" option followed by the "reset", "graph" and "quit" options should be selected. Upon selecting the "x" option, the range containing the data is requested. Entering for example "m6.m600" will indicate the range. Repeating this for the "a" option will render the operation complete. Select in order the following options: type; xy; options; format; graph; symbols; quit; grid; both; quit; and quit. Pressing "function 7" and "function 10" keys displays the required graph satisfying the criteria.

Macros, such as the one evoked by the "alt a" keys, are a set of commands that are frequently used. These commands placed in a single column are evoked as is the macro in the current spreadsheet. The uppermost cell in the column of macros is named using the "range", "name" and "create" options. A single alphabetic letter range name preceded by a backslash is then given.

The second, third and fourth floppy disks contain the dynamic data whose use has been limited and as such has been stored on high density IBM AT format because of its ability to store up to 1.2 Mbytes per floppy. Access to this data is therefore with an IBM AT or compatible and can the be incorporated into the spreadsheet for analysis as previously discussed. These files are stored in nine separate files named in series from "DYNAMIC1.PRN" to "DYNAMIC9.PRN".